Engineering Therapeutic Proteins for Immune Modulation

By

Tiffany F. Chen

B.S. Biomedical Engineering
The University of Texas at Austin, 2008

Submitted to the Department of Biological Engineering in
Partial Fulfillment of the Requirements for the Degree of

Doctor of Philosophy in Biological Engineering

at the

Massachusetts Institute of Technology

June 2014

SIGNATURE OF AUTHOR: _____
Department of Biological Engineering
May 21, 2014

CERTIFIED BY: _____
K. Dane Wittrup
C.P. Dubbs Professor of Chemical Engineering & Biological Engineering
Thesis Advisor

ACCEPTED BY: _____
Forest M. White
Associate Professor of Biological Engineering
Chair, Graduate Program Committee

THESIS COMMITTEE MEMBERS

Darrell Irvine, Ph.D. (Chair)
Professor of Materials Science & Engineering and Biological Engineering
Massachusetts Institute of Technology

Glenn Dranoff, M.D.
Professor of Medicine
Dana-Farber Cancer Institute
Brigham and Women's Hospital
Harvard Medical School

Engineering Therapeutic Proteins for Immune Modulation

By Tiffany F. Chen

Submitted to the Department of Biological Engineering on
May 21, 2014 in Partial Fulfillment of the Requirements for the
Degree of Doctor of Philosophy in Biological Engineering

ABSTRACT

Antibody-dependent cell-mediated cytotoxicity (ADCC) is implicated in the efficacy, to some degree, of most anti-cancer monoclonal antibodies. This interaction is mediated through Fc gamma receptor (FcγR) binding to the antibody Fc. Activating and inhibitory FcγRs are expressed on immune cells and bind to the Fc regions of IgGs, which either promote or hinder responses against the tumor cell. Since mouse models of cancer are currently the most established in this field, studying the effect of modulating individual murine FcγRs would provide insight into this type of therapeutic for humans. The ectodomains of murine FcγRs are highly homologous and therefore it has been difficult to engineer antibody Fc regions to specifically bind only one FcγR. To address this challenge, we engineered the human tenth type III fibronectin (Fn3) domain scaffold to bind individual murine FcγRs. The Fn3 scaffold has the advantage of binding at epitopes on the FcγR that are distinct from the Fc binding region.

Fn3 clones have been isolated with specificity to each known murine FcγR: FcγRI, FcγRIIB, FcγRIII, and FcγRIV. Measured K_Ds of Fn3 binding to FcγR range on the order of 1-100nM, which fall within the range of normal Fc-FcγR binding affinity or even higher affinity. Candidate Fn3 clones are fused to tumor antigen specific scFvs and a murine serum albumin (MSA) to maintain *in vivo* half-life. Each scFv-MSA-Fn3 construct was antigen specific and bound specifically to the FcγR that it was designed to target. To confirm the biological activity of the Fn3 clones, phagocytosis assays with peritoneal macrophages were conducted. Pharmacokinetic studies have shown all scFv-MSA-Fn3 constructs to have approximate beta half-lives of 25 hours in C56BL/6 mice. Biodistribution of scFv-MSA-Fn3 constructs demonstrate preferential accumulation in antigen positive subcutaneous tumors. Multiple *in vivo* models were optimized to detect anti-tumor efficacy of our engineered constructs. In a subcutaneous tumor model with aggressive prophylactic dosing, our binders to the activating FcγRI, FcγRIII, and FcγRIV demonstrate similar control to the mIgG2a antibody. These tools will allow us to conduct future studies on the immune response of triggering individual FcγR in models of cancer.

The binding of human IgG1 to human Fc gamma receptors (hFcγR) is highly sensitive to the presence of a single N-linked glycosylation site at asparagine 297 (N297) of the Fc, with deglycosylation resulting in a complete loss of hFcγR binding. Thus, aglycosylated variants that can bind to hFcγRs have the potential to allow therapeutic antibodies to be produced in virtually any expression system. Previously, we demonstrated that aglycosylated human IgG1 Fc variants are capable of engaging the human Fc gamma RII subset of the low-affinity hFcγRs, demonstrating that N-linked glycosylation of the Fc is not a strict requirement for hFcγR engagement. In the present study, we demonstrate that aglycosylated IgG variants can be engineered to productively engage with Fc gamma RIIIA, and that these variants can also bind the human Fc gamma RII subset. In this study, we also assess the biophysical properties and serum half-life of the aglycosylated IgG variants. Phagocytosis assays with monocytes and macrophages were performed to determine which constructs optimally drove tumor cell killing. A mathematical model of phagocytosis suggests that hFcγR dimers of hFcγRI were the main drivers of phagocytosis.

THESIS SUPERVISOR: K. Dane Wittrup
TITLE: C.P. Dubbs Professor of Chemical Engineering & Biological Engineering

ACKNOWLEDGEMENTS

This work was completed with help and contributions from many people. I would like to thank my advisor, Dane Wittrup, for his guidance, enthusiasm, and undying encouragement throughout my years in his lab. He has not only provided great scientific advice, but also has been a great mentor in helping me establish a career path in the industrial scientific field. My thesis committee members, Darrell Irvine and Glenn Dranoff, were key in driving my project in specific directions, and they provided tremendously helpful advice throughout the shaping of my project.

This project was funded by the Sanofi-Aventis Biomedical Innovation Award Program, which allowed us to work with our great collaborators Huawei Qiu and Julie Bird, who contributed to the aglycosylated antibody binding studies. Our collaborators Jeff Ravetch and David Dilillo from Rockefeller University helped with the aglycosylated antibody *in vivo* cancer model work. The Koch Institute Flow Cytometry Core, especially Mike Jennings, Michele Griffin, and Glenn Paradis, have been essential for the protein engineering portion of my project. The Biopolymers Core and the Microscopy Core were also very helpful in sequencing and microscopy image acquisition, respectively. Other funding sources include the Cunningham Immune Mechanisms in Cancer Fellowship and the NIH/NIGMS Biotechnology Training Program, which allowed me to gain invaluable experience with an internship in the Antibody Engineering department at Genentech.

I would also like to thank the group of talented undergraduates that have worked with me throughout my years here. My first undergraduate, Kevin Li, contributed greatly to this work on several of the projects throughout his 3 years working with me. His assistance was essential in the completion of much of the protein engineering, *in vitro,* and preliminary *in vivo* work. Undergraduates—Heeyoon Kim and Eta Atolia worked on the *in vivo* prophylactic model my last semester here. George Cheng assisted in the modeling aspect of the aglycosylated antibody work.

I am grateful for all of the colleagues I have worked with throughout the years. Benjamin Hackel was key in teaching me yeast surface display. Steve Sazinsky provided very useful advice on the aglycosylated work throughout the years and was kind enough to spend 2 hours chatting with me about his project when I was first interested in joining the lab. Margie Ackerman, Kelly Davis Orcutt, Mike Schmidt, Jamie Spangler, Chris Pirie, and David Liu were senior members of the lab that were great mentors and helped me with all of my trivial questions when I first started. John Rhoden was a great officemate and bench neighbor throughout my years here. He never failed to amuse me with his pranks and deadpan humor. Jordi Mata-Fink always entertained me with jokes and stories, along with providing very useful scientific advice. Annie Gai was not only a great scientific mentor but also a great friend, who cooked me many yummy meals. Xiaosai Yao and I joined the lab together and she has been one of my closest friends throughout the years. She has taught me many protocols, provided stimulating scientific and intellectual conversations, and been a great support the entirety of my Ph.D. Nicole Yang has also been a close friend, great lab buddy, and has been a pillar of support. Seymour de Picciotto, Alessandro Angelini, Jim Van Deventer, and Cary Opel have been great colleagues, providing scientific advice and being great sounding boards when I am working out ideas. Byron Kwan, Michael Santos, Alice Tzeng, Katie Maass, and Eric Zhu have been fun to work with and helpful in many aspects of science, from sharing reagents to advice. Michael Traxlmayr, Ryan Kelly, Monique Kauke, Adrienne Rothschilds, and Naveen Mehta have been great lab/officemates my last years here.

Outside of lab, I would like to thank my roommate, Yvonne Yamanaka, who has provided considerable scientific advice, been helpful in editing abstracts and presentations, and been a great friend and listener throughout my years here. I am also thankful for all of my friends that I have made from MIT Sport Taekwondo. Taekwondo has been a good stress reliever and great environment to workout in my last few years in graduate school. Lastly, I would like to thank my family, for their support, encouragement, and comfort throughout my Ph.D. I am thankful for my father for his advice and critical thinking, my mother for her patience and willingness to listen, and my sister for her support and random responses during my complaints about my proteins.

To my family for their unconditional love, support, wisdom, laughs, smiles, and quirkiness.

In memory of my aunts
小姑姑 and 舅媽
Who battled cancer.

TABLE OF CONTENTS

CHAPTER 1: BACKGROUND AND SIGNIFICANCE

The use of monoclonal antibodies (mAbs) is a growing field in anti-cancer therapy[1,2]. Several methods are currently being explored that utilize the specificity of antibodies to combat cancer. Currently, FDA-approved antibodies for cancer treatment operate through various mechanisms. One strategy employs antibodies as neutralizing molecules to competitively block receptors (cetuximab/erbitux) that promote cancer cell growth, such as epidermal growth factor receptor. An alternative method is through conjugating toxins or small molecules to antibodies (zevalin, bexxar, mylotarg) that target specific receptors on the surface of cancer cells that allow for delivery of the cytotoxic payload. Other antibodies that target tumor specific antigens have shown therapeutic efficacy by triggering the antibody-mediated adaptive immune response (rituximab/rituxan), which is typically reserved for infection clearance. Our current objective is to improve mAbs for optimized interactions with immune cells to promote increased effector function.

Role of antibody in the immune response

Antibodies are a part of the adaptive immune response and play key roles in pathogen neutralization and clearance. Antibodies coat the pathogen and mediate clearance through several mechanisms: neutralization of surface antigens essential for infection, opsonization, which promotes antibody dependent cellular cytotoxicity (ADCC) and phagocytosis by immune cells, and activation of the complement cascade. The belief is that these mechanisms can be directly transferred to the destruction of cancer cells. The typical IgG structure is in the shape of a "Y" where the two arms comprise the Fab region and the tail is the Fc region. The Fab region includes the variable portions of the antibody that bind to specific antigens. The Fc region is the constant region of the antibody that interacts with Fc receptors on immune cells, and other components of the immune system such as complement. The Fc region is also important in maintaining the long half-life of IgGs by binding

to FcRn for recycling, which is important when considering development of therapeutics. Our focus will be on engineering the Fc region, or scaffolds that mimic the Fc region to bind to Fc receptors on immune cells and promote their activation.

The significance in this type of antibody therapy lies in its possibility to promote immune cell memory against particular cancers[3]. Through the opsonization mechanism, antibodies can coat tumor cells and promote their phagocytosis through the Fc-Fc receptor interaction. If these tumor cells are phagocytosed by APCs, the cells will be degraded and their surface antigens will be displayed in the major histocompatibility complex molecules. These displayed antigens will be recognized by inactive T cells, which in turn become activated into cytotoxic T lymphocytes (CTLs) or T helper cells (T_H cells). CTLs are the main killing lymphocytes and will destroy tumor cells presenting the same antigens. The T_H cells will activate B cells, which can differentiate into plasma cells and become factories for antibodies against the tumor specific antigens. This entire process leads to immunologic memory against specific targeted tumor types[1].

FcγR and interactions with IgG

The key receptors modulating immune cell interaction with IgG Fc's are FcγRs. These receptors are expressed on various immune cell surfaces and form immune complexes upon binding of antibody Fc's. The FcγR family is comprised of both high and low affinity FcγRs. The high affinity FcγRs tend to bind soluble monomeric IgG and therefore lack a major role in binding antibodies bound to tumor surface antigens[3,4]. Low affinity FcγRs bind antibody Fc's with micromolar dissociation constants, and therefore the weak affinity requires multivalent interactions for FcγR activation. This ensures that these low affinity FcγRs interact with antibody coated targets.

The presence of FcγRs is conserved between humans and mice, allowing mice to be useful animal models for this system. Humans have the activating receptors FcγRI, FcγRIIA, and

FcγRIIIA, along with the inhibitory receptor FcγRIIB. The two FcγRIIA and FcγRIIIA receptors each have two polymorphisms FcγRIIA167R/H and FcγRIIIA176V/F. Mice have FcγRI (CD64), FcγRIII (CD16), and FcγRIV (CD16-2) as activating receptors and FcγRIIB (CD32) as the inhibitory receptor. It is believed that the receptors that play a key role in anti-tumor activity are low affinity FcγRs, which exclude both human and murine FcγRI[3–5]. Low affinity FcγRs tend to interact with immune complexes, and in the case of cancer, antibody coated tumors. FcγR expression varies depending on immune cell type. Cells of interest include macrophages and dendritic cells (DCs), Natural Killer (NK) cells, and neutrophils. Macrophages and monocytes express all of the murine FcγRs: FcγRI, FcγRIIB, FcγRIII, and FcγRIV, whereas dendritic cells express FcγRI, FcγRIIB, and FcγRIII. Neutrophils express the low affinity receptors: FcγRIII, FcγRIV and FcγRIIB. NK cells are unique in that they only express FcγRIII and do not possess an inhibitory FcγR[5]. Murine FcγR correspond to human FcγR with differential expression on the same types of immune cells. Therefore, murine FcγRIV, FcγRIII, and FcγRIIB have similar cell expression patterns as human FcγRIIA, FcγRIIIA, and FcγRIIB, respectively[3]. Strangely, based on sequence mapping it has been suggested that murine FcγRIV is homologous to human FcγRIIIA[6]. More recent evidence has also suggested that FcγRIV is actually a low affinity IgE receptor[7,8].

The typical structure of an FcγR is composed of an extracellular domain, which interacts with antibody Fc's and an intracellular domain for signaling. For the low affinity receptors, an α-chain consisting of two domains (D1 and D2) makes up the extracellular domain of the FcγRs of interest. The high affinity FcγRI, has an additional extracellular domain (D3). The intracellular domain typically consists of a signal-transducing γ-chain associated with the α-chain[3]. FcγRIIB is an exception in that its signal-transducing motif is on the α-chain and it does not have an associated γ-chain[5]. Intracellular signaling is dependent on the signal-transducing motif on each FcγR. Activating

FcγRs contain an immunoreceptor tyrosine-based activation motif (ITAM), whereas inhibitory FcγR contain an immunoreceptor tyrosine-based inhibitory motif (ITIM).

FcγR binding of antibody immune complexes triggers signaling pathways within the immune cells. Crosslinking or dimerization of the FcγRs occurs through multivalent binding, which leads to the phosphorylation of the receptor's signal-transducing motif. The dimerization of two activating FcγRs leads to the recruitment of SYK-family kinases and activation of various downstream targets, eventually leading to increased intracellular calcium levels. Crosslinking of an inhibitory FcγR with another receptor leads to phosphorylation of ITIM by LYN and recruits SHIP or SHP-1, which leads to the inhibition of recruitment of PH domain proteins and prevents calcium influx[9]. Activation of immune cells leads to secretion of cytokines, release of reactive oxidative species, phagocytosis, etc.

IgG interaction with FcγR is highly dependent on glycosylation and amino acid sequence. The mutation of N297Q in the CH2 domain of human IgG1 renders the antibody aglycosylated and abrogates all binding activity to FcγRs[10]. Shields *et al*, has shown that the mutation of the aspartic acid at position 265 to an alanine also abrogates binding activity with FcγRs, but maintains the glycosylation[11]. Lack of glycosylation has been a concern in the maintenance of antibody serum half-lives for therapeutic efficacy. It appears though that certain aglycosylated antibodies have similar clearance rates as wild-type[12]. The D265A mutation on mouse IgG2a & IgG2b shows similar results to that of human IgG where no binding is detected with mouse FcγRs or C1q in the case of IgG2a[13].

Current methods in improving Fc-FcγR engagement

Many factors impact FcγR binding affinity to IgGs, ranging from the amino acid sequence to the type of glycosylation at the Fc binding region[5]. In the past, aglycosylated antibodies showed

impaired FcγR binding, but recent studies have shown aglycosylated IgG1 variants productively engaging activating FcγRs[10]. Selection of amino acid mutants has also been performed through computational predictions and alanine scanning[4,14]. The FcγR monomer interacts with both domains of the CH2 portion of IgGs in a non-symmetric fashion. Therefore, it would be difficult to completely decouple binding with different FcγRs with only mutagenesis of the IgG Fc region, because the Fc is a homodimer. New exploration has begun in utilizing different scaffolds as binders for FcγRs with the eventual goal of creating bispecific antibodies[15].

FcγR and cancer

Two classes of thought encompass FcγRs and cancer. In cancer therapeutics with mAbs, activating FcγRs has been shown to play a key role in the elimination of tumor cells. The classic example is the α-CD20 mAb, rituximab, and its mechanism of action through FcγRIIIA engagement[16]. The role of different FcγRs has been studied through different knockout (KO) mice and antibody isotypes. Nimmerjahn and Ravetch, showed that *in vivo* the IgG2a isotype was key in mediating effector functions with the B16F10 lung metastasis mouse model treated with TA99. Then they tested different FcγR KO mice injected with B16F10 melanoma cells using the TA99 IgG2a antibody, and revealed that FcγRIV played the major role in tumor clearance[17]. Subsequent papers have shown evidence for overlapping roles between FcγRI and FcγRIV in tumor cytotoxicity[18,19]. Unfortunately, re-challenge of B16F10 in TA99 treated mice indicated that TA99 did not induce memory response[18].

The other school of thought centers on immune complex engagement with FcγRs and the promotion of cancer progression. FcγRs have been shown to be involved in inflammatory and autoimmune disease. Recently, in a squamous carcinogenesis mouse model, it was reported that activating FcγRs promote cancer development. Myeloid cells, in this case mast cells and M2

polarized macrophages, contributed to tumor formation[20]. The main difference between these two cases is that the former is a mAb therapeutic, and therefore transient, whereas the latter stems from accumulation of immune complexes over time. These immune complexes lead to a constant inflammatory response that polarizes tumor-associated macrophages towards a regulatory or M2 phenotype as opposed to the M1 polarized classically activated effector macrophages[21,22]. This suggests that mAb therapeutics probably interact with M1 macrophages or other effector cells for tumor clearance.

Yeast surface display with human tenth type III fibronectin domain scaffold

Yeast surface display (YSD) is a versatile platform for engineering proteins. Display of single-chain variable fragments (scFvs) for affinity maturation of already isolated scFvs or isolation of binders from naïve libraries are probably the most characterized applications of YSD[23–26]. Several other proteins including T cell receptors, cytokines, and green fluorescent protein (GFP) amongst others have been engineered using YSD for improved characteristics of binding affinity, expression, stability, etc.[27]. Yeast display libraries, which range from 10^7-10^9 transformants, are typically smaller than phage or ribosome display libraries, 10^{11}-10^{13}, but have the advantage of a eukaryotic expression machinery. This allows for isolation of clones that would have been missed using other display systems, which suggests more proper display of eukaryotic proteins[28].

In the YSD system, the protein to be engineered is fused to the C-terminal end of the Aga2p protein, which forms a covalent linkage to the Aga1p protein on the yeast surface through two disulfide bonds. YSD requires two main components: the yeast, EBY100, and the plasmid, pCT-CON. EBY100 is deficient in the machinery to synthesize the amino acid tryptophan and contains the Aga1p gene in the yeast genome. The pCT-CON plasmid encodes for (a) the gene TRP1, which is important for tryptophan synthesis, (b) the Aga2p protein fused to the protein of interest, and (c) ampicilin resistance, for plasmid production in *E. coli*. Both Aga1p and Aga2p mating proteins are

controlled under a galactose-inducible promoter. When yeast are properly transformed with the pCT-CON plasmid, they can grow in selective media deficient in tryptophan, whereas untransformed EBY100 will not propagate. Switching the yeast from glucose-rich media to galactose-rich media will induce proper display of the protein of interest.

Engineering binders from scFvs and antibodies has been the standard practice, but over the past decade the use of alternative scaffolds has been an emerging field in protein engineering[29,30]. Antibodies (150kDa) are quite complex protein structures comprised of several protein domains that require disulfide bonds and glycosylation for proper function. Alternative scaffolds such as anticalins, affibodies, darpins, and fibronectin domains are small proteins that have certain surface regions that can be highly diversified to bind to a variety of proteins[31–34]. The advantage of alternative scaffolds lies in the fact that they can be quite small, single domains yet fairly stable while lacking disulfide bonds. The alternative scaffold most developed with the yeast surface display platform is the 10th type III domain of the fibronectin (Fn3) protein; the primary domain involved in integrin binding[35–37]. This small, approximately 10 kDa, cysteine-free yet stable domain, is composed of two β-sheets comprising seven β-strands connected by three solvent-exposed loops on both sides, which resemble antibody CDRs.

A library of Fn3s was previously generated that had varying loop lengths compared to that of wild-type Fn3, with an amino acid repertoire similar to that of antibody CDR-H3. This library known as G4 is the naïve library used for our selection processes. The library diversity comprises 2.5x10^8 transformants with 60% of them being full-length Fn3s, yielding approximately 1.5x10^8 clones[38]. The current library size undersamples the immense sequence space created by the loop length and amino acid diversities. To compensate for this, diversity is constantly introduced into enriched sub-libraries by several mechanisms: high mutagenesis through error-prone PCR focused on the three loop areas (BC, DE, FG loops), low mutagenesis by error-prone PCR for the entire

Fn3 gene to introduce framework mutations, and shuffling of the loops during homologous recombination[36].

This library has yielded several binders to a variety of target proteins ranging from epidermal growth factor receptor (EGFR)[38], immunoglobulins of various species[37], carcinoembryonic antigen (CEA)[39], to human Fc gamma receptors[38]. Fn3 clones with high display levels correlate with increased stability as tested with circular dichroism thermal denaturation[37,38]. Ongoing work in our laboratory demonstrates the versatility of this library in producing Fn3 binders to a large panel of EGFR ligands, perfringolysin O, DEC-205, among many other targets. In this work, we engineered Fn3 binders to each individual murine FcγRs and with these binders demonstrated biological activity *in vitro* and *in vivo*.

References

1. Adams, G. P. & Weiner, L. M. Monoclonal antibody therapy of cancer. *Nat. Biotechnol.* **23,** 1147–1157 (2005).
2. Reichert, J. M. & Valge-Archer, V. E. Development trends for monoclonal antibody cancer therapeutics. *Nat. Rev. Drug Discov.* **6,** 349–356 (2007).
3. Desjarlais, J. R., Lazar, G. A., Zhukovsky, E. A. & Chu, S. Y. Optimizing engagement of the immune system by anti-tumor antibodies: an engineer's perspective. *Drug Discov. Today* **12,** 898–910 (2007).
4. Nimmerjahn, F. & Ravetch, J. V. Antibodies, Fc receptors and cancer. *Curr. Opin. Immunol.* **19,** 239–245 (2007).
5. Nimmerjahn, F. & Ravetch, J. V. Fcγ receptors as regulators of immune responses. *Nat. Rev. Immunol.* **8,** 34–47 (2008).
6. Nimmerjahn, F., Bruhns, P., Horiuchi, K. & Ravetch, J. V. FcγRIV: A Novel FcR with Distinct IgG Subclass Specificity. *Immunity* **23,** 41–51 (2005).
7. Mancardi, D. A. *et al.* FcγRIV is a mouse IgE receptor that resembles macrophage FcεRI in humans and promotes IgE-induced lung inflammation. *J. Clin. Invest.* **118,** 3738–3750 (2008).
8. Hirano, M. *et al.* IgEb immune complexes activate macrophages through FcγRIV binding. *Nat. Immunol.* **8,** 762–771 (2007).
9. Ravetch, J. V. & Bolland, S. IgG Fc receptors. *Annu. Rev. Immunol.* **19,** 275–290 (2001).
10. Sazinsky, S. L. *et al.* Aglycosylated immunoglobulin G1 variants productively engage activating Fc receptors. *Proc. Natl. Acad. Sci. U. S. A.* **105,** 20167–20172 (2008).
11. Shields, R. L. *et al.* High resolution mapping of the binding site on human IgG1 for Fc gamma RI, Fc gamma RII, Fc gamma RIII, and FcRn and design of IgG1 variants with improved binding to the Fc gamma R. *J. Biol. Chem.* **276,** 6591–6604 (2001).
12. Simmons, L. C. *et al.* Expression of full-length immunoglobulins in Escherichia coli: rapid and efficient production of aglycosylated antibodies. *J. Immunol. Methods* **263,** 133–147 (2002).
13. Baudino, L. *et al.* Crucial role of aspartic acid at position 265 in the CH2 domain for murine IgG2a and IgG2b Fc-associated effector functions. *J. Immunol. Baltim. Md 1950* **181,** 6664–6669 (2008).
14. Lazar, G. A. *et al.* Engineered antibody Fc variants with enhanced effector function. *Proc. Natl. Acad. Sci. U. S. A.* **103,** 4005–4010 (2006).
15. Behar, G. *et al.* Isolation and characterization of anti-FcγRIII (CD16) llama single-domain antibodies that activate natural killer cells. *Protein Eng. Des. Sel.* **21,** 1–10 (2008).
16. Cartron, G. *et al.* Therapeutic activity of humanized anti-CD20 monoclonal antibody and polymorphism in IgG Fc receptor FcγRIIIa gene. *Blood* **99,** 754–758 (2002).
17. Nimmerjahn, F. & Ravetch, J. V. Divergent Immunoglobulin G Subclass Activity Through Selective Fc Receptor Binding. *Science* **310,** 1510–1512 (2005).
18. Otten, M. A. *et al.* Experimental Antibody Therapy of Liver Metastases Reveals Functional Redundancy between FcγRI and FcγRIV. *J. Immunol.* **181,** 6829–6836 (2008).
19. Bevaart, L. *et al.* The High-Affinity IgG Receptor, FcγRI, Plays a Central Role in Antibody Therapy of Experimental Melanoma. *Cancer Res.* **66,** 1261–1264 (2006).
20. Andreu, P. *et al.* FcRgamma activation regulates inflammation-associated squamous carcinogenesis. *Cancer Cell* **17,** 121–134 (2010).
21. Mosser, D. M. & Edwards, J. P. Exploring the full spectrum of macrophage activation. *Nat. Rev. Immunol.* **8,** 958–969 (2008).

22. Sica, A., Schioppa, T., Mantovani, A. & Allavena, P. Tumour-associated macrophages are a distinct M2 polarised population promoting tumour progression: potential targets of anti-cancer therapy. *Eur. J. Cancer Oxf. Engl. 1990* **42,** 717–727 (2006).
23. Boder, E. T. & Wittrup, K. D. Yeast surface display for screening combinatorial polypeptide libraries. *Nat. Biotechnol.* **15,** 553–557 (1997).
24. Colby, D. W. *et al.* Engineering antibody affinity by yeast surface display. *Methods Enzymol.* **388,** 348–358 (2004).
25. Chao, G. *et al.* Isolating and engineering human antibodies using yeast surface display. *Nat. Protoc.* **1,** 755–768 (2006).
26. Boder, E. T., Raeeszadeh-Sarmazdeh, M. & Price, J. V. Engineering antibodies by yeast display. *Arch. Biochem. Biophys.* (2012). doi:10.1016/j.abb.2012.03.009
27. Gai, S. A. & Wittrup, K. D. Yeast surface display for protein engineering and characterization. *Curr. Opin. Struct. Biol.* **17,** 467–473 (2007).
28. Bowley, D. R., Labrijn, A. F., Zwick, M. B. & Burton, D. R. Antigen Selection from an HIV-1 Immune Antibody Library Displayed on Yeast Yields Many Novel Antibodies Compared to Selection from the Same Library Displayed on Phage. *Protein Eng. Des. Sel.* **20,** 81–90 (2007).
29. Binz, H. K., Amstutz, P. & Pl|[uuml]|ckthun, A. Engineering novel binding proteins from nonimmunoglobulin domains. *Nat. Biotechnol.* **23,** 1257–1268 (2005).
30. Skerra, A. Alternative non-antibody scaffolds for molecular recognition. *Curr. Opin. Biotechnol.* **18,** 295–304 (2007).
31. Koide, A. & Koide, S. Monobodies: antibody mimics based on the scaffold of the fibronectin type III domain. *Methods Mol. Biol. Clifton NJ* **352,** 95–109 (2007).
32. Skerra, A. Alternative binding proteins: anticalins - harnessing the structural plasticity of the lipocalin ligand pocket to engineer novel binding activities. *FEBS J.* **275,** 2677–2683 (2008).
33. Stumpp, M. T., Binz, H. K. & Amstutz, P. DARPins: a new generation of protein therapeutics. *Drug Discov. Today* **13,** 695–701 (2008).
34. Löfblom, J. *et al.* Affibody molecules: Engineered proteins for therapeutic, diagnostic and biotechnological applications. *FEBS Lett.* **584,** 2670–2680 (2010).
35. Lipovsek, D. *et al.* Evolution of an interloop disulfide bond in high-affinity antibody mimics based on fibronectin type III domain and selected by yeast surface display: molecular convergence with single-domain camelid and shark antibodies. *J. Mol. Biol.* **368,** 1024–1041 (2007).
36. Hackel, B. J., Kapila, A. & Wittrup, K. D. Picomolar affinity fibronectin domains engineered utilizing loop length diversity, recursive mutagenesis, and loop shuffling. *J. Mol. Biol.* **381,** 1238–1252 (2008).
37. Hackel, B. J. & Wittrup, K. D. The full amino acid repertoire is superior to serine/tyrosine for selection of high affinity immunoglobulin G binders from the fibronectin scaffold. *Protein Eng. Des. Sel. PEDS* **23,** 211–219 (2010).
38. Hackel, B. J., Ackerman, M. E., Howland, S. W. & Wittrup, K. D. Stability and CDR composition biases enrich binder functionality landscapes. *J. Mol. Biol.* **401,** 84–96 (2010).
39. Pirie, C. M., Hackel, B. J., Rosenblum, M. G. & Wittrup, K. D. Convergent potency of internalized gelonin immunotoxins across varied cell lines, antigens, and targeting moieties. *J. Biol. Chem.* **286,** 4165–4172 (2011).

CHAPTER 2: ENGINEERING THE FN3 SCAFFOLD FOR HIGHLY SPECIFIC BINDING TO INDIVIDUAL MURINE FC GAMMA RECEPTORS.

Introduction

Monoclonal antibodies (mAb) for cancer therapy operate through various mechanisms: blocking receptor signaling; delivery of toxic chemotherapy; or triggering antibody-dependent cellular cytotoxicity (ADCC)[1–4]. Fcγ receptors (FcγRs) modulate immune cell interaction with IgG Fc's. It has been proposed that the balance between activating and inhibiting FcγR signaling determines the effectiveness of ADCC, prompting extensive protein engineering and glycoengineering efforts to shift the balance of Fc binding affinity towards the activating receptors and away from the inhibitory receptor[5–13].

The distribution of FcγRs is approximately conserved between humans and mice, enabling mice to be useful animal models for therapeutics development[14]. Humans express the activating receptors FcγRI, FcγRIIA, and FcγRIIIA, along with the inhibitory receptor FcγRIIB. Mice express FcγRI (CD64), FcγRIII (CD16), and FcγRIV (CD16-2) as activating receptors and FcγRIIB (CD32) as an inhibitory receptor. The binding of FcγR to antibody immune complexes triggers signaling pathways within the immune cells, leading to release of reactive oxidative species, phagocytosis, etc.

Close homology amongst the FcγRs in any given species makes it virtually impossible to engineer the natural Fc/ FcγR interface for absolute specificity for any single FcγR. Both the amino acid sequence and the particular glycoforms attached to asparagine 297 of the Fc impact FcγR binding affinity to IgGs[14]. Past studies have shown the importance of different fucosylation and sialylation on antibody-dependent cellular cytotoxicity (ADCC)[6,15–17]. Selection of amino acid mutants has also been performed through computational predictions and alanine scanning[9,18]. The murine FcγRs (mFcγR) were homology modeled onto the equivalent human crystal structures (Figure 2-1a), and the Fc binding region is outlined in red, green, and blue. As noted, the areas of

interaction are all in the same region of the FcγRs. The sequence alignment shows the similarity between the different FcγRs, especially mFcγRIIB and mFcγRIII (Figure 2-1b). At the binding region, there is only one amino acid difference between mFcγRIIB and mFcγRIII, therefore making it especially difficult to engineer the antibody Fc to highly differentiate between the two receptors. Furthermore, the FcγR monomer interacts with each domain of the CH2 homodimer of IgGs in a non-symmetric fashion. Therefore, it would be difficult to completely decouple binding with different FcγRs with only mutagenesis of the IgG Fc region, because the Fc is a homodimer unless the Fc is engineered as a heterodimer[19]. An alternative approach is to utilize different scaffolds in place of the Fc region as binders for FcγRs.

Engineering alternative scaffolds to target human FcγRIIIA has shown promising *in vitro* and *in vivo* results[20,21]. In this study, we engineer binders based on the human tenth type III fibronectin (Fn3) scaffold[22–24] that are highly specific to each of the individual four mouse FcγRs.

Results

Sorting Methodology for Fn3 binders to mFcγRs

The Fn3 yeast surface-displayed G4 library was sorted separately against each mFcγR (RI, RIIB, RIII, and RIV). Unfortunately, after the first few rounds of magnetic bead sorting, a dominant clone was selected for in every case (data not shown). Therefore, sorting for individual mFcγR was restarted with the naïve G4 library with more stringent depletions (Figure 2-2a) to naked beads and other mFcγR (Figure 2-2b) before enrichment of binders to target mFcγRs (RI, RIIB, RIII, and RIV).

After low affinity Fn3 binders were enriched, sorting was performed by fluorescence-activated cell sorting (FACS). Two methods with FACS were used to isolate non-cross-reactive Fn3 binders. In one sorting method, Fn3 clones that bound to the target mFcγR were enriched before

sequentially depleting clones that bound to a different mFcγR (Figure 2-2c). Clones that displayed Fn3 properly but showed no cross-reactivity to the non-target mFcγR were enriched. The other sorting method required preincubation of biotinylated mFcγR with fluorophore labeled streptavidin at a 4:1 molar ratio, respectively to obtain mFcγR tetramers. Tetramers were then incubated with induced sublibraries and sorted for binders specific to the target mFcγR (Figure 2-2d).

Isolated Fn3 Clones Specific for Individual mFcγR

Sublibraries were sorted for 5 to 8 generations with mutagenesis introduced between each generation[25]. Periodic checks ensured that sublibraries maintained specificity to their target mFcγR and no cross-reactivity to other mFcγRs. Identification of individual clones from sublibraries was performed as previously noted[25]. From each sublibrary of binders to mFcγRI, mFcγRIIB, mFcγRIII, and mFcγRIV, 6 to 9 colonies were sequenced and unique clones were retransformed into EBY100 for display.

For binders to mFcγRI, 5/6 clones bottlenecked to the same BC, DE, and FG loops with the exception of a few point mutations and varying framework mutations (Table 2-1). Fn3 clones binding to mFcγRIIB also bottlenecked to a single clone with a BC loop of FPLHDEHAD, DE loop of GWMLA, and FG loop of SND-S/P-YSN. Binders to mFcγRIII narrowed down to two main clones with different loops. Interestingly, the DE loop, GWMLA, reappeared in one of the two main clones for mFcγRIII binders. It has been suggested that the DE loop often plays a role primarily in stabilization rather than antigen recognition,[24] and that might further support the reoccurrence of this DE loop. Since previous literature suggested the importance of mFcγRIV in tumor clearance,[5] two different sorts were conducted targeting mFcγRIV. In the first round of sorting, the population bottlenecked to the same BC loop with a few point mutations, two main DE

loops, and three different FG loops. The second round of sorting, resulted in a different clone, but the population still narrowed to a single clone with varying framework mutations.

Titrations of soluble target mFcγR ectodomain were performed on all isolated clones. A single clone from each group with the highest maximum fluorescence and lowest apparent K_D was chosen for further studies (Figure 2-3). The mFcγRI binder, I5.2.1, had a BC loop of HLPYHAI, DE loop of WSYTS, and a FG loop of YNGPPFFY. II8.5.6 was chosen as the mFcγRIIB binder with BC, DE, and FG loops of FPLHDEHAD, GWMLA, and SNDSYSN, respectively. The III5.3.2 clone to mFcγRIII contained a loop of HCPYCDSD, and DE loop of YWRFS, and FG loop of GRYWSE. Clone IV1.8.2.8 was isolated from the first round of sorting against mFcγRIV with a BC loop of DDPSGMCP, DE loop of EHVWM, and FG loop of DQGSSH. In the second round of sorting, clone IV2.6.2.5 was isolated with BC, DE, and FG loops of DIPCGDYLDY, WSIHT, and WKGPSPK, respectively. These clones were renamed I, II, III, IV1, and IV2 for Fn3 binders specific to mFcγRI, mFcγRIIB, mFcγRIII, and mFcγRIV, respectively. Because two different sorts were conducted against mFcγRIV, two different clones (IV1 and IV2) were chosen from each group.

Titrations of each mFcγR was conducted on each yeast displayed Fn3 clone to demonstrate low to no cross-reactivity (Figure 2-4). Clones I, IV1, and IV2 show very high specificity for mFcγRI and mFcγRIV respectively and no detectable binding to the other mFcγRs. Clone II appears to be high affinity to mFcγRIIB, but has very slight binding to mFcγRIII at 1μM concentration. Clone III is a weaker binder to mFcγRIII when compared to the other Fn3 clones and their respective mFcγRs, but still specific. Clone III shows slight cross-reactivity to mFcγRIV at 1μM concentration.

Competition assay

Once clones were isolated against individual mFcγR, a competition study was conducted to determine if the Fn3 binding epitope competed with the Fc binding epitope. Soluble mFcγR at 100nM was incubated with antibody of the mouse IgG2a (mIgG2a) isotype at 10μM concentration to be above the mFcγR-Fc K_D, which is in the single-digit micromolar range[26]. The mFcγR-Fc complex was then added to yeast displaying Fn3 clones I, II, III, IV1, or IV2. Fn3 binding to mFcγR was detected with a fluorescent anti-HIS antibody and compared to yeast binding mFcγR only. Results suggest that clones III and IV1 compete with mIgG2a, since mFcγR binding is knocked down drastically when preincubated with mIgG2a (Figure 2-5). The binding epitopes of III and IV1 to mFcγRIII and mFcγRIV, respectively, are most likely the same or overlapping with the mIgG2a binding epitope. Clones I and IV2 have decreased binding to mFcγR but not to the extent of clones III and IV1. This could possibly be due to the large antibody molecule preventing Fn3 binding through steric hindrance or conformation changes. In that, the Fn3 might not bind to the same epitope that the antibody Fc binds to, but the antibody in some way blocks Fn3 binding either through conformational changes caused by binding or blocking a nearby Fn3 binding epitope. Clone II shows very little competition with the antibody, which suggests that it binds to a different epitope on mFcγRIIB than the antibody Fc. Further characterization of binding was conducted through epitope mapping on mFcγRIV.

Mapping the Fn3 binding epitopes on mFcγRIV

The binding epitopes of two Fn3 binders IV1 and IV2 to mFcγRIV were determined using a yeast display epitope-mapping library of mFcγRIV. The ectodomain of mFcγRIV was introduced into the yeast display vector and low mutagenesis was introduced using a Mutazyme II polymerase. Based on the total residues of the mFcγRIV ectodomain, the theoretical diversity needed for a single

point mutation library of the 183 residues of the ectodomain is $3.48x10^3$. The engineered mFcγRIV single point mutation library size at $4.13x10^6$ sufficiently covered the diversity needed. The mFcγRIV epitope-mapping library was sorted through FACS with soluble Fn3s, IV1 and IV2, and only properly displayed cells with no binding to the Fn3s were collected. After 3-4 enrichment sorts, individual clones were sequenced to determine mutated residues that disrupted binding. IV1 was mapped to domain 2 of mFcγRIV at residues Q122/K127/K128 (Figure 2-6a and b), and IV2 was mapped to domain 1 at residues K38/R67/Q69 (Figure 2-6c and d). Interestingly, the IV2 epitope is distinct from the actual mFcγRIV/Fc interface; consequently, it is possible to test as below whether precise stereospecific engagement of FcγRs is required for activation.

Discussion

A current major focus in antibody therapeutic development is to drive greater therapeutic efficacy by engineering interactions with FcγRs. Much of the previous work aimed at understanding FcγR contributions have been conducted with knock-out mice, but unfortunately knock-out mice have been shown to change FcγR expression patterns to compensate for the lack of certain FcγRs[27]. By instead studying these interactions by modifying the protein interaction from the antibody side, we can invoke innate immune responses that utilize only individual FcγRs within a wild-type immune system.

In this work, we engineered individual Fn3 using yeast display of the Fn3 scaffold to bind with specificity to murine FcγRI, FcγRIIB, FcγRIII, and FcγRIV. In this process, we outline two different methods: 1) sequential enrichments and depletions and 2) two-color sorting that allow us to engineer binders to be able to differentiate between proteins that share a large percentage of homology to each other. Two separate sorts were conducted against FcγRIV because previous literature suggests its importance for tumor clearance, and we wanted to increase the variety of

binders engineered against this receptor. We chose to further study the Fn3 clones that bound their target FcγR with the highest affinity and had the highest expression on yeast.

The five Fn3 clones: I, II, III, IV1, and IV2 show specificity to their target FcγR based on yeast display titrations. The yeast display titrations show very little cross-reactivity of the Fn3 binders to other mFcγR. Competition studies suggested that clones III and IV1 competed with the Fc binding epitope on the FcγR, whereas clone II did not compete with the Fc binding epitope. Clones I and IV2 showed slight decrease in binding to their respective FcγRs in the presence of antibody, which suggests possible steric hindrance caused by the antibody. Clones IV1 and IV2 were epitope mapped on FcγRIV using a single point mutation yeast display library of the FcγRIV. Results confirmed that the clone IV1 epitope overlaps with that of the Fc binding epitope, whereas IV2 binds to an epitope on domain 1, which is distinct from the Fc binding epitope.

Materials and methods

Homology modeling and sequence alignment

Homology modeling of murine FcγR ectodomains was conducted using the protein structure modeling program MODELLER[28]. The crystal structure of human FcγRI (PDB ID: 3RJD) was used as a template for murine FcγRI (accession P26151). The inhibitory receptor human FcγRIIB (PDB ID: 2FCB) was used as the structural template for the inhibitory mouse receptor FcγRIIB (accession NP_034317). Murine FcγRIII (accession AAX13984) was modeled onto several crystal structures of human FcγRIIA (PDB ID: 1FCG, 1H9V, 3RY4, 3RY5, 3RY6). Lastly, human FcγRIIIA (PDB ID: 1E4K) shares the most sequence homology to murine FcγRIV (accession NP_653142)[29] and therefore served as the structural template. Structures were visualized with PyMOL.

Protein sequence alignment of the murine FcγRs was conducted using the bioinformatics software Geneious (Biomatters Ltd.). FcγR ectodomains were aligned with Geneious Alignment using the Blosum62 cost matrix, with a gap open penalty of 12, a gap extension penalty of 3, a global alignment with free end gaps, and two refinement iterations.

mFcγR protein production

RNA was collected from MH-S cells (ATCC) using a QIAshredder kit (Qiagen). The cDNA was constructed using a SuperScriptIII cDNA synthesis kit (Invitrogen). The mFcγR DNA was amplified out of the cDNA using the primers in Table 2-2. A biotin acceptor peptide and His6 tag was cloned onto each construct connected by a (Gly4Ser)2 linker to each mFcγR as a c-terminal fusion. Proteins were obtained through transient transfection of HEK293F cells with DNA and 2mg of polyethyleneimine per liter of culture per manufacturer's protocol. Supernatants were harvested and sterile filtered with a 0.2um filter one week after transfection. His6 tagged proteins were purified using Talon metal affinity resin (Clontech). After mFcγR purification, proteins are site-specifically biotinylated using the BirA enzyme (Avidity) per manufacturer's protocol.

Cell line

HEK293F cells (Invitrogen) were cultured in Freestyle 293 expression medium (Invitrogen) in suspension. Cells were maintained at 37°C with 5% CO2 in suspension and were subcultured every 2-3 days.

Yeast culture conditions

Yeast libraries and unique clones were cultured in SD-CAA minimal media (20 g/L D-glucose, 6.7 g/L yeast nitrogen base, 5 g/L casamino acids, 7.4 g/L citric acid monohydrate, 10.4 g/L sodium citrate, pH 4.5) at 30°C with shaking at 250 rpm and induced in SG-CAA media (18

g/L galactose, 2 g/L D-glucose, 6.7 g/L yeast nitrogen base, 5 g/L casamino acids, 5.4 g/L Na_2HPO_4, 8.6 g/L $NaH_2PO_4 \bullet H_2O$, pH 6.0) for at least 8 hours at 20°C with shaking at 250 rpm.

Engineering and screening approach of Fn3s

Fn3 engineering was conducted as noted previously[25,30]. The G4 yeast surface display Fn3 library was initially screened against biotinylated mouse FcγRs immobilized on biotin binder dynabeads (Invitrogen). The library was depleted of binders first to naked dynabeads and then to other irrelevant murine FcγRs before enrichment of binders to the target mFcγR. To prevent cross-reactivity of binders, two different flow cytometry sorting methods were used to isolate Fn3 binders specific to individual mFcγR. The first method required sequential enrichments to the target mFcγR and subsequent depletions of binders to other mFcγRs. Induced yeast were incubated for fully displayed Fn3s with chicken anti-c-Myc antibody (Gallus Immunotech) and soluble biotinylated mFcγR. Enrichment sorting windows collected high display and high binding to target mFcγR. Depletion sorting windows collected only properly displayed Fn3s that showed no binding to the irrelevant mFcγRs. The second method consists of two color labeling. Biotinylated mFcγRs are precomplexed in a 4:1 molar ratio to Alexa Fluorophore labeled streptavidin before incubation with induced yeast. Cells that show binding to the target mFcγR and no binding to the other mFcγRs are collected and expanded. Both methods were used to isolate Fn3 binders to individual mFcγRs. Sorting was performed on a MoFlo (Beckman Coulter) or a FACS Aria (Becton Dickinson) instrument.

Binding analysis

Yeast display titrations were performed as noted previously[31]. Yeast were stained for full display using a chicken anti-c-Myc antibody (Gallus Immunotech) and also incubated with different dilutions of soluble biotinylated mFcγR. Secondary labeling was performed with a goat anti-chicken

Alexa Fluor 488 conjugated antibody and streptavidin conjugated with Alexa Fluor 647 at recommended dilutions. Titrations were analyzed on a FACSCalibur HTS (Becton Dickinson) instrument.

Competition assay

Soluble mFcγR at a 100nM concentration in 1x PBS + 0.1% BSA (PBSA) was incubated with a 10μM concentration of antibody of the mIgG2a isotype for greater than 1 hr. Single clones of yeast displaying Fn3s I, II, III, IV1, and IV2 were incubated with a chicken anti-c-Myc antibody for display and either soluble mFcγR at 100nM, mIgG2a antibody at 10μM, or soluble mFcγR complexed with mIgG2a antibody at 4°C shaking for greater than 30 min. Cells were then washed with 200μL of PBSA and pelleted at 3000xg for 3min. Supernatant was removed and cells were stained with an anti-6X HIS allophycocyanin (APC) conjugated antibody (Abcam) and a goat anti-chicken Alexa Fluor 488 conjugated antibody for at least 15min at 4°C. Cells were analyzed on an Accuri C6 cytometer (Becton Dickinson).

Epitope mapping

The mFcγRIV gene was amplified with Mutazyme II polymerase (Agilent Technologies) to introduce a low rate of mutagenesis. The amplified product was then run on a 1.5% agarose gel, purified, and recombined into the pCTCON vector during yeast electroporation. Total library size was determined to be $2.31x10^7$ by plating dilutions of the transformation. To determine the library diversity, the plasmids from the library were extracted using the Zymoprep™ Yeast Plasmid Miniprep II (Zymo Research) and transformed into XLI-Blue supercompetent cells. A plate of 96 clones were sent for sequencing and results showed that 18% of all sequences were single mutants therefore the single mutant library size was calculated to be $4.13x10^6$, which is greater than the theoretical diversity needed of $3.48x10^3$. The yeast library of mutagenized mFcγRIV was displayed

on the surface of yeast and clones that showed no binding to the Fn3s IV1 and IV2 were collected. Two to four enrichments of non-binding clones were conducted and then sent for sequencing to determine the residues important for binding.

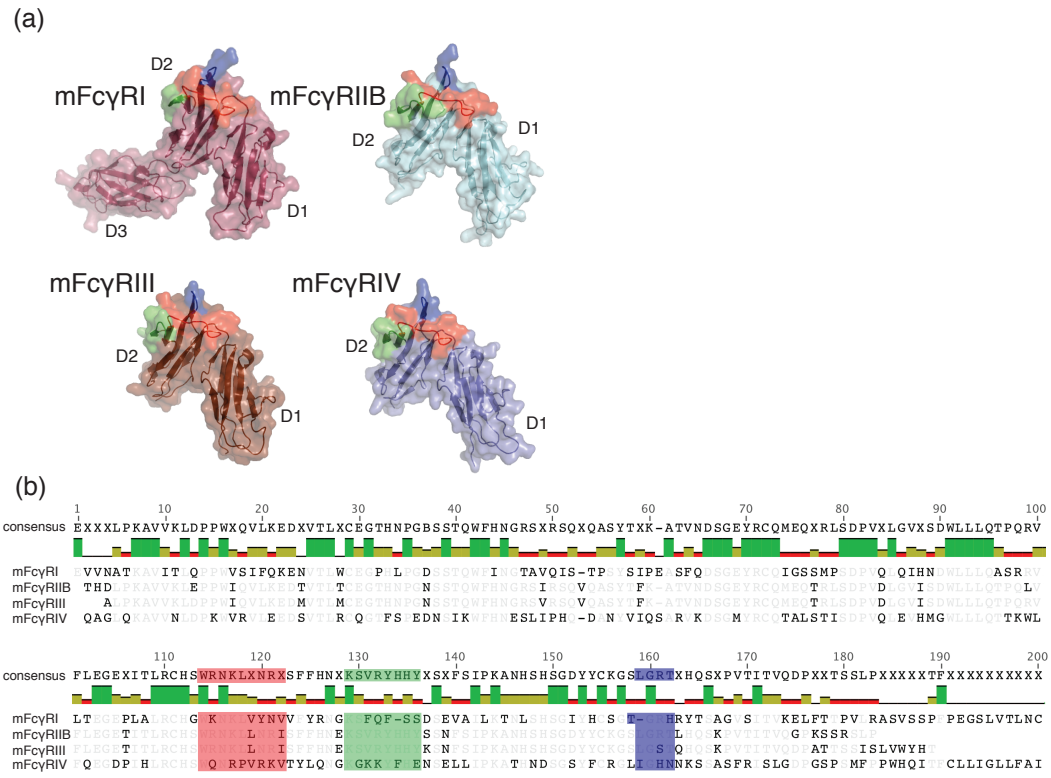

Figure 2-1: Similarity between Murine FcγR Ectodomains.

(a) Homology models of murine FcγRs (mFcγR) with their human FcγR (hFcγR) equivalent. mFcγRI, mFcγRIIB, mFcγRIII, and mFcγRIV are modeled to hFcγRI (Protein Data Bank (PDB) ID: 3RJD), hFcγRIIB (PDB ID: 2FCB), hFcγRIIA (PDB ID: 1FCG, 1H9V, 3RY4, 3RY5, 3RY6), and hFcγRIIIA (PDB ID: 1E4K), respectively. Domains 1, 2, and 3 on the FcγRs are labeled D1, D2, and D3 respectively. (b) Sequence alignment of domains 1 and 2 of the murine FcγRs. Surfaces on the FcγR that interact with the BC loop (shown in red), C'E loop (green), and FG loop (blue) of the Fc region of an IgG are highlighted. Only the first 200 residues of mFcγRI are shown.

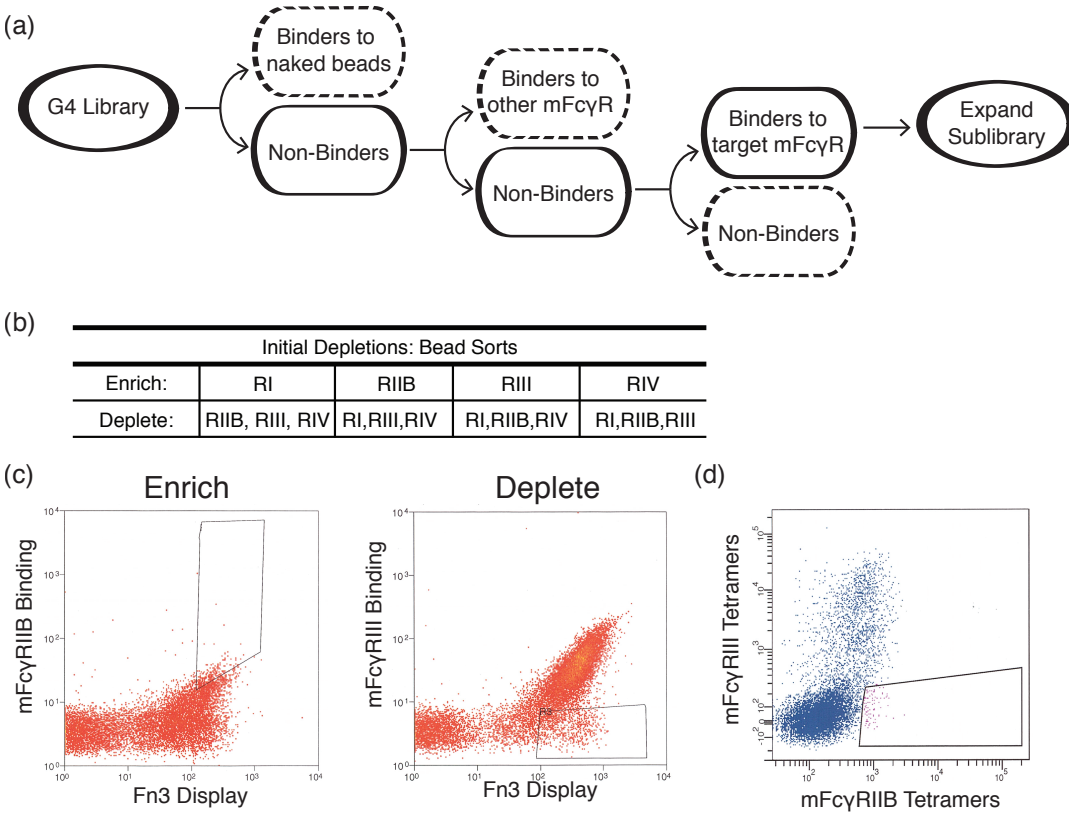

Figure 2-2: Sorting Protocol

(a) Flow chart of sorting protocol with depletions of binders to naked beads and other mFcγR from the naïve G4 library before enrichment in binders to the target mFcγR. (b) Table of enriched targets and their respective mFcγR depletions. (c-d) Representative flow cytometry dot plots of two different sorting protocols designed for enrichment of binders specific for individual FcγRs. (c) Enrichment of binders to the target FcγR (mFcγRIIB) and then depletion of cross reactive binders to another FcγR (mFcγRIII). (d) Two color sorting of FcγRs by incubating yeast with mFcγRs precomplexed with fluorophore labeled streptavidin. The collection window is drawn only on binders specific for the target FcγR (mFcγRIIB).

Table 2-1 Binder sequences

Clone	BC Loop	DE Loop	FG Loop	Framework
WT Fn3	DAPAVTVR	GSKST	GRGDSPASSK	
mFcγRI binders				
Clone	BC Loop	DE Loop	FG Loop	Framework
I5.2.1	**HLPYHAI**	**WSYTS**	**YNGPPFFY**	**Y31F,V45A,I85T**
I5.2.2	YLPYHAI	WSYTS	YNGPPFSY	Y31F,Y36H,G41R,I70V
I5.2.3	HLPYHAI	GTESI	TCGFDFCPSG	Y31L,T35A,T39S
I5.2.4	HLPYRAI	WSYTS	YNGPPFSY	Y31F,G41R,S89T,Y92C,K98R
I5.2.5	HLPYHAI	WSYTS	YNGPPFLY	Y31F,S43G,T49P
I5.2.6	HLPYHAI	WSYTS	YNGPPFSY	I20V,Y31F,Y36H,G41R,V66I,Y73H,S100P
mFcγRII binders				
Clone	BC Loop	DE Loop	FG Loop	Framework
II8.5.1	FPLHDELAD	EWMLA	SNDSYSN	V1L,D7V,A12T,Q36R,T58P,T69S
II8.5.2	FPLHDEHAD	GWMLA	SNDPYSN	V1L,D7V,E9D,A12T,Y32F,D97G
II8.5.3	FPLHDEHAD	GWMLA	SSDPYSN	V1L,D7V,E9D,A12T,Y32F,I34V,N42D,V45A,E47G,T58P
II8.5.5	FPLHDEHAD	GWMLA	PNDSYSN	V1L,D7V,A12T,T58P,S100F
II8.5.6	**FPLHDEHAD**	**GWMLA**	**SNDSYSN**	**D7V,A12T,Y32F,T58P**
mFcγRIII binders				
Clone	BC Loop	DE Loop	FG Loop	Framework
III5.3.2	**HCPYCDSD**	**YWRFS**	**GRYWSE**	**Y31S,V66I,V72M**
III5.3.3	YFHDSTLG	GWMLA	PNDSHTE	Y31S,G61D
III5.3.4	YFHDSTLG	GWMLA	PNDPYSD	Y31S
III5.3.5	HCPYCDSD	YWRFS	HNDFGSSFSL	Y31S,G40R,V45A,N91D,E95G
III5.3.6	YFHDSTLG	GWMLA	PNGSYPN	V4A,Y31S,V45A,G61D,P99L
mFcγRIV binders (1st sort)				
Clone	BC Loop	DE Loop	FG Loop	Framework
IV1.8.2.1	DDPYGMCP	QHMWM	EDGYASH	N41D
IV1.8.2.2	DDPYGMCP	QHMWM	YQGYSH	V1A,2SP
IV1.8.2.3	DDPYGMCP	EHTWM	HQGYSH	G40R,K62R
IV1.8.2.4	DDPGGMCP	EHVWM	YQGYSC	
IV1.8.2.5	DDPYGMCP	QHMWM	EDGYPSR	
IV1.8.2.6	DDPYGMCP	QHMWM	FRGYTD	
IV1.8.2.7	DDPYGMCP	QHMWM	EGNYASH	
IV1.8.2.8	**DDPSGMCP**	**EHVWM**	**DQGSSH**	
IV1.8.2.9	DDPYGMCP	QHMWM	DQGSSH	K62E
mFcγRIV binders (2nd sort)				
Clone	BC Loop	DE Loop	FG Loop	Framework
IV2.6.2.1	DIPCGDYLNY	WSIHT	WKGSSPK	S17C,T36A,T50A,K64E
IV2.6.2.2	DIPCGDYLNY	WSIHT	WKGSSPK	I35V,F49L,D68G
IV2.6.2.3	DIPCGDYLNY	WSIHT	WKGSSPK	D3G,D7G,T50A,K64E
IV2.6.2.4	YSLANPYLNY	WSLHT	WKGSSPK	T50A,I89T,Y93C
IV2.6.2.5	**DIPCGDYLDY**	**WSIHT**	**WKGPSPK**	**R6G,R34K,E48K,T50A**
IV2.6.2.7	DAYYDDYLNY	WSLHT	WKGPSPK	T50A,T95A,E96K
IV2.6.2.8	DIPCGDYLNY	WSLHT	WKGSSPK	T16A,T50A,I71V,I97T

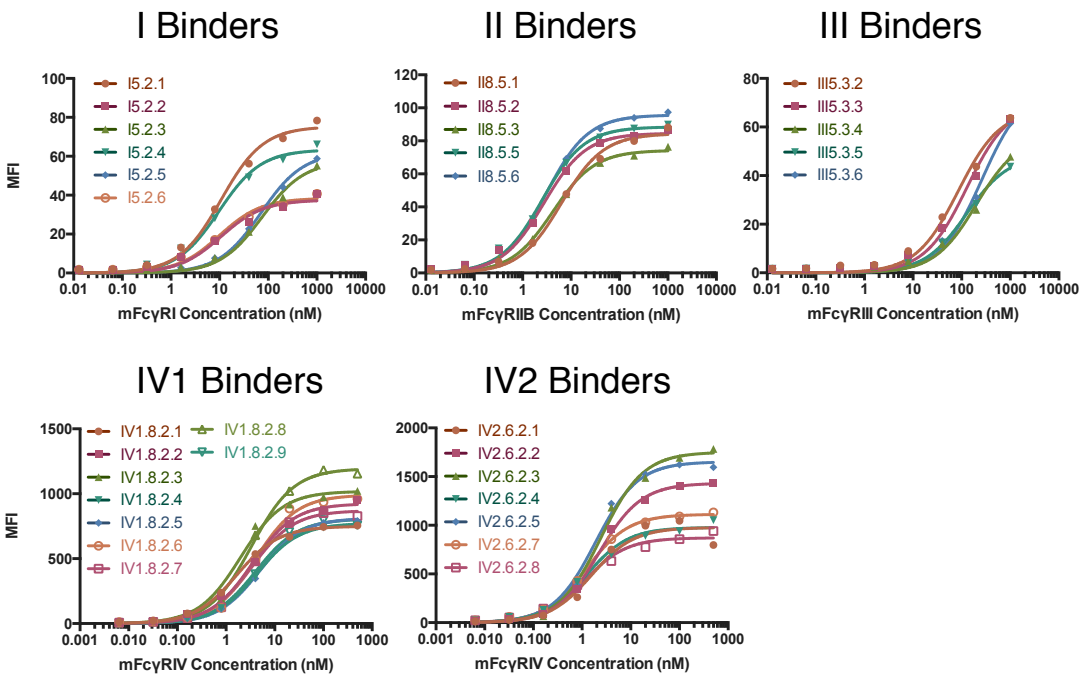

Figure 2-3: Multiple Isolated Fn3s that Bind Individual mFcγRs

Yeast displaying individual clones of Fn3 that were incubated with varying concentrations of soluble mFcγRs used for selection. Individual clones with high expression (high MFI) and low K_D were chosen as lead candidates for further studies.

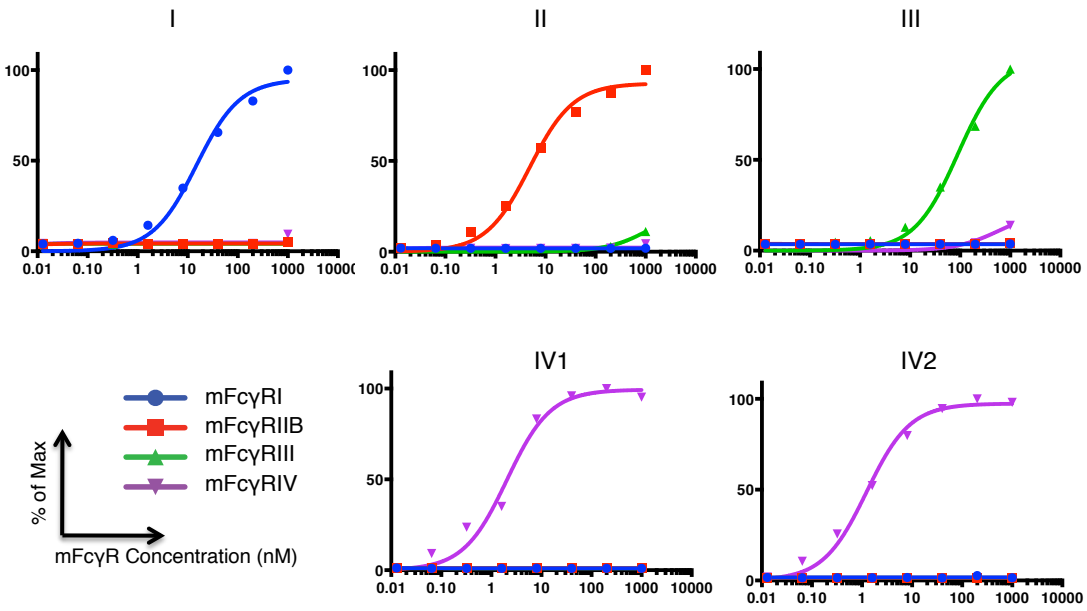

Figure 2-4: Select Fn3s that Bind Individual mFcγRs

Yeast displaying Fn3 clones I, II, III, IV1, and IV2 incubated with titrations of all four mFcγRs. mFcγRI (blue circle), mFcγRIIB (red square), mFcγRIII (green triangle), mFcγRIV (purple transposed triangle). Each clone is specific for its target mFcγR with little cross-reactivity to the other mFcγR.

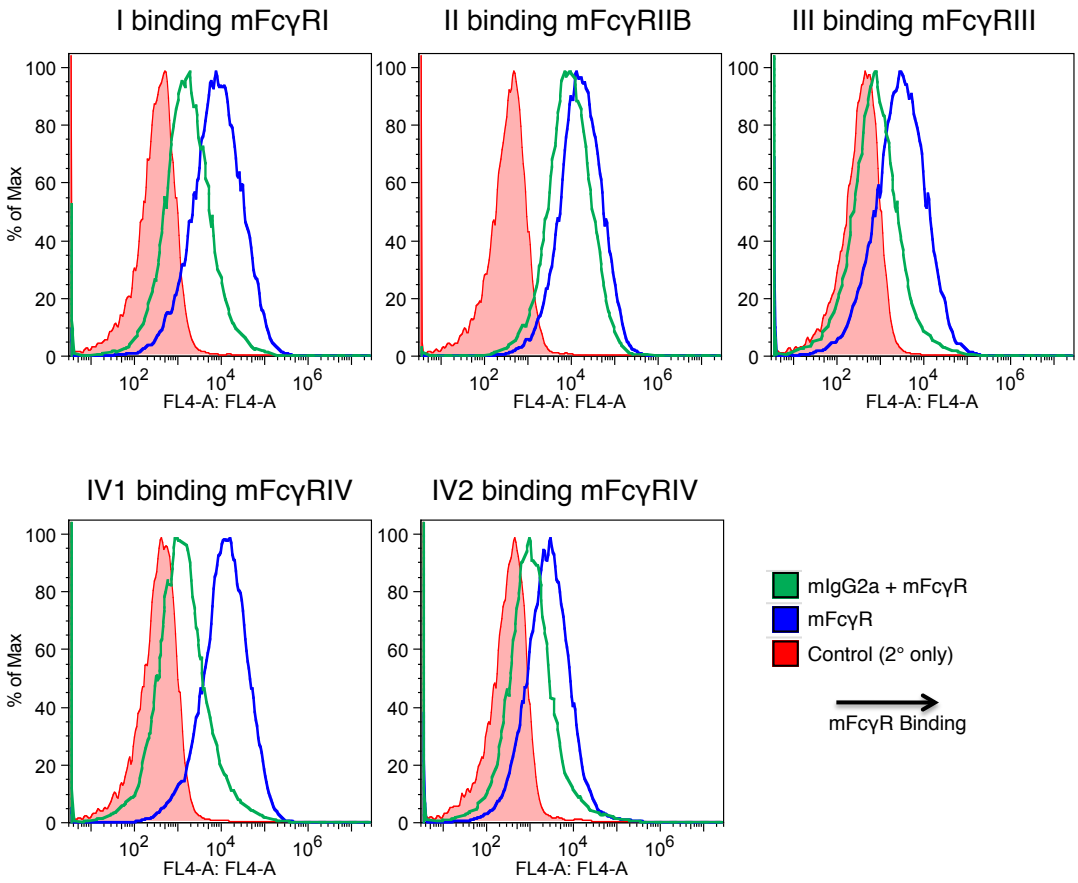

Figure 2-5: Competition of mFcγR Binding to Fn3 with mIgG2a

Yeast displaying individual Fn3 clones I, II, III, IV1, and IV2 incubated with 100 nM of mFcγR (blue), 100 nM of mFcγR and 10 μM of mIgG2a (green), or secondary only (red). If there is competition, the green histogram will shift left towards the secondary control histogram. If there is no competition, the green histogram will not shift much from the blue binding histogram. Fn3 clones I, III, and IV1 show a greater downward shift of binding with the addition of mIgG2a, suggesting competition between the Fn3 and mIgG2a. Clone II shows very little change in binding with the addition of mIgG2a and IV2 shows a slight shift in binding.

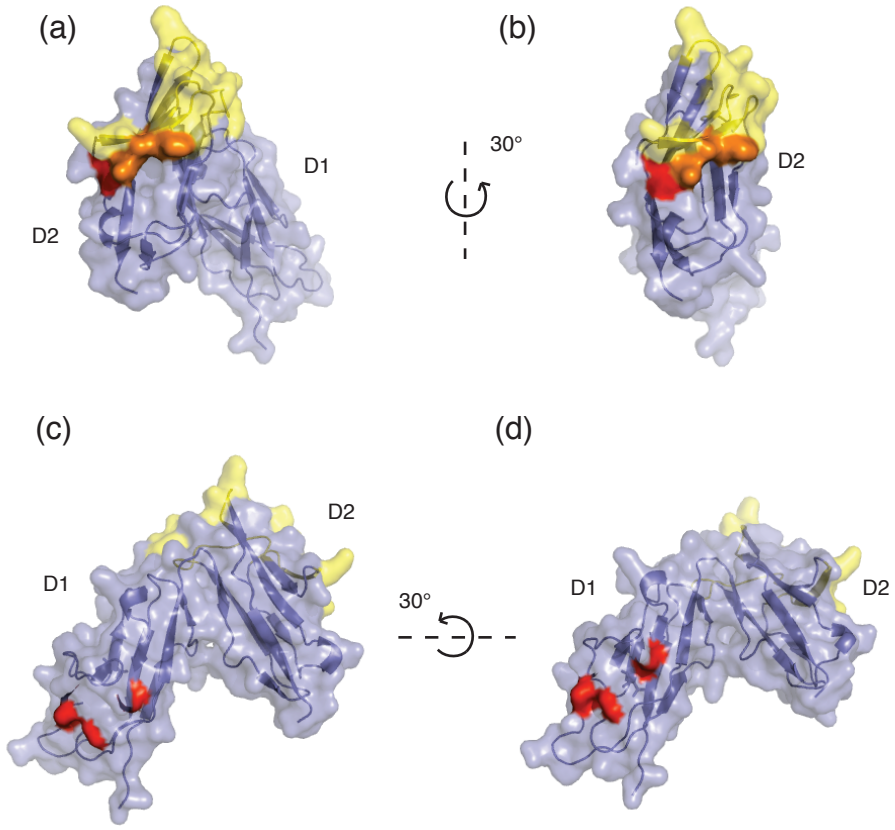

Figure 2-6: Epitope mapping of IV binders to mFcγRIV

Mapping of Fn3 binding epitopes on the homology model of mFcγRIV. The IgG Fc binding region is show in yellow. Fn3 binding epitopes are shown in red and the epitopes that overlap with the Fc binding region are shown in orange. The IV1 binding epitope is on domain 2 of the mFcγRIV shown in (a) and (b), where (b) is a 30° y-axis rotation from (a). The IV1 binding region overlaps with that of the Fc binding epitope. The IV2 binding epitope is on domain 1 of the mFcγRIV shown in (c) and (d), where (d) is a 30° x-axis rotation from (c). The IV2 binding epitope is at a region distinct from the Fc binding epitope.

Table 2-2

Gene		Sequence
mFcγRI	5’ Primer	ATGATTCTTACCAGCTTTGGAGATGAC
	3’ Primer	TAAGTTGTATTTCTTCTCTCTCTGC
mFcγRIIB	5’ Primer	ATGGAGAGCAACTGGACTGTCCATGTG
	3’ Primer	CTAAATGTGGTTCTGGTAATCATGCTCTG
mFcγRIII	5’ Primer	ATGTTTCAGAATGCACACTCTGGAAGC
	3’ Primer	TCACTTATCTTGAGGAGCCTGGCGCTTTC
mFcγRIV	5’ Primer	ATGTGGCAGCTACTACTACCAACAG
	3’ Primer	TCACTTGTCCTGAGGTTCCTTGCTCC

References

1. Adams, G. P. & Weiner, L. M. Monoclonal antibody therapy of cancer. *Nat. Biotechnol.* **23,** 1147–1157 (2005).
2. Reichert, J. M. & Valge-Archer, V. E. Development trends for monoclonal antibody cancer therapeutics. *Nat. Rev. Drug Discov.* **6,** 349–356 (2007).
3. Harris, M. Monoclonal antibodies as therapeutic agents for cancer. *Lancet Oncol.* **5,** 292–302 (2004).
4. Boross, P. & Leusen, J. H. W. Mechanisms of action of CD20 antibodies. *Am. J. Cancer Res.* **2,** 676–690 (2012).
5. Nimmerjahn, F. & Ravetch, J. V. Divergent Immunoglobulin G Subclass Activity Through Selective Fc Receptor Binding. *Science* **310,** 1510–1512 (2005).
6. Shields, R. L. *et al.* Lack of Fucose on Human IgG1 N-Linked Oligosaccharide Improves Binding to Human FcγRIII and Antibody-dependent Cellular Toxicity. *J. Biol. Chem.* **277,** 26733–26740 (2002).
7. Weng, W.-K. & Levy, R. Two immunoglobulin G fragment C receptor polymorphisms independently predict response to rituximab in patients with follicular lymphoma. *J. Clin. Oncol. Off. J. Am. Soc. Clin. Oncol.* **21,** 3940–3947 (2003).
8. Richards, J. O. *et al.* Optimization of antibody binding to FcgammaRIIa enhances macrophage phagocytosis of tumor cells. *Mol. Cancer Ther.* **7,** 2517–2527 (2008).
9. Lazar, G. A. *et al.* Engineered antibody Fc variants with enhanced effector function. *Proc. Natl. Acad. Sci. U. S. A.* **103,** 4005–4010 (2006).
10. Tai, Y.-T. *et al.* Potent in vitro and in vivo activity of an Fc-engineered humanized anti-HM1.24 antibody against multiple myeloma via augmented effector function. *Blood* **119,** 2074–2082 (2012).
11. Jung, S. T. *et al.* Aglycosylated IgG variants expressed in bacteria that selectively bind FcgammaRI potentiate tumor cell killing by monocyte-dendritic cells. *Proc. Natl. Acad. Sci. U. S. A.* **107,** 604–609 (2010).
12. Jung, S. T. *et al.* Effective phagocytosis of low Her2 tumor cell lines with engineered, aglycosylated IgG displaying high FcγRIIa affinity and selectivity. *ACS Chem. Biol.* **8,** 368–375 (2013).
13. Sazinsky, S. L. *et al.* Aglycosylated immunoglobulin G1 variants productively engage activating Fc receptors. *Proc. Natl. Acad. Sci. U. S. A.* **105,** 20167–20172 (2008).
14. Nimmerjahn, F. & Ravetch, J. V. Fcγ receptors as regulators of immune responses. *Nat. Rev. Immunol.* **8,** 34–47 (2008).
15. Peipp, M. *et al.* Antibody fucosylation differentially impacts cytotoxicity mediated by NK and PMN effector cells. *Blood* **112,** 2390–2399 (2008).
16. Kaneko, Y., Nimmerjahn, F. & Ravetch, J. V. Anti-Inflammatory Activity of Immunoglobulin G Resulting from Fc Sialylation. *Science* **313,** 670–673 (2006).
17. Scallon, B. J., Tam, S. H., McCarthy, S. G., Cai, A. N. & Raju, T. S. Higher levels of sialylated Fc glycans in immunoglobulin G molecules can adversely impact functionality. *Mol. Immunol.* **44,** 1524–1534 (2007).
18. Nimmerjahn, F. & Ravetch, J. V. Antibodies, Fc receptors and cancer. *Curr. Opin. Immunol.* **19,** 239–245 (2007).
19. Liu, Z. *et al.* Asymmetrical Fc engineering greatly enhances ADCC effector function and stability of the modified antibodies. *J. Biol. Chem.* (2013). doi:10.1074/jbc.M113.513366

20. Behar, G. *et al.* Isolation and characterization of anti-FcγRIII (CD16) llama single-domain antibodies that activate natural killer cells. *Protein Eng. Des. Sel.* **21,** 1–10 (2008).
21. Rozan, C. *et al.* Single-Domain Antibody–Based and Linker-Free Bispecific Antibodies Targeting FcγRIII Induce Potent Antitumor Activity without Recruiting Regulatory T Cells. *Mol. Cancer Ther.* **12,** 1481–1491 (2013).
22. Koide, A. & Koide, S. Monobodies: antibody mimics based on the scaffold of the fibronectin type III domain. *Methods Mol. Biol. Clifton NJ* **352,** 95–109 (2007).
23. Koide, A., Bailey, C. W., Huang, X. & Koide, S. The fibronectin type III domain as a scaffold for novel binding proteins. *J. Mol. Biol.* **284,** 1141–1151 (1998).
24. Hackel, B. J., Ackerman, M. E., Howland, S. W. & Wittrup, K. D. Stability and CDR composition biases enrich binder functionality landscapes. *J. Mol. Biol.* **401,** 84–96 (2010).
25. Chen, T. F., de Picciotto, S., Hackel, B. J. & Wittrup, K. D. Engineering fibronectin-based binding proteins by yeast surface display. *Methods Enzymol.* **523,** 303–326 (2013).
26. Ravetch, J. V. & Bolland, S. IgG Fc receptors. *Annu. Rev. Immunol.* **19,** 275–290 (2001).
27. Bruhns, P. Properties of mouse and human IgG receptors and their contribution to disease models. *Blood* **119,** 5640–5649 (2012).
28. Šali, A. & Blundell, T. L. Comparative Protein Modelling by Satisfaction of Spatial Restraints. *J. Mol. Biol.* **234,** 779–815 (1993).
29. Nimmerjahn, F., Bruhns, P., Horiuchi, K. & Ravetch, J. V. FcγRIV: A Novel FcR with Distinct IgG Subclass Specificity. *Immunity* **23,** 41–51 (2005).
30. Hackel, B. J., Kapila, A. & Wittrup, K. D. Picomolar affinity fibronectin domains engineered utilizing loop length diversity, recursive mutagenesis, and loop shuffling. *J. Mol. Biol.* **381,** 1238–1252 (2008).
31. Chao, G. *et al.* Isolating and engineering human antibodies using yeast surface display. *Nat. Protoc.* **1,** 755–768 (2006).

CHAPTER 3: CHARACTERIZATION OF FN3 BINDING FUNCTIONALITY AND BIOLOGICAL ACTIVITY

Introduction

The role of antibody-dependent cellular cytotoxicity (ADCC) in antibody mediated tumor clearance has been very apparent in past studies[1–4]. The key receptors modulating immune cell interaction with antibody Fc's are Fcγ receptors (FcγRs). The binding of FcγR to antibody immune complexes triggers signaling pathways within the immune cells. Multiple cell types express FcγRs, the main ones of interest being macrophages and monocytes, neutrophils, dendritic cells, and natural killer (NK) cells. FcγR expression varies depending on immune cell type. Macrophages and monocytes express murine FcγRI, FcγRIIB, FcγRIII, and FcγRIV, whereas dendritic cells mainly express FcγRI, FcγRIIB, and FcγRIII. Neutrophils express the low affinity receptors: FcγRIII, FcγRIV and FcγRIIB. NK cells are unique in that they only express FcγRIII and do not possess an inhibitory FcγR.[5] Murine FcγR correspond to human FcγR with differential expression on the same types of immune cells. Therefore, murine FcγRIV, FcγRIII, and FcγRIIB have similar cell expression patterns as human FcγRIIA, FcγRIIIA, and FcγRIIB, respectively.[6] Bispecific antibodies linking tumor antigens and human CD16 (FcγRIIIa) have proven successful in preclinical models in directing NK activity against tumor models.[7,8]

In the previous study, we worked with the human tenth type III fibronectin (Fn3) domain, a small, 10 kDa protein, that maintains its native fold without disulfide bonds. We used a yeast display library of Fn3s, named the G4 library,[9] to engineer to binders to the different murine FcγRs (mFcγRs). Using this technology, we engineered and validated a bispecific construct that engages with a specific tumor antigen and FcγRs on immune cells. In this study, we measure the binding affinity of our Fn3 binders in our tumor targeting construct format, and confirm its binding functionality by targeting tumor cells and FcγRs concurrently. We also study the biological activity

of our constructs that target the individual mFcγR specifically in the context of activating phagocytosis of tumor cells. The approach described here will be useful for studying antibody effector functions in future mouse models.

Results

Engineered dsSSMSA-Fn3 Construct

A tumor targeting fusion protein was engineered using an scFv, mouse serum albumin, and Fn3, with the scFv at the N-terminus followed by the serum albumin and then a particular mFcγR-binding Fn3. The scFv known as sm3E was previously engineered to have high affinity to the tumor antigen carcinoembryonic antigen (CEA) with a K_D of 30pM.[10] The scFv was disulfide stabilized by introducing two cysteine residues at R44C in framework region 2 (FR2) of the heavy chain and G100C in FR4 of the light chain.[11] Murine serum albumin (MSA) was used for the protein fusion construct for several useful characteristics: 1) enhanced serum half-life,[12–14] 2) no residual interaction with mFcγR, and 3) low immunogenicity. Serum albumin exhibits a long serum half-life through its interactions with FcRn,[15] while not interacting with any of the mFcγRs.[16] The murine albumin should exhibit low immunogenicity in mouse studies. The Fn3 clone was fused to the scFv-MSA construct at the c-terminus separated by a linker (Figure 3-1a). A construct was made with each mFcγR binding Fn3 and a control Fn3, L7.5.1, a picomolar binding to hen-egg lysozyme,[17] renamed L. Construct nomenclature is "dsSSMSA-Fn3", with ds representing disulfide stabilized and the SS representing sm3E scFv.

Label-Free Method to Measure Binding Affinity

Equilibrium binding constants of each Fn3 to their respective mFcγR was determined through a label-free method using a ForteBio BLitz machine. Biotinylated mFcγR were immobilized on streptavidin biosensors, which are then dipped into different dilutions of dsSSMSA-Fn3 (Figure

3-1b). Using the k_{on} and k_{off} rates determined by global fits with the Langmuir model, the equilibrium binding constants of each Fn3 clone was determined (Figure 3-1c). All Fn3 binders range from mid to low nM K_Ds with binder I having a K_D of 19.9nM, II with a 7.49nM K_D, III with a 44nM K_D, and with binders IV1 and IV2 having similar equilibrium binding constants of 29.1 and 28.9 nM, respectively. Binder I has a slower k_{on} than the other binders, but also has a slower k_{off} and therefore is a mid-affinity binder. The mFcγRIIB binder II, on the other hand, has relatively average k_{on} but a slower k_{off} leading to a lower K_D than the other binders. The III binder has a slightly higher K_D compared the other binders which agrees with the yeast surface titration data. The mFcγRIV binder IV1 has a slightly slower k_{on} and k_{off} compared to IV2, therefore leading to similar K_D values.

Binding Functionality of dsSSMSA-Fn3

Binding functionality of the dsSSMSA-Fn3 constructs were determined on four cell lines: the antigen positive MC38-CEA and B16-CEA cell lines along with the antigen negative cell lines MC38 and B16-F10. The constructs were first tested for the scFv binding on antigen positive and negative cells to determine that sm3E maintained binding specificity to CEA (Figure 3-2). All constructs showed specific binding to only CEA positive cell lines and no binding to antigen negative cell lines. Two different cell lines were used to confirm that this format is applicable to various model systems.

Constructs were then tested to see if they could simultaneously bind CEA positive cells and their target mFcγR. To do so, both MC38-CEA and B16-CEA were incubated with each dsSSMSA-Fn3 construct and then streptavidin-loaded tetramers of mFcγR were added (Figure 3-3a). As expected, dsSSMSA-L shows no binding to any of the mFcγRs. The remaining constructs show exquisite specificity to their respective mFcγR: dsSSMSA-I to mFcγRI, dsSSMSA-II to mFcγRIIB, dsSSMSA-III to mFcγRIII, and dsSSMSA-IV1 and dsSSMSA-IV2 to mFcγRIV (Figure 3-3b and c). The amount of binding of dsSSMSA-III is slightly less than the other dsSSMSA-Fn3s, in agreement

with the calculated K_D of the III Fn3. The IV1 Fn3 also has lower binding to mFcγRIV than IV2, and these results are true for both MC38-CEA and B16-CEA. This could be due to the slower k_{on} of IV1 versus IV2, though according to the BLItz data both of them have similar K_Ds. These binding results show that the engineered dsSSMSA-Fn3 constructs can simultaneously bind CEA positive tumor cells and engage with mFcγRs, enabling specific bridging of target cells to individual mFcγRs.

We also wanted to confirm that our constructs could bind to cells expressing FcγRs. Our initial studies were conducted with macrophages, since according to literature they express all four of the FcγRs[1]. Unfortunately, on flow cytometry, macrophages showed binding to all of our constructs including our control (data not shown), which confirms the general sentiment that macrophages are known to be "sticky"[18,19]. Therefore, we decided to work with HEK293 cells that expressed individual FcγRs. HEK293 cells were transiently transfected with the full mFcγRs along with the common γ-chain for the activating FcγRs or only the mFcγRIIB, since it does not associate with the common γ-chain. We measured FcγR expression by staining for the c-Myc tag followed by a fluorescent anti-c-Myc secondary antibody. Our results show varying transfection levels between the different FcγRs with mFcγRI, II, III, and IV1 at approximately 31.29±0.96%, 6.48±0.62%, 7.16±1.25%, and 19.65±0.8%, respectively of measured HEK293 cells (Figure 3-4a). Our dsSSMSA-I, III, IV1, and IV2 constructs showed very specific binding to their target FcγRs (Figure 3-4b). Unfortunately our dsSSMSA-II binding was undetectable, which most likely was a result of the low transfection levels of the mFcγRIIB in the HEK293 cells.

In order to confirm dsSSMSA-II binding to mFcγRIIB expressing cells, we decided to test binding on B-cells since they only express mFcγRIIB[1]. We isolated primary splenocytes from a mouse and stained for the CD19+B220+ B-cell markers along with dsSSMSA-II binding. We gated on CD19+B220+ cells and within that population we detected a small population that bound

dsSSMSA-II while not binding the control dsSSMSA-L. We therefore confirmed that not only do our constructs specifically bind antigen positive tumor cells, but also are able to bind mFcγR expressing cells (Figure 3-4c).

Phagocytosis Assay

We conducted a phagocytosis assay in order to determine if these engineered constructs promote mFcγR-driven effector functions such as phagocytosis. Tumor cells labeled with carboxyfluorescein succinimidyl ester (CFSE) were pre-coated with bispecific protein constructs and then incubated with peritoneal macrophages. All proteins were tested to have endotoxin levels of less than 0.2 EU/ml before use in the assay. Cells were gated on F4/80 and CD11b positive macrophages that were CFSE positive for tumor cells (Figure 3-5a and b). The antibody version of sm3E on mouse isotype IgG2a (mIgG2a) served as a positive control of phagocytosis, while dsSSMSA-L and uncoated cells were negative controls. Increased phagocytosis only occurred with the CEA positive cells MC38-CEA and B16-CEA, whereas with the antigen negative cells MC38 and B16-F10, phagocytosis levels were comparable to those of the negative controls. Sm3E mIgG2a coated cells show increased phagocytosis on MC38-CEA and B16-CEA cells compared to MC38 and B16-F10 cells, respectively. The Fn3s that bind to the activating receptors mFcγRI, mFcγRIII, and mFcγRIV promoted increased phagocytosis with the constructs dsSSMSA-I, dsSSMSA-III, dsSSMSA-IV1, and dsSSMSA-IV2 when coated on CEA positive cells as opposed to CEA negative cells (Figure 3-6a and b). On the other hand dsSSMSA-II does not promote phagocytosis, consistent with the fact that the II Fn3 binds to the inhibitory mFcγRIIB. The significant ($p\text{-val} < 0.05$) increases in phagocytosis further confirm that these Fn3s are specific for their mFcγRs and show proper activity. Phagocytosis was further confirmed with deconvolution microscopy (Figure 3-6c).

This demonstrates that macrophages were actually engulfing tumor cells, which agrees with the flow cytometry data collected.

Discussion

In the dsSSMSA-Fn3 format, the five Fn3 clones: I, II, III, IV1, and IV2 show specificity to their target FcγR based on binding studies. At high concentrations, using a non-label-free method of detection, proteins can become stickier and therefore slight cross-reactivity is detected at high concentrations. Although the binding affinities of these Fn3 binders are not necessarily higher than that of the wild-type antibody with the mIgG2a isotype for each mFcγR, the ratio of binding to the activating receptors versus inhibitory receptors, (known as the A/I ratio[20]) is dramatically larger (Figure 3-1c). These binders to the activating receptors have several hundred to thousand fold higher A/I ratios compared to that of the wild-type antibody Fc.

This dsSSMSA-Fn3 construct functionally, if not structurally, mimics an antibody except that it exhibits monospecific FcγR binding and is monovalent for the target antigen. Antigen-binding, FcRn-mediated lifetime extension, and FcγR engagement are all present in these constructs, which are very modular in that the scFv can be switched out to target other antigens and the Fn3s are also easily swapped out. The MSA extends *in vivo* serum half-life and increases protein expression yields. The engineered dsSSMSA-Fn3 constructs show specificity of the scFv to the target antigen, CEA, and demonstrates that they can simultaneously bind cells and FcγR.

The phagocytosis assays demonstrate that our dsSSMSA-Fn3 constructs can drive biological activity *in vitro*. Macrophages were used for this biological assay because they are known to express all four mFcγR.[5] The constructs that were engineered to bind to the activating receptors: mFcγRI, mFcγRIII, and mFcγRIV all drive increased phagocytosis when compared to antigen-negative cells or the construct with the control Fn3. The construct with the II Fn3 specific for inhibitory

mFcγRIIB showed no phagocytosis, which is consistent with the fact that mFcγRIIB sends inhibitory signals when cross-linked and therefore would not drive phagocytosis. This assay also demonstrates that our constructs can bridge two types of cells together, tumor cells and macrophages.

We have shown that it is possible to engineer Fn3-based binders specific to each individual mFcγR. This allows us to parse out the individual contribution of each mFcγR from the protein level. By engineering binders instead of altering the Fc portion of an antibody, this allows us to bypass allelic restrictions. Our current construct is also designed to be optimal for *in vivo* work with the presence of the serum albumin, which would provide an extended half-life. The Fn3 binders also provide a powerful toolkit that can be used to study many different ailments ranging from cancer to autoimmune diseases.

Materials and methods

Protein production

DNA for transfection was obtained using a PureLink HiPure Plasmid FP Maxiprep Kit (Invitrogen). Proteins were obtained through transient transfection of HEK293F cells with DNA and 2mg of polyethyleneimine per liter of culture per manufacturer's protocol. Supernatants were harvested and sterile filtered with a 0.2 μm filter one week after transfection. His6 tagged proteins were purified using Talon metal affinity resin (Clontech). Size-exclusion chromatography of dsSSMSA-Fn3 constructs was performed using a HiLoad 16/600 Superdex 200 pg column (GE healthcare) on an Akta FPLC system (GE healthcare). Sm3E mIgG2a antibodies were purified using Protein A resin (Genscript) per manufacturer's protocol. All proteins tested for endotoxin presence with an Endpoint Chromogenic LAL assay (Lonza) before use in assays.

Cell lines

HEK293F cells (Invitrogen) were cultured in Freestyle 293 expression medium (Invitrogen) in suspension. The chemically induced murine colon adenocarcinoma cell lines MC38 and MC38-CEA, which is transfected with human CEA,[21] were obtained from Dr. Jeffrey Scholm (National Cancer Institute, Bethesda, MD). Cell lines were cultured in DMEM (Corning Cellgro) with 10% heat inactivated FBS (Invitrogen) and 100 U/ml penicillin and 100 μg/ml streptomycin (Corning Cellgro), with the addition of 500 μg/ml G418-sulfate (Corning Cellgro) for MC38-CEA. The murine melanoma cell line B16-F10 (ATCC) was cultured in DMEM (ATCC) with 10% heat inactivated FBS (Invitrogen) and 100 U/ml penicillin and 100 μg/ml streptomycin (Corning Cellgro).

For the generation of B16-CEA cells (by Cary Opel), the vector pcDNA-CEA-GFP was generated using In-Fusion (Clontech) cloning. The sequence coding for human CEA (CEACAM5, UniProt: P06731) was synthesized (Genscript) and the sequence for eGFP was cloned from pEGFP-C2 (Clontech). The two sequences were separated by a 2A skip peptide sequence to generate two separate polypeptides, and cloned into pcDNA3.1(+) (Invitrogen). B16-F10 cells were transfected with pcDNA-CEA-GFP using Xfect (Clontech) according to manufacturer's instructions. 24 hours after transfection, the cells were cultured in media containing 5 mg/mL G418 (Corning Cellgro). A stable polyclonal pool was generated by sorting for GFP positive cells using a MoFlo Cytometer (Beckman Coulter) several times until a homogenous population was achieved. Single clones were selected from this pool based on double positive signals from GFP and 647-labeled sm3E also using a MoFlo Cytometer. Of these, a two clones, one showing high expression and the other showing physiological levels of CEA was identified and designated B16-CEA B and F, respectively. B16CEA F cells were used in the phagocytosis assays. These cells were cultured in DMEM (Corning Cellgro), with the addition of 5 mg/ml G418-sulfate. All cell lines were maintained

at 37°C with 5% CO2. Cells were subcultured every 2-3 days and when necessary detached using 0.25% trypsin and 1mM EDTA (Invitrogen).

dsSSMSA-Fn3 construction

A scFv-serum albumin-Fn3 construct was engineered as our tumor targeting protein therapeutic. The scFv is a disulfide stabilized version of sm3E that binds to carcinoembryonic antigen (CEA) at high affinity. Murine serum albumin (MSA) was used to increase the serum half life of the protein construct while decreasing immunogenicity by being of mouse origin. Different Fn3 clones were fused to the c-terminus of the MSA by a Gly3Ser linker. The MSA and scFv were linked by a Gly4Ser linker.

Label-free binding analysis

The BLitz system (ForteBio) was used to as the label-free method of determining binding affinities. All proteins are diluted into 1X Kinetics Buffer, 1XPBS pH 7.4 with 0.002% Tween-20 and 0.1% bovine serum albumin (BSA). Biotinylated mFcγR was immobilized on a streptavidin biosensor at a concentration of 100 nM for 180 seconds. dsSSMSA-Fn3 constructs to their respective mFcγR are incubated with the tips at different concentrations. Association times for dsSSMSA-I, II, III, and IV2 were 240 seconds and 120 seconds for dsSSMSA-IV1. Dissociation times were 360 seconds for dsSSMSA-I, II, III, and IV2 and 180 seconds for dsSSMSA-IV1. Tips were regenerated each time for 60 seconds with 0.1M Glycine HCl pH 3.5. A new tip was used for mFcγRIIB for each concentration since it was sensitive to Glycine regeneration.

Binding analysis on cells

Cell lines were detached using 0.25% trypsin and 1mM EDTA, pelleted, and resuspended in 1XPBS and 0.1% BSA (PBSA). $1x10^5$ cells were stained with each dsSSMSA-Fn3 construct at room temperature for 30 minutes. Cells were the washed with excess PBSA and stained with preincubated

tetramers of mFcγR with streptavidin Alexa Fluor 647 at a concentration of 100nM or secondary anti-HIS6 antibody (Biolegend). Samples were analyzed on an Accuri C6 cytometer (BD Accuri Cytometers). The median fluorescence intensity was normalized to the highest sample per cell line and plotted as a heat map with MATLAB (MathWorks).

The genes for full length mFcγRI, IIB, III, and IV were cloned into separate gWiz vectors with a c-Myc tag at the N-terminus. The common gamma chain was also cloned into the gWiz vector. HEK293 cells were seeded over night at $1x10^6$ cells per 10 cm dish in DMEM (Corning Cellgro) with 10% heat inactivated FBS (Invitrogen) and 100 U/ml penicillin and 100 μg/ml streptomycin (Corning Cellgro). Cells were transiently transfected using transit-LT1 (Murius Bio) as per manufacturer's protocol. Transfections were with both the gWiz mFcγR plasmid and the common gamma chain plasmid or in the case of mFcγRIIB, only the gWiz mFcγRIIB plasmid was transfected. Two days after transfection, cells were detached with Versene (Invitrogen) and resuspended in PBSA. Full expression of the mFcγR was detected using a chicken anti-c-Myc antibody (Gallus Immunotech) and a secondary goat anti-chicken Alexa Fluor 488 (Invitrogen). Binding of the Fn3 was determined using Alexa Fluor 647 labeled dsSSMSA-Fn3 and a control anti-CD32/CD16 conjugated to APC antibody (BD biosciences). Samples were analyzed on an Accuri C6 cytometer (BD Accuri Cytometers).

For splenocyte isolation and B-cell staining, spleens were harvested from three mice and manually dissociated between two frosted glass slides. Cells were strained through a 70 μm strainer, pelleted, and red blood cells (RBC) were lysed. Cells resuspended in PBSA and split approximately $5x10^6$ cells per sample. Samples were stained with anti-CD19 conjugated with Alexa Fluor 488 (Biolegend) and anti-CD45R/B220 conjugated with phycoerythrin (Biolegend) to detect B-Cells. Cells were then stained with either anti-CD32/CD16 APC as a positive control or Alexa Fluor 647

labeled dsSSMSA-L as a negative control and dsSSMSA-II. Samples were analyzed on an Accuri C6 cytometer (BD Accuri Cytometers).

Phagocytosis Assay

Murine peritoneal macrophages were isolated from C57BL/6 mice four days after intraperitoneal (IP) injection of 1ml of fluid thioglycollate (Becton Dickinson). Macrophages were seeded into a 96-well tissue culture plate at $1x10^5$ cells per well and treated with 25 ng/ml of IFN-γ (Biolegend) in RPMI (Corning Cellgro) with 10% heat-inactivated fetal bovine serum (Invitrogen) and 1X penicillin-streptomycin solution for 24-40 hours.

Cell lines were detached with 0.25% trypsin and 1mM EDTA, and washed and resuspended with 1XPBS and 0.1% Bovine serum albumin (PBSA) at $5x10^6$ cells/ml. Cells were labeled with 5μM carboxyfluorescein succinimidyl ester (CFSE) for 10 minutes at room temperature in the dark. Cells were then quenched with excess PBSA and washed two more times with serum free DMEM. Cell lines were then incubated with 100 nM of Sm3E mIgG2a or dsSSMSA-Fn3 for 30 minutes at room temperature in the dark. Cells incubated in protein were then transferred to the 96-well plate the peritoneal macrophages were seeded in 24-40 hours previously. Plates were incubated at 37°C with 5% CO_2 for at least 3 hours to allow for phagocytosis.

After phagocytosis, plates were pelleted, supernatants removed, and incubated with Versene (Invitrogen) for 15 min at 37°C with 5% CO_2. Cells were transferred to a new plate and washed with excess PBSA before staining for 1 hour at 4°C with anti-F4/80 Alexa Fluor 647(Biolegend) and anti-CD11b PE (Biolegend) antibodies as macrophage markers. Plates were analyzed on a FACSCalibur HTS instrument.

Microscopy

Imaging was performed on an Applied Precision DeltaVision (GE healthcare) deconvolution microscope. The phagocytosis assay was prepared as stated above with $5x10^5$ peritoneal macrophages on a 3.5mm glass bottom petri dish (MatTek). $1x10^5$ CFSE labeled MC38-CEA cells were incubated with the proteins for at least 3 hours before imaging. Samples were stained with anti-F4/80 Alexa Fluor 647 before imaging on the DeltaVision microscope. Images were recorded on the 60X oil lens.

Statistical Analysis

Unpaired student's t-tests were performed between phagocytosis percentages (%F4/80+CD11b+CFSE+) of CEA positive and CEA negative cells. Statistical significance was determined for p-values below 0.05.

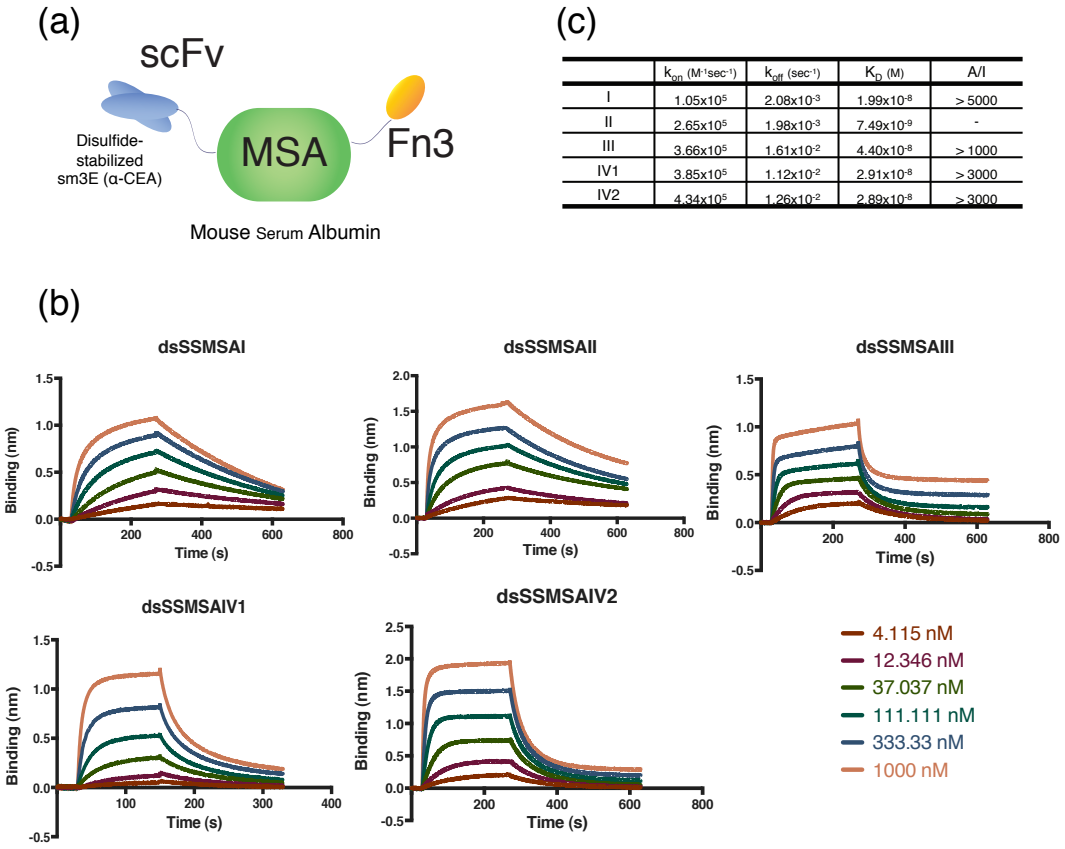

	k_{on} ($M^{-1}sec^{-1}$)	k_{off} (sec^{-1})	K_D (M)	A/I
I	$1.05x10^{5}$	$2.08x10^{-3}$	$1.99x10^{-8}$	> 5000
II	$2.65x10^{5}$	$1.98x10^{-3}$	$7.49x10^{-9}$	-
III	$3.66x10^{5}$	$1.61x10^{-2}$	$4.40x10^{-8}$	> 1000
IV1	$3.85x10^{5}$	$1.12x10^{-2}$	$2.91x10^{-8}$	> 3000
IV2	$4.34x10^{5}$	$1.26x10^{-2}$	$2.89x10^{-8}$	> 3000

Figure 3-1: Binding of dsSSMSA-Fn3 Constructs

(a) Diagram of dsSSMSA-Fn3 construct consists of the anti-CEA scFv, sm3E, fused to a murine serum albumin, fused to an individual Fn3 binder (b) Binding curves obtained using a ForteBio BLitz system. Overlaid sensorgrams correspond to different concentrations of the analyte (dsSSMSA-Fn3) incubated with the immobilized ligand (mFcγR) to each respective binder. (c) Kinetic on rates (K_{on}), off rates (K_{off}), and affinity constants (K_D) determined by global fits to the Langmuir model (1:1 kinetics) with the BIAevaluation software. An activating to inhibitory (A/I) ratio was determined by approximating the K_D of each Fn3 clone to the inhibitory receptor from Figure 2-4 titrations.

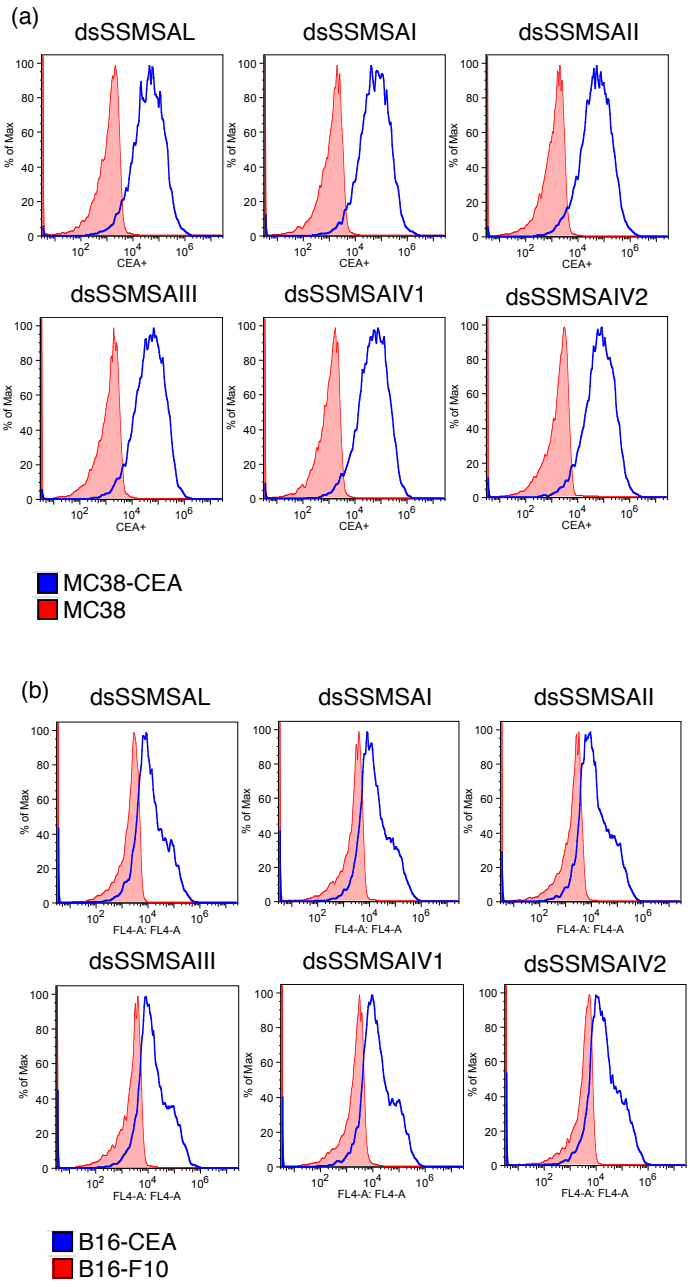

Figure 3-2: dsSSMSA-Fn3 binding CEA positive cell lines

Binding histograms of dsSSMSA-Fn3 constructs to (a) antigen negative cell line MC38 (red) and CEA positive cell line MC38-CEA (blue). (b) CEA negative cell line B16-F10 (red) and CEA positive cell line B16-CEA. All constructs only bind to the CEA positive cell line through the disulfide stabilized sm3E scFv on the dsSSMSA-Fn3 constructs.

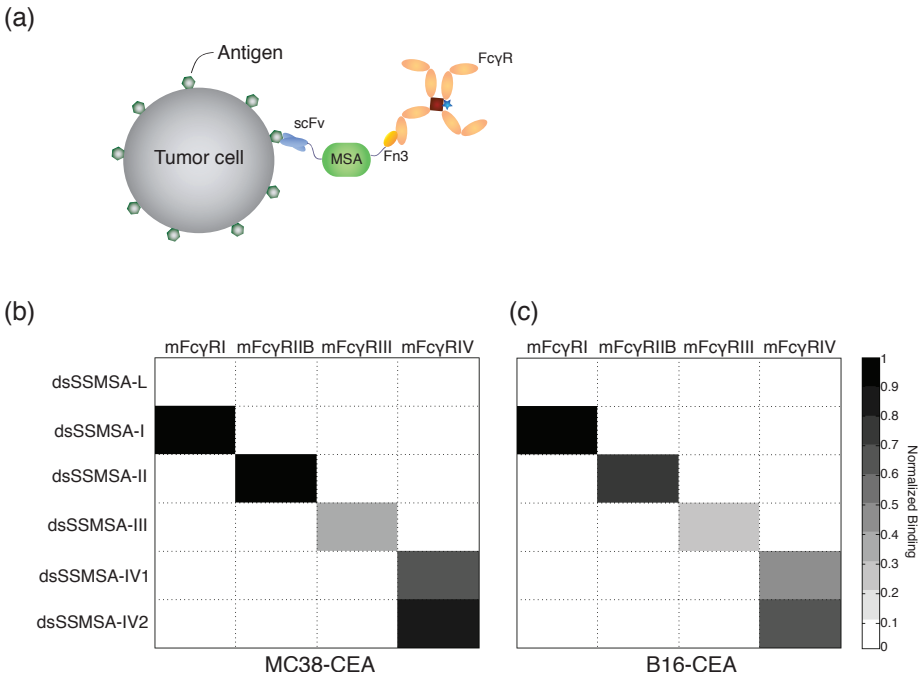

Figure 3-3: dsSSMSA-Fn3 constructs bind to tumor cells and specific mFcγRs

(a) Diagram of dsSSMSA-Fn3 constructs binding the tumor cell with the antigen specific scFv and engaging with tetramers of mFcγRs with the mFcγR specific Fn3. (b) heat map showing binding specificity of each dsSSMSA-Fn3 construct to each mFcγR on MC38-CEA cells. (c) same as (b) except on B16-CEA cells.

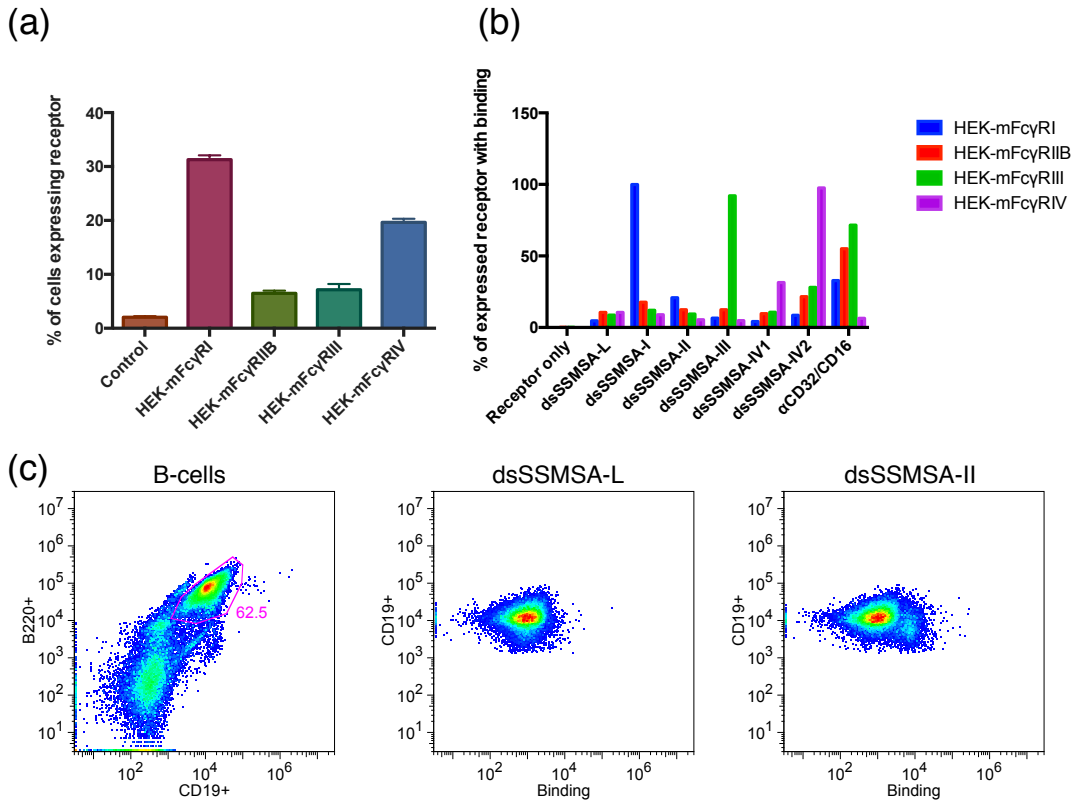

Figure 3-4: dsSSMSA-Fn3 binding to Cells Expressing mFcγRs

(a) Percent receptor expression of HEK cells transiently transfected with full mFcγRs and the common γ-chain (activating receptors only). Receptor was detected with a c-Myc tag. (b) Gated on cells expressing receptor, percent of cells that bind the respective dsSSMSA-Fn3 constructs. Constructs appear to be specific for the cells expressing their targeted receptor. An anti-CD32/CD16 antibody served as a positive control and dsSSMSA-L served as a negative control. (c) Isolation of B-cells from spleens using CD19 and B220 as B-cell markers. Gated on CD19+/B220+ cells. Detected dsSSMSA-II binding over dsSSMSA-L (control) binding.

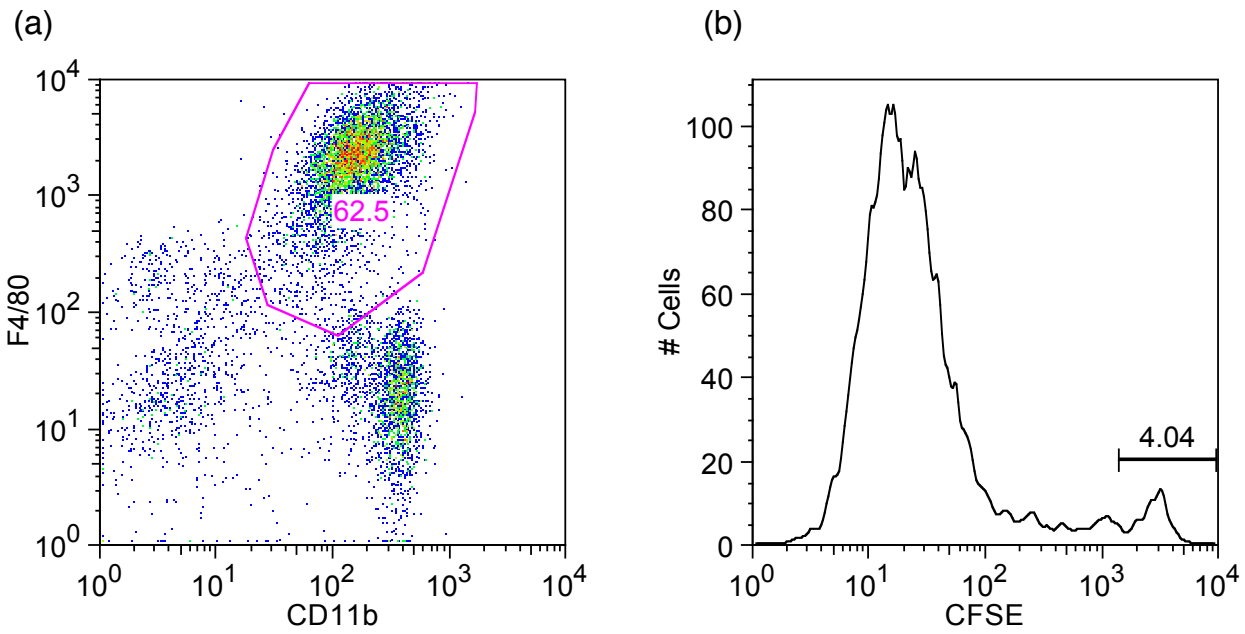

Figure 3-5: Phagocytosis Gating for Analysis

Example flow cytometry plots for phagocytosis analysis. (a) Gating on macrophages by selecting F4/80 and CD11b positive cells. (b) From the population selected in (a) CFSE positive cells were gated on, indicating macrophages that have engulfed CFSE labeled tumor cells.

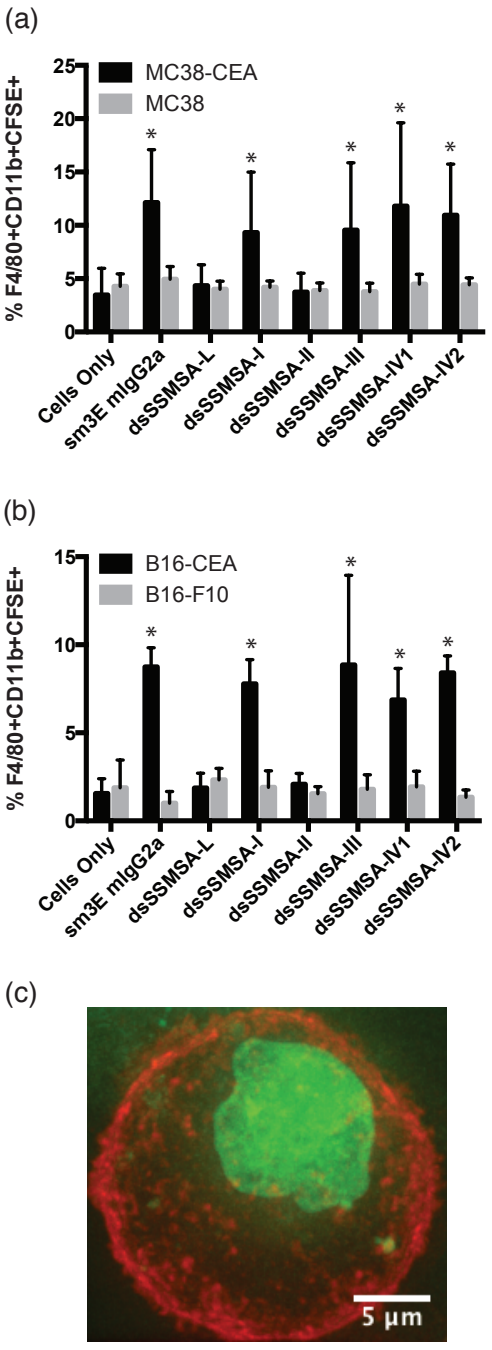

Figure 3-6: Phagocytosis driven by activating mFcγRs

Phagocytosis measured by the percentage of CFSE positive F4/80 and CD11b positive IFNγ treated peritoneal macrophages taken by flow cytometry. Grey bars represent antigen negative cells and black bars represent CEA positive cells. Cells only represent background levels of phagocytosis when tumor cells are incubated with peritoneal macrophages. Cells were incubated with antibody sm3E mIgG2a isotype as a positive control for phagocytosis. Cells were the incubated with different dsSSMSA-Fn3 constructs. The current graphs are representative data of at least three separate experiments with four samples per condition. Unpaired student's t-tests were used to determine statistical significance between antigen positive and antigen negative cells. Statistical significance denoted by * for p-values < 0.05 (a) Phagocytosis comparisons measured on MC38 and MC38-CEA cells. (b) Phagocytosis comparisons between B16-F10 and B16-CEA cells. (c) Deconvolution microscopy of a macrophage (shown in red) phagocytosing a tumor cell (green).

References

1. Griggs, J. & Zinkewich-Peotti, K. The state of the art: immune-mediated mechanisms of monoclonal antibodies in cancer therapy. *Br. J. Cancer* **101,** 1807–1812 (2009).
2. Carter, P. Improving the efficacy of antibody-based cancer therapies. *Nat. Rev. Cancer* **1,** 118–129 (2001).
3. Cassard, L. *et al.* Fc gamma receptors and cancer. *Springer Semin. Immunopathol.* **28,** 321–328 (2006).
4. Adams, G. P. & Weiner, L. M. Monoclonal antibody therapy of cancer. *Nat. Biotechnol.* **23,** 1147–1157 (2005).
5. Nimmerjahn, F. & Ravetch, J. V. Fcγ receptors as regulators of immune responses. *Nat. Rev. Immunol.* **8,** 34–47 (2008).
6. Desjarlais, J. R., Lazar, G. A., Zhukovsky, E. A. & Chu, S. Y. Optimizing engagement of the immune system by anti-tumor antibodies: an engineer's perspective. *Drug Discov. Today* **12,** 898–910 (2007).
7. McCall, A. M. *et al.* Isolation and characterization of an anti-CD16 single-chain Fv fragment and construction of an anti-HER2/neu/anti-CD16 bispecific scFv that triggers CD16-dependent tumor cytolysis. *Mol. Immunol.* **36,** 433–446 (1999).
8. Vallera, D. A. *et al.* Heterodimeric Bispecific Single-Chain Variable-Fragment Antibodies Against EpCAM and CD16 Induce Effective Antibody-Dependent Cellular Cytotoxicity Against Human Carcinoma Cells. *Cancer Biother. Radiopharm.* (2013). doi:10.1089/cbr.2012.1329
9. Hackel, B. J., Ackerman, M. E., Howland, S. W. & Wittrup, K. D. Stability and CDR composition biases enrich binder functionality landscapes. *J. Mol. Biol.* **401,** 84–96 (2010).
10. Graff, C. P., Chester, K., Begent, R. & Wittrup, K. D. Directed evolution of an anti-carcinoembryonic antigen scFv with a 4-day monovalent dissociation half-time at 37°C. *Protein Eng. Des. Sel.* **17,** 293–304 (2004).
11. Reiter, Y., Brinkmann, U., Lee, B. & Pastan, I. Engineering antibody Fv fragments for cancer detection and therapy: Bisulfide-stabilized Fv fragments. *Nat. Biotechnol.* **14,** 1239–1245 (1996).
12. Halpern, W. *et al.* AlbugraninTM, a Recombinant Human Granulocyte Colony Stimulating Factor (G-CSF) Genetically Fused to Recombinant Human Albumin Induces Prolonged Myelopoietic Effects in Mice and Monkeys. *Pharm. Res.* **19,** 1720–1729 (2002).
13. Subramanian, G. M., Fiscella, M., Lamousé-Smith, A., Zeuzem, S. & McHutchison, J. G. Albinterferon α-2b: a genetic fusion protein for the treatment of chronic hepatitis C. *Nat. Biotechnol.* **25,** 1411–1419 (2007).
14. Andersen, J. T. *et al.* Single-chain Variable Fragment Albumin Fusions Bind the Neonatal Fc Receptor (FcRn) in a Species-dependent Manner IMPLICATIONS FOR IN VIVO HALF-LIFE EVALUATION OF ALBUMIN FUSION THERAPEUTICS. *J. Biol. Chem.* **288,** 24277–24285 (2013).
15. Kim, J. *et al.* Albumin turnover: FcRn-mediated recycling saves as much albumin from degradation as the liver produces. *Am. J. Physiol. - Gastrointest. Liver Physiol.* **290,** G352–G360 (2006).
16. Chaudhury, C., Brooks, C. L., Carter, D. C., Robinson, J. M. & Anderson, C. L. Albumin Binding to FcRn: Distinct from the FcRn−IgG Interaction†. *Biochemistry (Mosc.)* **45,** 4983–4990 (2006).
17. Hackel, B. J., Kapila, A. & Wittrup, K. D. Picomolar affinity fibronectin domains engineered utilizing loop length diversity, recursive mutagenesis, and loop shuffling. *J. Mol. Biol.* **381,** 1238–1252 (2008).

18. Put, S. *et al.* Macrophages have no lineage history of Foxp3 expression. *Blood* **119,** 1316–1318 (2012).
19. Baumgarth, N. & Roederer, M. A practical approach to multicolor flow cytometry for immunophenotyping. *J. Immunol. Methods* **243,** 77–97 (2000).
20. Nimmerjahn, F. & Ravetch, J. V. Divergent Immunoglobulin G Subclass Activity Through Selective Fc Receptor Binding. *Science* **310,** 1510–1512 (2005).
21. Robbins, P. F. *et al.* Transduction and Expression of the Human Carcinoembryonic Antigen Gene in a Murine Colon Carcinoma Cell Line. *Cancer Res.* **51,** 3657–3662 (1991).

CHAPTER 4: TESTING *IN VIVO* EFFICACY OF MURINE FC GAMMA RECEPTOR BINDERS

Introduction

In mAb cancer therapeutics, activating FcγRs has been shown to play a key role in the elimination of tumor cells[1]. A landmark example is the α-CD20 mAb, rituximab, and its mechanism of action through FcγRIIIA engagement, where polymorphisms play a major role in clinical efficacy[2]. The role of different FcγRs has been studied through different knockout (KO) mice and antibody isotypes - Nimmerjahn and Ravetch showed that *in vivo* the IgG2a isotype was key in mediating effector functions with the B16F10 lung metastasis mouse model treated with TA99[3]. Different FcγR KO mice injected with B16F10 melanoma cells and treated with the TA99 IgG2a antibody, revealed that FcγRIV played the major role in tumor clearance[3]. Subsequent work has revealed overlapping roles for FcγRI and FcγRIV in tumor cytotoxicity[4,5]. It is hypothesized that the IgG2a isotype has a high activating to inhibitory (A/I) ratio where the Fc binds to the activating FcγR with higher affinity than the inhibitory FcγR[3]. These studies suggest that there are two main areas of improvement of therapies: increasing affinity to activating FcγR and decreasing binding to the inhibitory FcγR, and thereby increasing the A/I ratio.

Although, a mouse model with human FcγRs has been developed,[6] it is not widely available and therefore the approach of targeting mouse FcγRs would be useful in studying many diseases in mouse models. Previously engineered Fn3 domains, have been characterized to have approximately 10-50 nM binding affinity to their respective FcγR, which is of higher affinity than the current μM affinity of the murine IgG2a (mIgG2a) isotype to the low affinity FcγRs. Only the Fn3 binder to mFcγRI has slightly lower affinity than that of the wild-type mIgG2a. The Fn3 binders are also very specific to their respective mFcγR, and therefore the Fn3s that bind the activating mFcγRI, III, and IV have very high A/I ratios.

Previous studies demonstrated that the scFv-MSA-Fn3 construct maintained binding functionality along with promoted phagocytosis. *In vivo* pharmacokinetics and biodistribution of these constructs were evaluated in this study. This panel of Fn3s that bind specifically to individual mFcγR fused to a tumor-targeting serum albumin construct was used to help parse out the roles of individual murine FcγRs in a model system. Several murine tumor model systems were evaluated with various treatment regimens to determine if these constructs behaved like tumor targeting antibodies.

Results

In vivo *characterization of dsSSMSA-Fn3 constructs*

Constructs were first evaluated for proper *in vivo* characteristics before conducting any efficacy studies. Initial pharmacokinetic studies were conducted in C56BL/6 mice with Alexa Fluor 647 labeled dsSSMSA-Fn3 constructs. Results from intraperitoneal injections show that these constructs have approximate alpha half-lives of 4.9±1.5 hours and beta half-lives of 29.7±0.4 hours (Figure 4-1a). Because the protein is delivered intraperitoneally, there is a delay in the protein reaching the blood and its maximum signal. The alpha and beta half-lives are fit to the points after the signal has reached its peak at approximately 3 hours.

Pharmacokinetic studies were repeated in CEA.Tg mice with dsSSMSA-Fn3 constructs labeled with Alexa Fluor 647 to determine if the endogenous CEA expressed in the mice were acting as a sink for the proteins. Results suggest that the constructs are clearing much faster in CEA.Tg mice. When fit to a two-phase decay non-linear fit, some of the constructs have beta half-lives ranging from 9-12 hours (Figure 4-1b). The data was not very clean though, so the study will have to be redone to have better curve fits. It does suggest that most likely endogenous CEA is acting as a sink for these constructs, so their serum half-life is actually shorter than previously predicted.

Initial biodistribution studies were performed in albino C56BL/6 mice for ease of imaging, since the melanin in the black pigments of wild-type C56BL/6 mice can interfere with the fluorescent imaging. MC38-CEA and MC38 tumors were inoculated two weeks prior to dosing with Alexa Fluor 647 labeled dsSSMSA-Fn3 constructs. After injection of labeled construct, mice were imaged at 4, 8, and 24 hrs. By 24 hrs most of the construct as cleared from the organs imaged on the ventral side, but much still remains in the tumors (Figure 4-2a). Although the intensity of the antigen free tumor appears to be higher than that of the antigen positive tumor, this is because of the size difference. When tumors are removed and homogenized, it appears that the constructs have significantly more accumulation in the antigen positive tumor as compared to the antigen negative tumor when normalized by mass (Figure 4-2b). These results demonstrate that our engineered dsSSMSA-Fn3 can localize specifically to CEA positive tumors.

MC38-CEA tumor model

Initial studies with the dsSSMSA-Fn3 constructs were conducted on the MC38-CEA tumor model in CEA transgenic (CEA.Tg) mice that are on the C56BL/6 background. CEA.Tg mice were used because they were tolerant to the CEA that is stably expressed on the MC38 colon adenocarcinoma cell line. Therefore, any immune response generated by the mouse should be from activation caused by the therapy and not by the presence of the "foreign" human CEA protein.

The initial MC38-CEA model was conducted with only the dsSSMSA-I, dsSSMSA-IV1, and dsSSMSA-IV2 constructs. These were chosen because literature suggested that mFcγRI and mFcγRIV played the main roles in tumor clearance in ADCC[4]. The antibody sm3E mIgG2a was used as our positive control, which should control the tumor through ADCC. Unfortunately, the tumor growth curves for the sm3E mIgG2a treated mice were not significantly different from the PBS negative control mice (Figure 4-3a). Our constructs also showed no significant difference in tumor growth as compared to the control.

To further determine if immunoediting of the CEA was leading to the lack of tumor control, we tested the treated tumors for CEA expression. Interestingly, it did not appear that CEA was being immunoedited from the MC38-CEA tumors (Figure 4-3b). Tumors from all treatments stained for CEA expression above background level. We also tested serum from the same mice to determine if antibodies specifically against CEA were being produced. Results show that there was no antibody detected in the mouse serum against MC38-CEAs against the background level of MC38s other than the mice treated with sm3E mIgG2a (Figure 4-3c). The antibody detected in the serum in this case was most likely remaining sm3E mIgG2a from previous dosing.

Optimization of B16CEA tumor model

Since the original MC38-CEA tumor model with sm3E mIgG2a antibody dosing failed to show tumor growth control, as would be expected, we had to switch mouse models. Previous studies of the antibody TA99, which targets the TYRP-1 protein on the B16F10 cell line, with the mIgG2a isotype elicited ADCC and demonstrated tumor control when conducted on the B16F10 mouse tumor model[3]. Our lab has generated single clones of B16F10s stably expressing varying levels of human CEA. Clones were designated B16CEA B, B16CEA D, and B16CEA F and expressed $1.5x10^6$ CEA/cell, $1.2x10^6$ CEA/cell, and $1.8x10^5$ CEA/cell respectively.

Previous studies with B16F10s demonstrating tumor control with the TA99 mIgG2a antibody were conducted in lung metastasis models. In order to determine if the new B16CEA cells maintained the same metastatic properties as the original B16F10 cell line, $1x10^6$ cells of each B16CEA cell line was injected intravenously through the tail vein to metastasize to the lungs. After two weeks, lungs were harvested and qualitatively evaluated for lung metastases. Interestingly, the cell line that expresses the lowest amount of CEA, B16CEA F had the highest metastatic potential, while the cell line with the most CEA on the surface, B16CEA B had the least amount of lung

metastases (Figure 4-4a). Qualitatively, B16CEA F appeared to metastasize in the lungs most similarly to B16F10s so we conducted initial tumor control studies with this cell line.

B16CEA Fs were injected intravenously through tail vein into mice and then dosed intraperitoneally (IP) with sm3E mIgG2a or TA99 mIgG2a antibody prophylatically, starting on day 0. The antibody treatment regimen followed that of previous literature[7]. After two weeks, lungs were harvested and lung metastases were preliminarily evaluated qualitatively. Results showed that sm3E mIgG2a antibody had very little effect on controlling tumor growth (Figure 4-4b). The TA99 mIgG2a antibody, which previously showed very good control of B16F10 lung metastases[3], also had very little effect on controlling tumor growth in this model. This led us to either believe that B16CEA F cells were either very hardy or our single agent treatment was not strong enough.

Combination treatment with persistent serum half-life IL-2 with dsSSMSA-Fn3 constructs

Previous studies with persistent serum half-life IL-2 either in the form of Fc/IL-2 or MSA/IL-2 in combination with the TA99 mIgG2a antibody treatment showed strong tumor control of B16F10 subcutaneous tumors (unpublished data). A preliminary experiment was conducted with this combination therapy on B16CEA F lung metastases. Results showed that Fc/IL-2 only and Fc/IL-2 in combination with sm3E mIgG2a were better at clearing lung metastases as compared to the no treatment control (Figure 4-4c). Unfortunately, the results from the preliminary treatment were not very conclusive other than suggesting that this combination therapy has an effect on the B16CEA Fs, whereas the original antibody monotherapy did not.

We decided to pursue this combination therapy with B16CEA F and B subcutaneous tumors. CEA.Tg mice were inoculated with either B16CEA F or B cells and treated with MSA/IL-2 in combination with sm3E mIgG2a or TA99 mIgG2a as our positive control or the dsSSMSA-Fn3 constructs. In the B16CEA F model, all of the treatments are unable to control the tumors except for the MSA/IL-2 combination with TA99 mIgG2a, which controlled 2 out of 5 mice (Figure 4-5a).

These results suggested that the B16CEA F cell line is extremely potent and difficult to treat. Conversely, the B16CEA B cell line showed outgrowth of tumors in the PBS and MSA/IL-2 only controls, whereas there was tumor control in 5 out of 5 mice treated with MSA/IL-2 and TA99 mIgG2a and 2 out of 5 mice in the MSA/IL-2 and sm3E mIgG2a treatment group (Figure 4-5b).

Initial studies were only conducted with MSA/IL-2 in combination with dsSSMSA-IV1 or dsSSMSA-IV2. Treatment with the combination therapy and dsSSMSA-IV1 showed delayed tumor outgrowth of 1 out of 5 mice and tumor control in 1 out of 5 mice. Treatment with dsSSMSA-IV2 showed tumor control in 1 out of 5 mice (Figure 4-5b). It appears that these two treatments are comparable, which would be logical since they both only interact with FcγRIV.

Varying degrees of vitiligo was observed on 6 out of the 8 mice initially injected with B16CEA B, whereas there was no vitiligo observed in the B16CEA F injected mice. All mice that demonstrated tumor control were rechallenged with their respective tumor cell line. The mice initially injected with B16CEA F tumors all failed to control the rechallenged tumor (Figure 4-5c). In the B16CEA B rechallenge mice only 3 out of 8 mice failed to control the rechallenged tumor. The remaining mice all demonstrated memory against the B16CEA B line (Figure 4-5d).

A second study was conducted to include all of the different dsSSMSA-Fn3 constructs. The negative control of MSA/IL-2 and dsSSMSA-L showed outgrowth of all tumors (Figure 4-6d). MSA/IL-2 in combination with dsSSMSA-I showed delayed tumor growth of 2 out of 5 mice and tumor control in 1 out of 5 mice (Figure 4-6e). Interestingly, dsSSMSA-II and MSA/IL-2 treated mice showed delayed growth in 1 out of 5 mice and tumor control in 2 out of 5 mice (Figure 4-6f). This is surprising since dsSSMSA-II should bind to the inhibitory receptor and prevent tumor cell killing, which logically would suggest that the tumors would grow out faster. Unfortunately, when mice are treated with MSA/IL-2 with dsSSMSA-III there is no tumor control but 1 out of 5 mice have slight tumor growth delay (Figure 4-6g). Treatments of MSA/IL-2 in combination with either

dsSSMSA-IV1 or dsSSMSA-IV2 have similar results. In the dsSSMSA-IV1 treatment group 2 out of 5 mice are delayed and 1 out of 5 mice demonstrate tumor control (Figure 4-6h). In the dsSSMSA-IV2 treatment group 3 out of 5 mice have delay in tumor outgrowth and 1 out of 5 mice have tumor control (Figure 4-6i). The survival curves of MSA/IL-2 combination treatment are all significantly different from the PBS control (Figure 4-7a). MSA/IL-2 only survival is already statistically significant compared to the PBS control, therefore the increase in survival for the combination treatments over PBS is masked by MSA/IL-2 treatment. In order to detect a difference in survival, combination treatments were compared to the MSA/IL-2 + dsSSMSA-L negative control treatment. With this comparison, combination treatments of MSA/IL-2 + sm3E mIgG2a, MSA/IL-2 + dsSSMSA-I, and MSA/IL-2 + dsSSMSA-IV2 were considered significantly different compared to the control (Figure 4-7b).

The third replication of the study was a repetition of the dsSSMSA-Fn3s doses that were not previously replicated. Unfortunately in this repetition, 1 out of 5 mice showed tumor control in the MSA/IL-2 only treatment (Figure 4-8b). Therefore, this confounded much of the results since any tumor control could be attributed to the MSA/IL-2 treatment only. In this study, none of the dsSSMSA-I treated tumors showed control or delay in tumor growth (Figure 4-8e). Interestingly, the dsSSMSA-II treated mice had 1 out of 5 mice show control (Figure 4-8f). Finally, in the dsSSMSA-III treated mice there was also 1 out of 5 mice demonstrating tumor control (Figure 4-8g). The mice in this replication were slightly older, which could have also confounded the results.

Prophylactic studies of single agent treatments

As noted previously, the addition of MSA/IL-2 increased chances of tumor control, but confounded the results since some mice showed tumor control when dosed with only MSA/IL-2. Since it was determined that the B16CEA B cell line was easier to treat, a prophylactic monotherapy was conducted on subcutaneous tumors of this type in CEA.Tg mice. Controls used were PBS as a

vehicle control, sm3E mIgG2a as a positive control, and dsSSMSA-L as a negative control. Results show that both PBS and dsSSMSA-L treated tumors grow out whereas sm3E mIgG2a treated tumors had delayed tumor growth, until treatment termination (Figure 4-9a-c). Interestingly, our constructs that interact with the activating mFcγRs: dsSSMSA-I, dsSSMSA-III, dsSSMSA-IV1, and dsSSMSAIV2 (Figure 4-9d, f, g, and h) all seemed to control the tumor in a similar fashion as sm3E mIgG2a. Our construct that binds the inhibitory receptor dsSSMSA-II shows no tumor control and behaves similarly to PBS and our negative control dsSSMSA-L (Figure 4-9e). Survival curves show a statistical difference between PBS and sm3E mIgG2a treated mice, whereas there is no statistical difference between PBS and dsSSMSA-L treated mice. The survival curves for dsSSMSA-I, dsSSMSA-III, dsSSMSA-IV1, and dsSSMSA-IV2 treated mice were also statistically different from the negative control dsSSMSA-L (Figure 4-9i). On the other hand, survival curves for dsSSMSA-II treated mice were not different from dsSSMSA-L treated mice.

Discussion

In order to test the *in vivo* stability of our engineered constructs, we performed initial pharmacokinetic studies in wild-type C56BL/6 mice. The constructs had reasonable serum half-lives and had detectable protein in the blood even on the fifth day after injection. These results convinced us to move forward with *in vivo* biodistribution studies. The biodistribution studies were conducted in albino C56BL/6 mice that were inoculated with antigen positive and antigen negative MC38 tumor cell lines. Both the cell lines and mice were chosen for ease of imaging since melanin pigments in wild-type C56BL/6 mice and the B16F10 melanoma cell line interfere with fluorescence imaging. It appears that the constructs are cleared from the organs when imaged on the IVIS and accumulate within the tumors after 24 hours. Most of the accumulation is probably due to the enhanced permeability and retention (EPR) effect, where the constructs accumulate passively in the tumors because of the lack of lymphatic drainage. When quantified and calculated by percent-

injected dose per gram, results indicate that the constructs have higher accumulation in the antigen positive tumor.

These results allowed us to move forward in attempting tumor control experiments. The initial experiment with the MC38-CEA tumor model in CEA.Tg mice showed no difference between treatments with the PBS vehicle versus dsSSMSA-Fn3 constructs that only interacted with mFcγRI and mFcγRIV. Although it was disappointing that our constructs failed to control tumor growth, the positive control with the sm3E mIgG2a antibody monotherapy also failed to control tumor growth. This suggested that our model was not a good representation to determine the efficacy of mFcγR driven tumor control. The study was also ended early at only 14 days after tumor inoculation, which is standard for lung metastasis models, but perhaps too early for subcutaneous models. It is possible that if the study was extended, we would have observed more of a difference in tumor control with our constructs and sm3E mIgG2a compared to the PBS treated mice. Tumors were analyzed and blood samples were taken to detect immunoediting or specific anti-CEA antibodies. Results show that CEA levels did not go down on the MC38-CEA tumors and no detectable anti-CEA antibodies were in the serum. Since this study was so short, it would make sense that a robust B-cell response had not yet occurred to produce anti-CEA antibodies. Another explanation would be that since this study was conducted in CEA.Tg mice, the mice are already tolerized to CEA as a self-antigen and therefore would not produce anti-CEA antibodies.

Previous mouse models used to demonstrate mFcγR driven tumor control were conducted with B16F10 melanoma cells in a lung metastasis model. Therefore, we switched our mouse model to B16F10 cell lines that stably expressed CEA and inoculated them via tail vein for lung metastases. The lung metastasis model has a greater discrepancy in outcomes between treatment options and was useful for optimization tumor model and treatments. Preliminary studies with the three different B16CEA cell lines suggested that B16CEA F metastasized to the lung most similarly to B16F10s

whereas B16CEA B and D were less fit. Unfortunately, B16CEA F lung metastases that were treated with antibody monotherapies of either sm3E mIgG2a or TA99 mIgG2a, which both bind to the cell line, were not controlled, in stark contrast to normal B16F10s when treated with TA99 mIgG2a[3]. When B16CEA F lung metastases were treated with Fc/IL-2 or the combination therapy of Fc/IL-2 and sm3E mIgG2a, there was a decrease of lung metastases compared to the PBS controls. These results suggested that combination therapy of antibody with Fc/IL-2 or a long serum half-life IL-2 molecule would be able to demonstrate slowed tumor growth.

The tumor model was switched to a subcutaneous model since all previous antibody combination treatments with long serum half-life IL-2 molecules were conducted in this format. The subcutaneous models showed that the B16CEA F cell line was incredibly difficult to control even with the combination treatment, but the B16CEA B cell line demonstrated some efficacy. Replicates of the combination treatment on B16CEA B with the dsSSMSA-Fn3 suggested that some dsSSMSA-I, dsSSMSA-IV1, and dsSSMSA-IV2 treated mice had significantly delayed or controlled tumor growth. Interestingly, dsSSMSA-II combination treatment also appeared to have a few controlled tumors, along with the MSA/IL-2 only treatment. The combination therapy with MSA/IL-2 confounded much of the results since treatment with only MSA/IL-2 demonstrated efficacy and therefore efficacy from the combinations could just be due to the addition of MSA/IL-2 and not the dsSSMSA-Fn3 constructs.

In order to work with a simpler model, monotherapies in very aggressive dosing regimens were given to mice inoculated subcutaneously with B16CEA B tumors. In this case, all tumors were expected to grow out, except at different rates. When treated with sm3E mIgG2a antibody only, tumor growth is delayed as compared to the PBS negative control. The dsSSMSA-Fn3 constructs that bind to the activating receptors dsSSMSA-I, dsSSMSA-III, dsSSMSA-IV1, and dsSSMSA-IV2 all seemed to delay tumor growth as compared to the vehicle control PBS and the negative control

dsSSMSA-L. The dsSSMSA-II monotherapy does not control tumor growth since it binds to the inhibitory receptor. All of the treatments that showed efficacy appear to behave similarly except for dsSSMSA-III which decreased tumor growth compared to the controls but did not work as well as the others. This could be due to the fact that the Fn3 binder has a lower binding affinity to the mFcγRIII. Technically all of the Fn3 binders to the activating receptors have very high A/I ratios, since they do not cross-react with the inhibitory receptor. This appears to agree with the A/I ratio hypothesis in that as long as there is decreased binding to the inhibitory receptor, interaction with any of the activating receptors and drive tumor control. The data from the tumor control studies with the monotherapy suggests that all of the activating mFcγRs behave in a similar fashion regarding tumor control, which also agrees with the phagocytosis data.

Although the prophylactic treatment of subcutaneous tumors with sm3E mIgG2a antibody or the dsSSMSA-Fn3 constructs demonstrated decrease in tumor growth, the results were not as drastic as previously published TA99 mIgG2a antibody treatment[7]. Multiple factors could explain the differences in results, one of which could be that the tumor inocula for our study is one order of magnitude larger ($5x10^5$ B16CEA B cells) than the amount that Nimmerjahn *et al.* used ($5x10^4$ B16F10 cells). We used this higher number because the B16CEA B cells were less fit than the B16F10 cells and were harder to establish even in CEA.Tg mice. Another factor could be that since we were using CEA.Tg mice, the endogenous CEA was acting as a sink by binding a large percentage of our constructs before they could reach the tumor. Performing pharmacokinetic studies in the CEA.Tg mice with our constructs tested this hypothesis. Preliminary studies suggested that our constructs clear faster in CEA.Tg mice as compared to C56BL/6 mice. This could also be due to the fact that CEA is known to shed, which could also act as another sink for our therapeutics[8]. Our mouse model demonstrated the potential of our constructs to drive tumor

control, but suggests that CEA as a target antigen is not the best at promoting anti-tumor responses driven by mFcγR.

Materials and methods

Proteins

Proteins were prepared as mentioned previously in Chapter 3. TA99 mIgG2a antibodies in addition to sm3E mIgG2a antibodies were purified using Protein A resin (Genscript) per manufacturer's protocol. All proteins were tested with an Endpoint Chromogenic LAL assay (Lonza) for endotoxin levels. All endotoxin units (EU) in the proteins were measured to be less than 0.1 EU before injection in mice.

Proteins used for the pharmacokinetic (PK) study are fluorescently labeled with IRDye 800 CW (LI-COR Biosciences) through a NHS-esther reaction mechanism. Proteins used for the biodistribution study are fluorescently labeled with Alexa Fluor 647 dye (Invitrogen) through the same non-specific NHS-esther reaction mechanism.

Pharmacokinetic Study

C56BL/6 or CEA.Tg mice were injected intraperitoneally with 140 μg of labeled dsSSMSA-Fn3 or 100 μg of labeled antibody. Time points are measured by taking samples of blood at the tip of the tail immediately after injection at 0 hour and then subsequent hours after at 1, 3, 5, 8, 12, hrs and then at 1, 2, 3, 4, and 5 days after injection. Fluorescent readings are read on the Odyssey scanner (LI-COR Biosciences) and taken on serum only. All readings are normalized to the highest reading and fit to: $C(t) = Ae^{-\alpha t} + Be^{-\beta t}$. All PK studies were conducted in triplicate with three separate mice.

Biodistribution

Albino C56BL/6 mice were injected subcutaneously with $5x10^6$ MC38CEA cells in the right flank and $5x10^6$ MC38 cells in the left flank on day 0. On day 14, mice are dosed with fluorescently labeled dsSSMSA-Fn3 and imaged on the IVIS Spectrum-bioluminescent and fluorescent imaging system (Xenogen Corporation). Images are taken at 4, 8 and 24 hours after injection. Mice are euthanized after the 24 hour time point and tumors are then harvested and frozen at -80°C. Tumors are then thawed on ice in the dark. Approximately 100 mg of each tumor is added to 500 μL of cold 1xPBS and disassociated using zirconium beads (KSE scientific). Samples are read on a plate reader in 384-well black microplates. The plate was read under fluorescence readings with excitation at 650 nm and emission read at 665 nm.

Subcutaneous tumor model

For the MC38CEA subcutaneous model, CEA.Tg mice are injected subcutaneously with $1x10^6$ cells. Mice were treated with 100 μL PBS as a vehicle control, 200 μg of sm3E mIgG2a as a positive control, and 140 μg of dsSSMSA-L as a negative control. Experimental categories were only conducted with dsSSMSA-I, dsSSMSA-IV1, and dsSSMSA-IV2 with doses of 140 μg each. Dosing was every other day starting on day 0 and ending on day 12. Mice were euthanized and the experiment was ended at day 14.

For the combination therapy subcutaneous model, CEA.Tg mice were injected subcutaneously with either $1x10^6$ B16CEA B or B16CEA F cells. Mice were treated, with 5 mice per group, with PBS as a negative control, 30 μg of MSA/IL-2 only, 30 μg of MSA/IL-2 and 200 μg of sm3E mIgG2a as a positive control, 30 μg of MSA/IL-2 and 200 μg of TA99 mIgG2a as another positive control, and 30 μg of MSA/IL-2 and 140 μg of dsSSMSA-Fn3. Doses were given after

tumor injection on day 6, 12, 18, 24, and 30. Rechallenged tumors were given subcutaneously on the opposite flank of either $1x10^5$ B16CEA B or B16CEA F cells.

The subcutaneous tumor model for the prophylactic monotherapy was conducted with B16CEA B cells only. CEA.Tg mice, with 5 mice per group, were injected subcutaneously with $5x10^5$ B16CEA B and treated with either PBS as a vehicle control, 200 μg of sm3E mIgG2a as a positive control, and 140 μg of dsSSMSA-Fn3. Doses were given on day 0, 2, 4, 7, 9, 11, 14, 16, and 18 after tumor inoculation. All mice were euthanized after tumor size reached greater than 10 mm in width and length.

Lung metastasis model

The three different B16CEA lines B, D, and F were injected intravenously through tail vein at $1x10^6$ cells unless otherwise noted. Cells were allowed to metastasize in the lungs for two weeks (14 days) before euthanasia and analysis of the lungs. Lungs were harvested and fixed in Fekete's solution before imaged. B16CEA F cells were injected via tail vein at $5x10^5$ cells per mouse and then treated with 200 μg of either sm3E mIgG2a or 200 μg TA99 mIgG2a on days 0, 2, 4, 7, 9, and 11. Mice were euthanized on day 14 and lungs were harvested and fixed with Fekete's solution. For Fc/IL-2 combination treatment with sm3E mIgG2a, $5x10^5$ B16CEA F cells were tail vein injected and allowed to metastasize to the lung. Mice were either not treated, treated with 25 μg of Fc/IL-2 only on day 1, or treated with 25 μg of Fc/IL-2 on day 1 and 200 μg sm3E mIgG2a on days 1, 3, 5, 7, 9, and 11, with 5 mice per group. Mice were euthanized on day 14 and lungs were harvested and fixed in Fekete's solution.

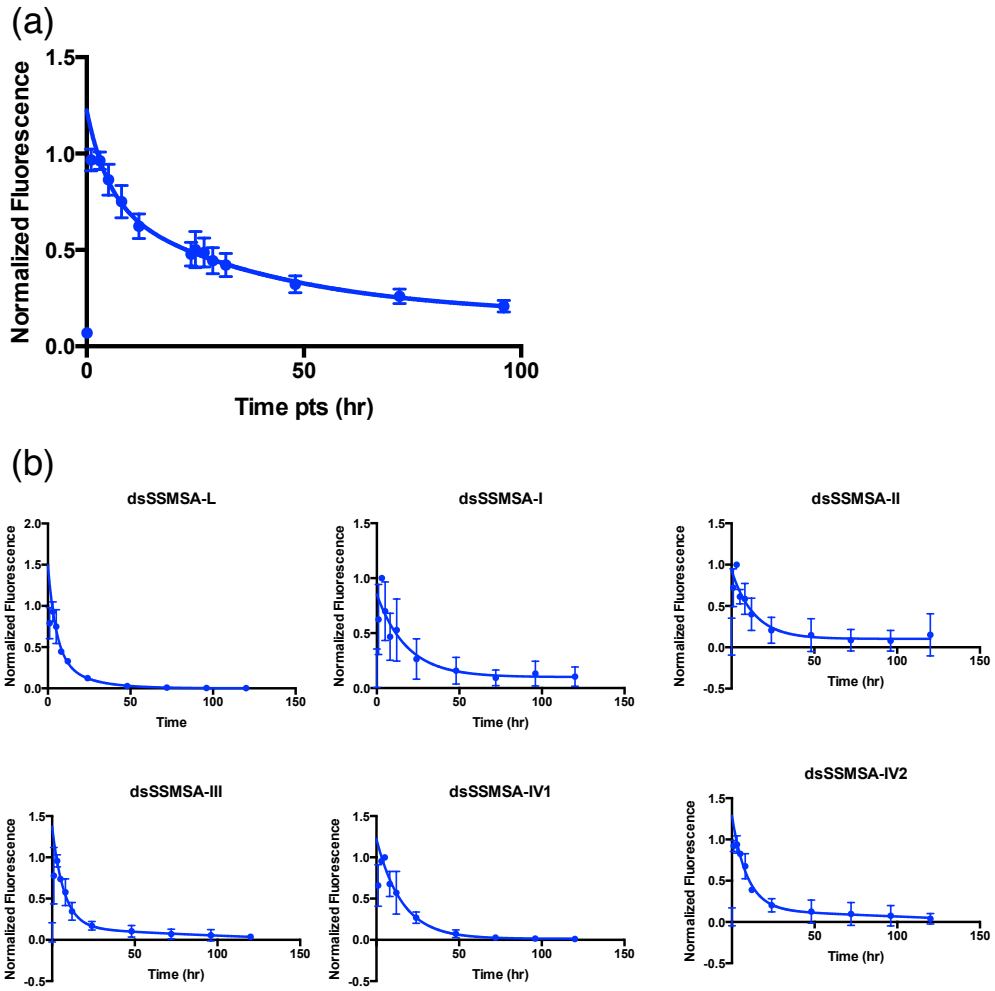

Figure 4-1: Pharmacokinetic Studies of dsSSMSA-Fn3 Constructs

(a) The pharmacokinetics of dsSSMSA-Fn3 constructs were tested in C56BL/6 mice. Constructs were injected intraperitoneally and time points were taken via the tail. (b) The pharmacokinetics of the individual dsSSMSA-Fn3 constructs in triplicate in CEA.Tg mice. Constructs were injected intraperitoneally and time points were taken via the tail.

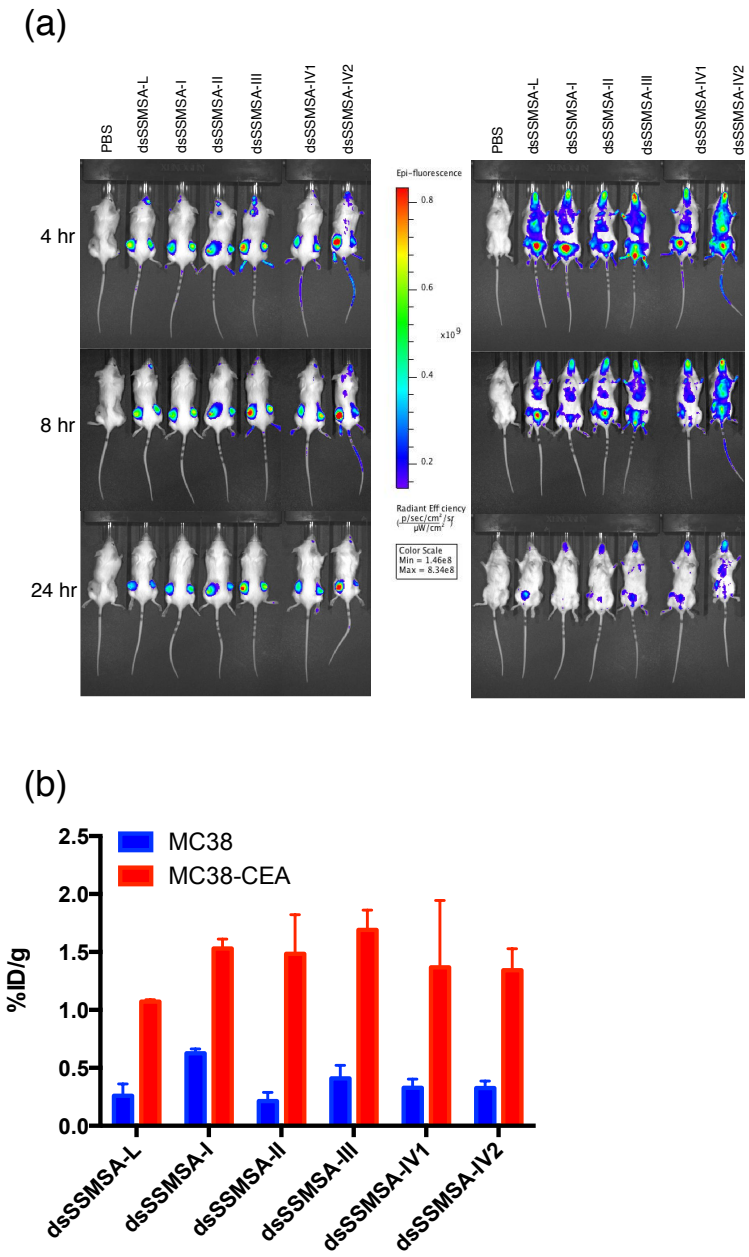

Figure 4-2: Biodistribution of dsSSMSA-Fn3 Constructs

(a) IVIS imaging of C56BL/6 albino mice injected retro-orbitally with dsSSMSA-Fn3 constructs labeled with Alexa Fluor 647. Times imaged were at 4, 8, and 24 hours after injection. MC38-CEA (antigen positive) tumors on the right flank and MC38 (antigen negative) tumors on the left flank. Left images are taken on the dorsal side of the mice and images on the right are taken of the ventral side of the mice. (b) Percent injected dose per gram of injected dsSSMSA-Fn3 construct in antigen negative tumors MC38 (blue) versus antigen positive tumors MC38-CEA (red).

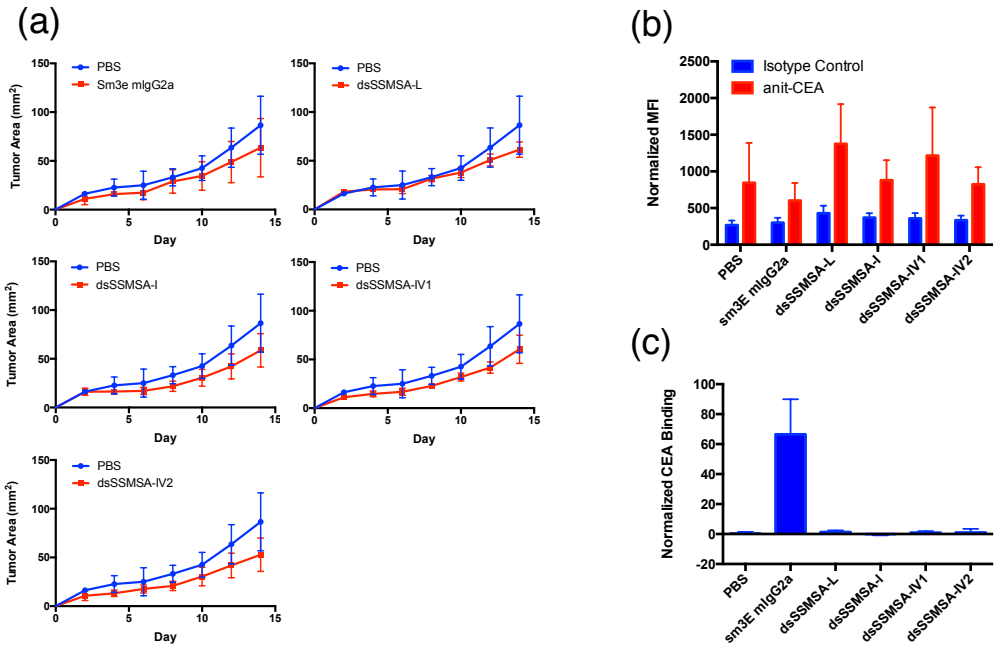

Figure 4-3: MC38-CEA tumor model

(a) MC38-CEA tumors injected subcutaneously in CEA.Tg mice and treated with PBS as a vehicle control or sm3E mIgG2a, dsSSMSA-L, dsSSMSA-I, dsSSMSA-IV1, or dsSSMSA-IV2. No statistical difference between the growth curves. (b) Detection of CEA expression on harvested subcutaneous tumors. All levels greater than or equivalent to that of the PBS control. (c) Testing serum of treated mice for anti-CEA antibodies. Serum samples were used to stain MC38 cells and MC38-CEA cells. MC38-CEA staining was normalized over MC38 staining. Only mice treated with sm3E mIgG2a had detectable levels of anti-CEA antibodies, most likely from residual antibody in the blood after treatment.

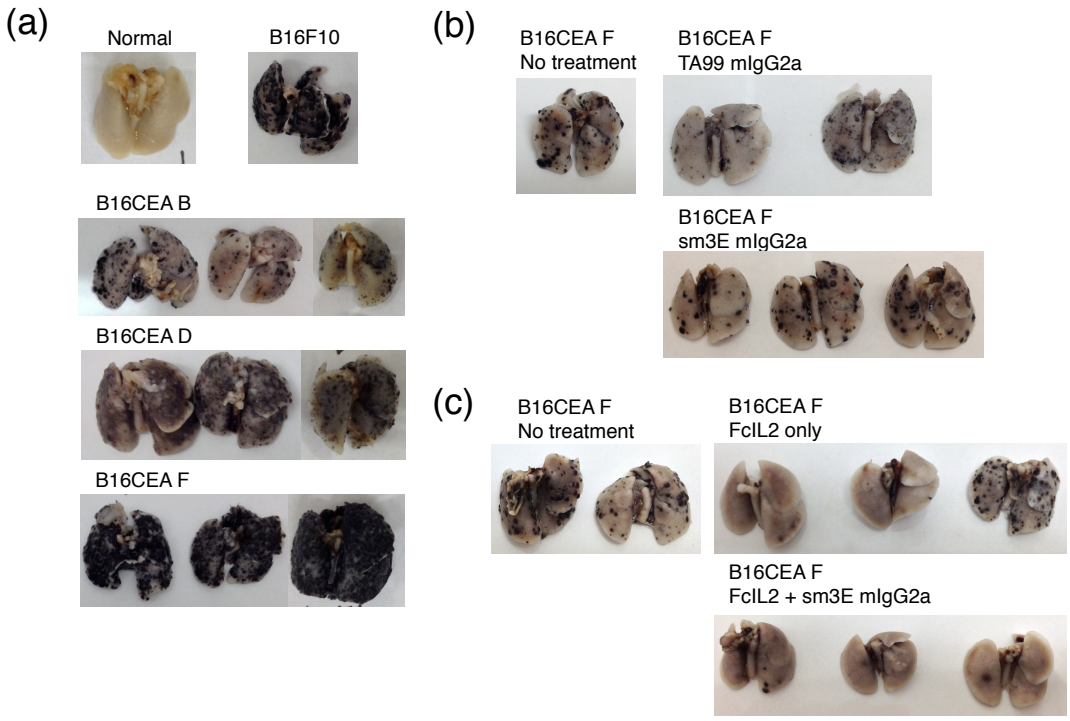

Figure 4-4: B16CEA Mouse Model

Optimization of the B16CEA mouse model. (a) Mice were injected via tail vein with $1x10^6$ cells of B16CEA B, D, or F and compared to the normal B16F10 cell line. In terms of lung metastases, B16CEA B < D < F nodules. B16CEA F lung metastases most resemble the normal B16F10 lung metastases. (b) B16CEA F cells were injected via tail vein at $5x10^5$ cells and treated with TA99 mIgG2a or sm3E mIgG2a. (c) B16CEA F cells were injected via tail vein at $5x10^5$ cells and treated with Fc/IL-2 only or Fc/IL-2 in combination with sm3E mIgG2a.

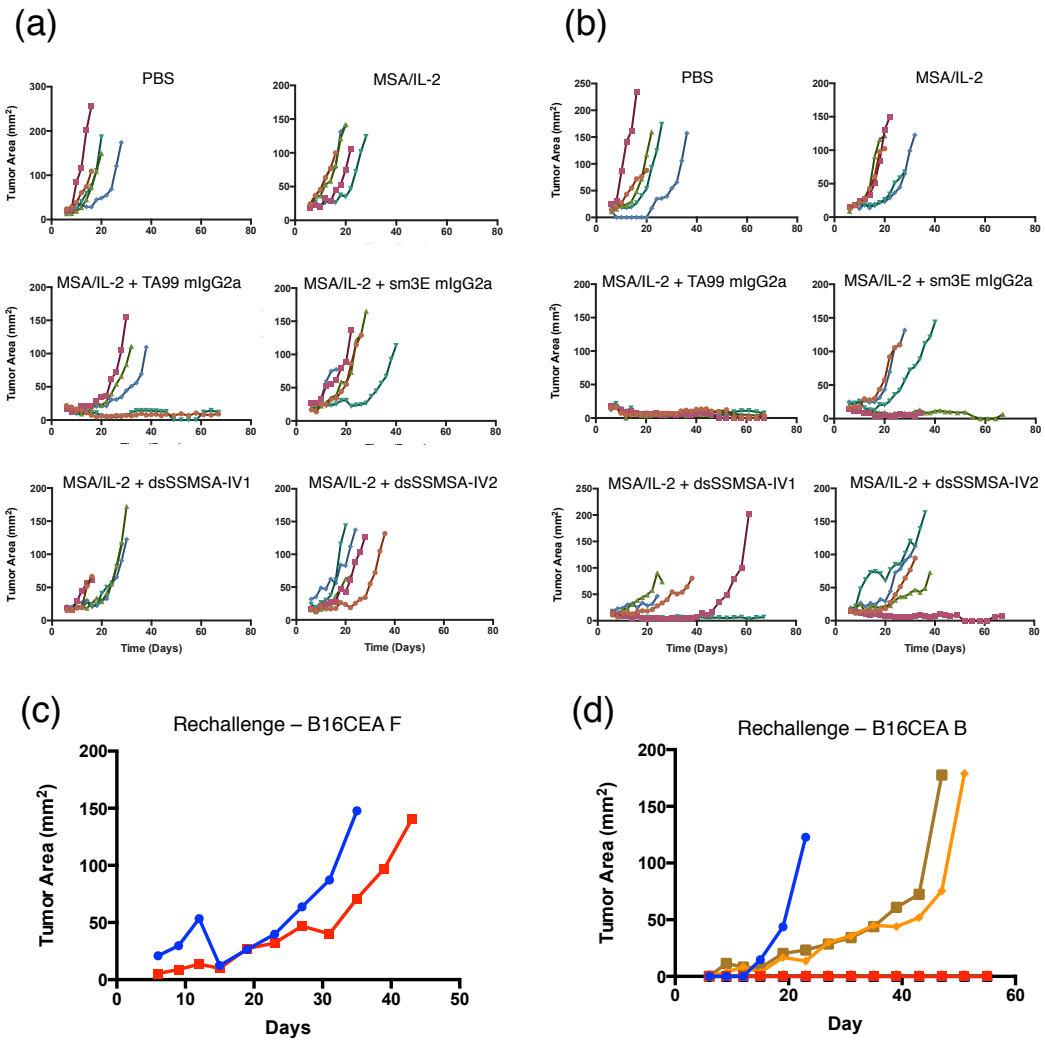

Figure 4-5: Initial Combination Treatment on B16CEA F and B Tumors

Testing MSA/IL-2 combination treatments on B16CEA F and B cells. (a) B16CEA F tumors treated with PBS, MSA/IL-2 only, or combinations of MSA/IL-2 and TA99 mIgG2a, sm3E mIgG2a, dsSSMSA-IV1, and dsSSMSA-IV2. (b) B16CEA B tumors treated with PBS, MSA/IL-2 only, or combinations of MSA/IL-2 and TA99 mIgG2a, sm3E mIgG2a, dsSSMSA-IV1, and dsSSMSA-IV2. (c) Mice with controlled B16CEA F tumors were rechallenged with $1x10^5$ B16CEA F cells in the opposite flank. (d) Mice with controlled B16CEA B tumors were rechallenged with $1x10^5$ B16CEA B cells in the opposite flank.

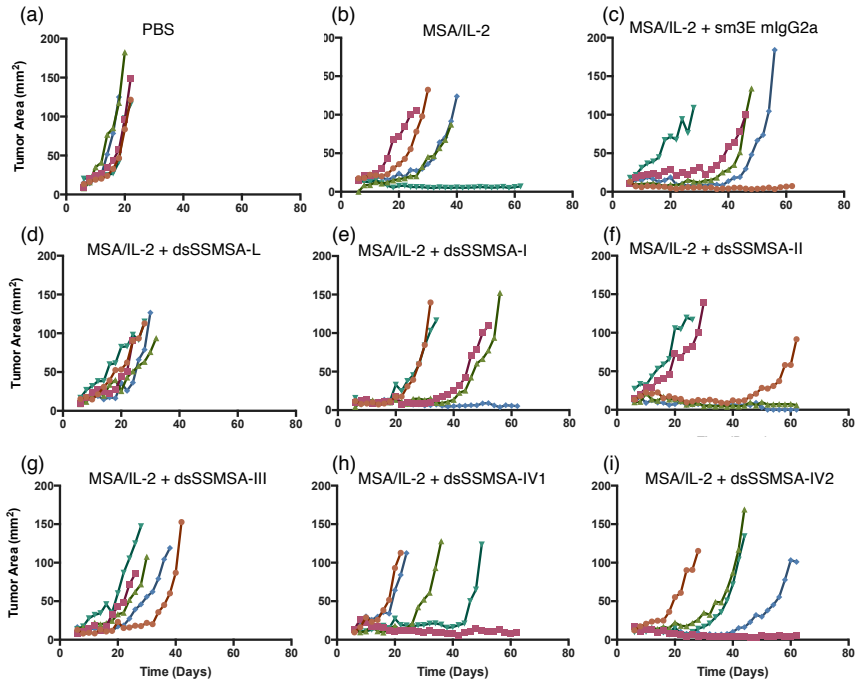

Figure 4-6: Combination MSA/IL-2 Treatment with dsSSMSA-Fn3

Expanded mouse study with all dsSSMSA-Fn3. B16CEA B cells were injected subcutaneously at $1x10^6$ cells per mouse and measured starting on day 6. (a) PBS as the vehicle control (b) MSA/IL-2 only as a negative control (c) MSA/IL-2 in combination with sm3E mIgG2a as the positive control and (d) MSA/IL-2 + dsSSMSA-L as a negative control (e)-(i) different dsSSMSA-Fn3 combination treatments for each group of mice.

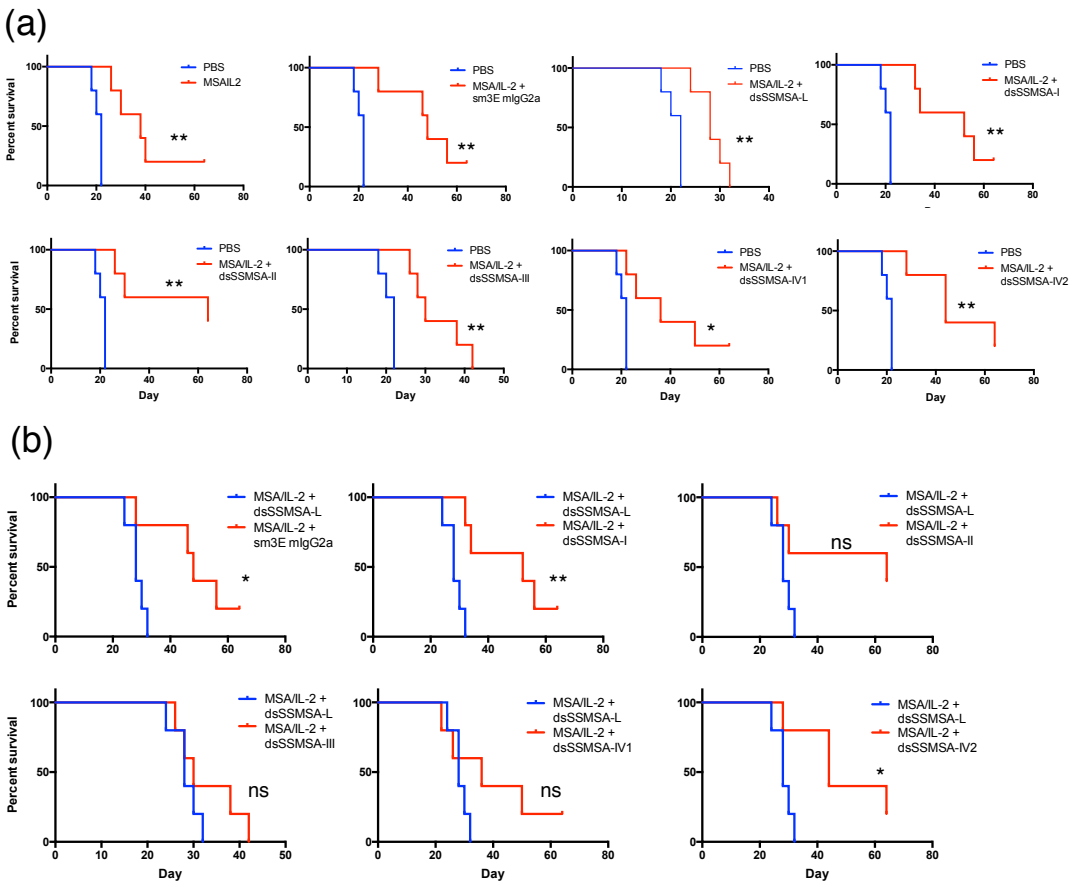

Figure 4-7: Survival Curves of MSA/IL-2 Combination Treatments

(a) Survival curves of the different treatments as compared to PBS. All treatments are considered statistically different from PBS. (b) Different treatments as compared to the negative control MSA/IL-2 + dsSSMSA-L. Only MSA/IL-2 combination treatments with sm3E mIgG2a, dsSSMSA-I, or dsSSMSA-IV2 are considered statistically significant. * p-value < 0.05, ** p-value < 0.01, ns p-value > 0.05

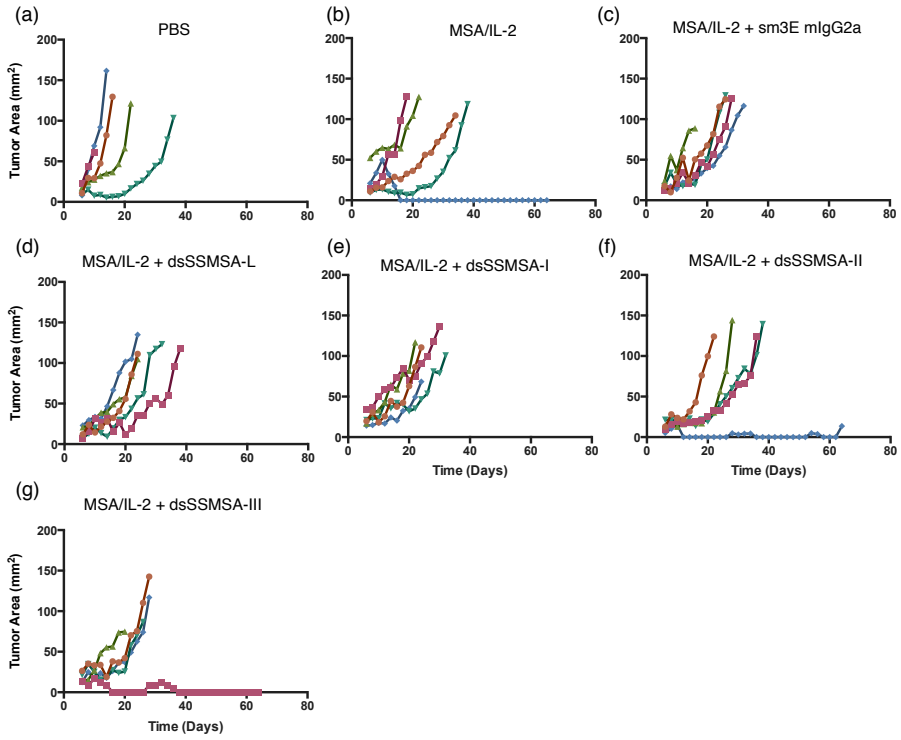

Figure 4-8: Combination MSA/IL-2 Treatment

The third replicate of the MSA/IL-2 combination treatment were conducted on slightly older mice approximately 11-12 weeks old. (a) PBS as the vehicle control (b) MSA/IL-2 only as a negative control (c) MSA/IL-2 in combination with sm3E mIgG2a as the positive control and (d) MSA/IL-2 + dsSSMSA-L as a negative control (e)-(g) different dsSSMSA-Fn3 combination treatments for each group of mice. Almost all tumors grew out except for 1 out of 5 in MSA/IL-2 treated mice, 1 out of 5 in MSA/IL-2 + dsSSMSA-II treatment, and 1 out of 5 in MSA/IL-2 + dsSSMSA-III.

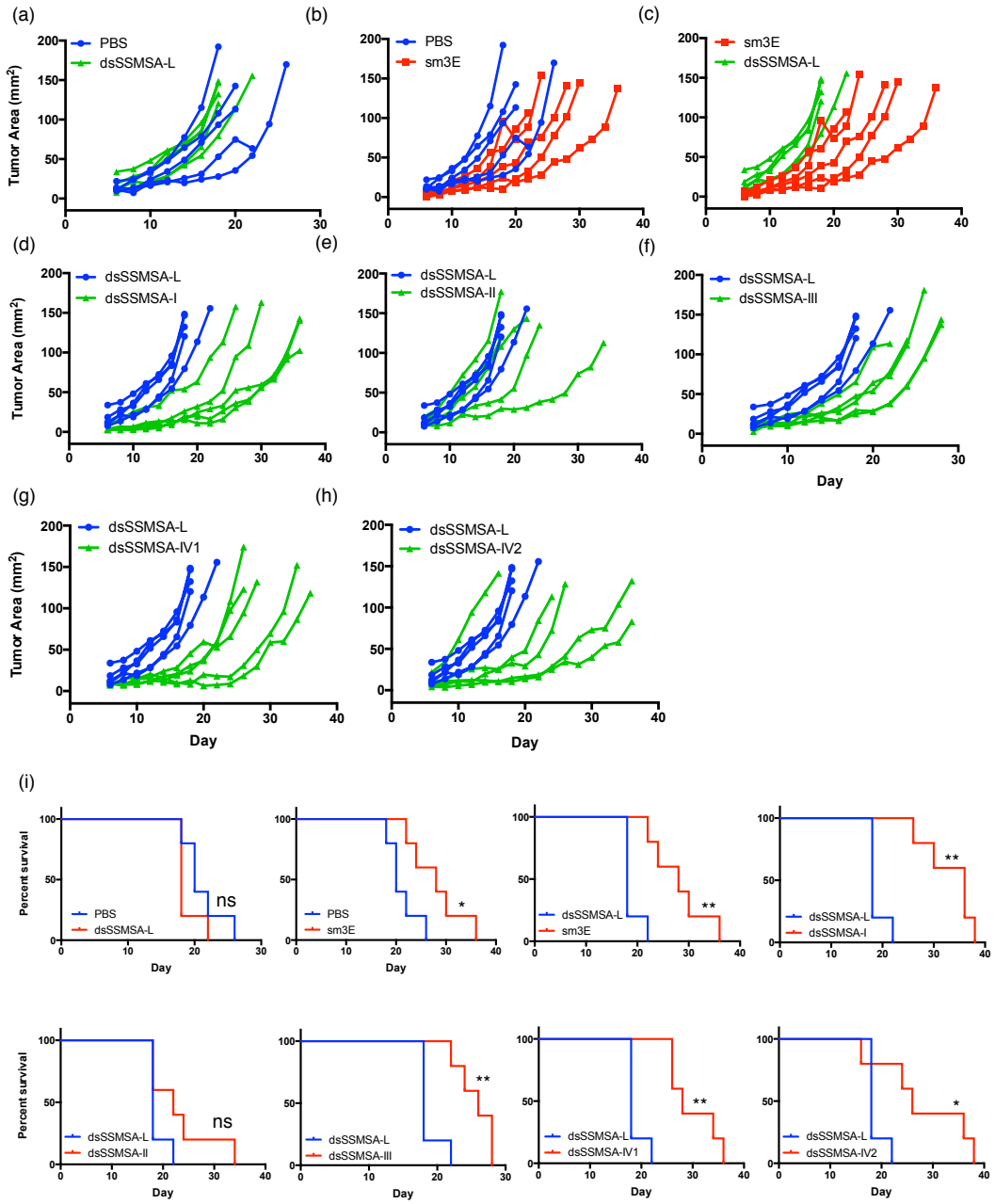

Figure 4-9: Subcutaneous B16CEA B Tumors with Prophylatic Treatment

Mice were inoculated subcutaneously with B16CEA B tumors and treated on the day of tumor injection. PBS was used as the vehicle control, sm3E mIgG2a as the positive control, and dsSSMSA-L as a negative control. (a) and (b) Comparison of tumor growth curves of PBS treated mice to the negative control, dsSSMSA-L and positive control sm3E mIgG2a, respectively. (c) Comparison of tumor growth curves of the negative and positive controls. (d)-(h) Tumor growth curves of different dsSSMSA-Fn3 treatments compared to the control dsSSMSA-L. (i) survival curves of the different treatments as compared to the controls: PBS and dsSSMSA-L. * p-value < 0.05, ** p-value < 0.01, ns p-value > 0.05

References

1. Clynes, R. A., Towers, T. L., Presta, L. G. & Ravetch, J. V. Inhibitory Fc receptors modulate in vivo cytoxicity against tumor targets. *Nat. Med.* **6,** 443–446 (2000).
2. Weng, W.-K. & Levy, R. Two immunoglobulin G fragment C receptor polymorphisms independently predict response to rituximab in patients with follicular lymphoma. *J. Clin. Oncol. Off. J. Am. Soc. Clin. Oncol.* **21,** 3940–3947 (2003).
3. Nimmerjahn, F. & Ravetch, J. V. Divergent Immunoglobulin G Subclass Activity Through Selective Fc Receptor Binding. *Science* **310,** 1510–1512 (2005).
4. Otten, M. A. *et al.* Experimental Antibody Therapy of Liver Metastases Reveals Functional Redundancy between FcγRI and FcγRIV. *J. Immunol.* **181,** 6829–6836 (2008).
5. Bevaart, L. *et al.* The High-Affinity IgG Receptor, FcγRI, Plays a Central Role in Antibody Therapy of Experimental Melanoma. *Cancer Res.* **66,** 1261–1264 (2006).
6. Smith, P., DiLillo, D. J., Bournazos, S., Li, F. & Ravetch, J. V. Mouse model recapitulating human Fcγ receptor structural and functional diversity. *Proc. Natl. Acad. Sci.* **109,** 6181–6186 (2012).
7. Nimmerjahn, F. *et al.* FcγRIV deletion reveals its central role for IgG2a and IgG2b activity in vivo. *Proc. Natl. Acad. Sci. U. S. A.* **107,** 19396–19401 (2010).
8. Watson, S. A. *et al.* Inhibition of tumour growth by marimastat in a human xenograft model of gastric cancer: relationship with levels of circulating CEA. *Br. J. Cancer* **81,** 19–23 (1999).

CHAPTER 5: CHARACTERIZATION OF ENGINEERED AGLYCOSYLATED ANTIBODY VARIANTS THAT ENGAGE WITH HUMAN FC GAMMA RECEPTORS

Introduction

The majority of current monoclonal antibody therapies against human cancers are of human IgG1 isotype (hIgG1). There are various different mechanisms of action that contribute to the efficacy of the current broad range of antibody therapies. One of which, that has emerged is through antibody effector function by which the antibody Fc interacts with FcγR on immune cells and promote anti-tumor responses through multiple immune mechanisms i.e. antibody dependent cellular cytotoxicity (ADCC), antibody dependent cellular phagocytosis (ADCP), etc[1–3].

The human IgG1 isotype interacts with and stimulates signaling when cross-linking human FcγRI, FcγRIIA, FcγRIIB, and FcγRIIIA[4]. Similar to the mouse receptors, the human FcγR (hFcγR) are separated into two groups, the activating FcγRs, which signal through ITAMs and an inhibitory FcγRIIB that signals through ITIMs. The human receptors have polymorphisms that impact clinical efficacy of the antibody therapeutic, which are dependent on the binding affinity to the Fc of hIgG1[5–7]. It is widely known that aglycosylated antibodies or loss of glycosylation at the N-linked glycosylation site at asparagine 297 (N297) of the Fc resulted in loss of binding to the hFcγR and loss of effector function[8,9]. Previously in our lab, we engineered variants of aglycosylated antibodies that recovered binding to hFcγRIIA and hFcγRIIB and found that variant S298G/T299A (SGTA) restored binding affinity to both polymorphisms of hFcγRIIA167R/H and hFcγRIIB to close to wild-type or higher binding affinity[10].

Literature suggests that therapeutic efficacy of clinical antibodies strongly correlates with the allelic form of hFcγRIIIA. The hFcγRIIIA176V variant binds to hIgG1 with higher affinity than the hFcγRIIIA176F variants, and patients have better response rates[5,6,11]. Building upon previous work, hIgG1 aglycosylated variants were engineered to recover binding to hFcγRIIIA along with binding

to the other hFcγRs. Initial aglycosylated Fc screening was focused on engineering the C'/E loop, which contains the N-linked glycosylation site along with FcγR contact residues. In this new round of screening, saturation libraries of the lower hinge, B/C loop, and F/G loop were screened in a glycosylated background using full-length hIgG1 variants in a yeast secretion and surface capture system. Variants were screened against the lower affinity hFcγRIIIA176F allele since it represents more stringent criteria for screening. From the yeast screens, only variants in the BC loop and FG loop were enriched. Further binding studies from isolated HEK secretions suggested that two main F/G loop variants, K326I/A327Y/L328G (IYG) and K326I/A327E/L328E (IEA) contributed greatly to the increase of binding to hFcγRIIIA176F.

Since these screens were initially on a glycosylated background, these F/G loop variants were transferred onto an aglycosylated background of T299A and characterized for binding. The IYG aglycosylated mutant bound hFcγRIIIA176F to a slightly greater degree than wild-type hIgG1, whereas the IEA aglycosylated mutant bound hFcγRIIIA176F to a slightly lesser degree, and both variants showed detectable binding to hFcγRIIIA176V, hFcγRIIA167R, and hFcγRIIB. In order to restore binding of aglycosylated hIgG1 to the panel of low-affinity hFcγRs the K326I/A327Y/L328G (IYG) F/G loop variant was combined with different C'/E loop variants previously isolated. Aglycosylated double mutants, N297D/S298T (DTT), N297D/S298A (DAT), and N297H/S298A (HAT) that were previously isolated had weak binding to hFcγRIIIA176V, but no detectable binding to hFcγRIIA167R. Preliminary binding profiles of these aglycosylated variants suggest that DTT-IYG, DAT-IYG, and HAT-IYG have relatively similar binding to both alleles of hFcγRIIIA but have varying degrees of binding to hFcγRIIA and the inhibitory hFcγRIIB. T299A/IYG on the other hand had detectable binding to all of the of the low affinity hFcγRs. In this study we further characterize all of these aglycosylated mutants and perform phagocytosis assays

with them to demonstrate biological activity. We also developed a mathematical model to explain the contributions of each type of receptor to their efficacy in our system.

Results

Characterization of aglycosylated variants with improved binding to FcγRIIA and FcγRIIIA

The original hIgG1 variants were isolated as full antibodies in the yeast secretion and surface capture assay with a 4m5.3 variable region, which binds to fluorescein isothiocyanate with femtomolar binding affinity. These were then switched out with the TA99 variable region, which binds to the model melanoma tumor antigen TRP-1. The aglycosylated variants exhibit higher mobility on a reducing SDS-PAGE gel, as compared to the glycosylated wild-type heavy chain (Figure 5-1a). All aglycosylated TA99 variants in addition to the wild-type hIgG1 antibody run at the expected molecular weight on size-exclusion chromatography with less than 0.5% of high molecular weight species (Figure 5-1b). Samples were analyzed with dynamic light scattering (DLS) to characterize protein stability. Variants had a hydrodynamic radius from the range of 5.1-5.6 nm (Figure 5-1c), which is within the range of reported hydrodyanmic radii 5-6 nm of normal monoclonal antibodies[12]. The majority of the variants are monodisperse with a % polydispersity of < 20% when analyzed two days after purification. When protein preparations are allowed to remain at 4°C for an extended period of time (approximately 2 weeks), % polydispersity levels tend be higher. This suggests that some of the aglycosylated variants might not be very stable for extended periods of time unlike wild-type glycosylated antibodies. All other characteristics of the aglycosylated hIgG1 variants seem to suggest that they behave similarly to wild-type antibodies.

Binding affinities of these aglycosylated variants to human FcγRI, FcγRIIA167H, FcγRIIA167R, FcγRIIB, FcγRIIIA176F, and FcγRIIIA176V were determined on Biacore. Wild-type antibody has approximately 3 nM binding to FcγRI and low levels of binding in the single-digit μM

range for all of the remaining low-affinity FcγRs (Table 5-1) in agreement with literature[4]. As expected the N297Q aglycosylated variant showed no detectable binding to the low affinity FcγRs and decreased binding by two orders of magnitude to the high-affinity FcγRI. The S298G/T299A (SGTA) variant only has detectable binding to the FcγRIIA and FcγRIIB receptors and not the FcγRIIIA receptor, in agreement with previous data[10]. Since SGTA is on an aglycosylated background, it has approximately the same binding affinity as the aglycosylated N297Q variant to FcγRI. The K326I/A327Y/L328G (IYG) F/G loop variant was isolated based on screens against FcγRIIIA176F and therefore the when combined with various C'/E loop aglycosylated variants are expected to retain binding to FcγRIIIA with various degrees of binding to the other FcγRs. The N297D/S298T/K326I/A327Y/L328G (DTT-IYG) variant has no detectable binding to FcγRIIA167H or FcγRIIB, but has approximately 1-3 μM binding affinity to both allelic variants of FcγRIIIA and FcγRIIA167R. Interestingly, although aglycosylated, DTT-IYG has restored binding to FcγRI with a measured binding affinity of 5 nM. The N297D/S298A/K326I/A327Y/L328G (DAT-IYG) variant displays single-digit μM binding affinity to both allelic variants of FcγRIIIA. This variant also has binding to the inhibitory FcγRIIB and slight binding to FcγRIIA167R, though no detectable binding to the FcγRIIA167H variant. DAT-IYG has reduced binding to FcγRI of approximately one order of magnitude at 29 nM, but is still one order of magnitude better than the aglycosylated N297Q mutant. In preliminary binding studies, the N297H/S298A/K326I/A327Y/L328G (HAT-IYG) mutant displayed the most reduced binding for FcγRIIA and FcγRIIB, and was the most FcγRIIIA specific. In the Biacore studies, it suggests that the HAT-IYG variant has no detectable binding to both allelic variants of FcγRIIA or FcγRIIB, but has approximately 1-2 μM binding affinity to both allelic variants of FcγRIIIA. The last aglycosylated variant T299A/K326I/A327Y/L328G (299A-IYG) has restored binding to all of the

low affinity FcγRs with either wild-type or improved binding affinity. The binding affinity of 299A-IYG to the high-affinity FcγRI is on the same order of magnitude of N297Q, suggesting that binding to FcγRI was not restored. With this panel of aglycosylated variants we now have restored binding to the low affinity FcγR to wild-type or better affinities, along with different combinations of binding characteristics.

Aglycosylated variants promote phagocytosis of tumor cells

In order to determine if these aglycosylated variants displayed biological activity along with their restored binding to the various human FcγR, we conducted a phagocytosis assay. Initial phagocytosis was performed using monocytes isolated from human peripheral blood. B16F10 melanoma cells were incubated under different conditions, with or without antibodies and then combined with the isolated monocytes. Monocytes were identified by staining with an anti-CD14 antibody and analyzed on flow cytometry. Results show that DTT-IYG, DAT-IYG, HAT-IYG, and 299A-IYG aglycosylated constructs have increased phagocytosis levels over the basal level of phagocytosis of only B16F10 cells incubated with monocytes, labeled as cells only (Figure 5-2a). From this initial phagocytosis assay, it appears that the DTT-IYG construct has comparable phagocytosis levels to that of wild-type glycosylated hIgG1.

Subsequent phagocytosis assays were conducted with macrophages that were differentiated from monocytes isolated from human peripheral blood using GM-CSF. Macrophages that were either untreated or pre-treated with interferon gamma (IFN-γ) were combined with B16F10 cells that were preincubated with or without antibodies. Phagocytosis results with macrophages that were not pretreated with IFN-γ indicate that besides the wild-type glycosylated antibody, only the DTT-IYG and DAT-IYG constructs promote significant levels of phagocytosis above the negative controls of cells only and the aglycosylated variant with decreased binding to all FcγR, N297Q

(Figure 5-2b). Macrophages that were pre-treated with IFN-γ show increased phagocytosis of the SGTA, HAT-IYG, and 299A-IYG constructs that were originally undetectable with untreated macrophages. The DTT-IYG and DAT-IYG constructs show higher phagocytosis levels as compared to the wild-type glycosylated antibody (Figure 5-2c).

Phagocytosis was further confirmed using microscopy. Images were taken at a 20x magnification to visually validate the data obtained by flow cytometry. Cells only and N297Q treated cells show very little phagocytosis, whereas cells treated with wild-type antibody or DTT-IYG have high levels of phagocytosis. Aglycosylated variants SGTA, DAT-IYG, HAT-IYG and 299A-IYG show intermediate levels of phagocytosis (Figure 5-3a). Higher magnification at 60x visually confirms engulfment of tumor cells in macrophages on an individual cell level for samples treated with wild-type, SGTA, DTT-IYG, DAT-IYG, HAT-IYG, and 299-IYG antibodies (Figure 5-3b). Phagocytosis assays confirm restoration of biological activity in the new aglycosylated variants that initially lost their ADCP activity with loss of glycosylation as represented by the N297Q variant.

In vivo *activity of aglycosylated variants*

Aglycosylated variants were evaluated for proper *in vivo* characteristics and stability through pharmacokinetic (PK) studies. The PK of each antibody through intraperitoneal dosing was measured in triplicate (Figure 5-4a). The wild-type glycosylated antibody has the longest beta half-life of approximately 108 hours, whereas the aglycosylated antibodies N297Q, SGTA, DTT-IYG, DAT-IYG and 299A-IYG have similar beta half-lives ranging from approximately 70-90 hours. The aglycosylated variant HAT-IYG has a faster beta half-life of 54 hours, which suggests that it is slightly less stable than the other antibodies (Figure 5-4b). The PK studies suggests that the aglycosylated antibodies are slightly less stable than the wild-type glycosylated antibody, but still have fairly long beta half-lives that would allow them to be viable therapeutics.

Preliminary *in vivo* tumor control studies were conducted with select aglycosylated variants in mice transgenic for the human FcγR with the murine FcγR knocked out. The HAT-IYG and 299A-IYG constructs were initially chosen since HAT-IYG showed basically no binding to any of the FcγRIIA and FcγRIIB receptors and only binding to FcγRIIIA, for a maximum A/I ratio. The 299A-IYG variant was chosen because it restored binding to all of the low affinity human FcγR that was initially lost in the aglycosylated format. Antibody efficacy was determined by number of lung metastasis foci of the B16F10 cell line. Wild-type antibody has decreased numbers of foci as compared to the PBS control, unfortunately it appears the initial study shows no statistical decrease in tumor foci in the HAT-IYG and 299A-IYG treated mice as compared to PBS (Figure 5-5). It appears that HAT-IYG might control tumors slightly better than 299A-IYG, which could be because of its lack of binding to the inhibitory receptor FcγRIIB. Future studies will be carried out with aglycosylated variants DTT-IYG and DAT-IYG, since they showed better biological activity in phagocytosis assays.

Mathematical modeling of complete FcγR system

A mathematical model of phagocytosis was devised to understand the importance of each receptor in driving the phagocytosis of tumor cells. A previous model developed by the Georgiou group[13] to model the FcγRIIA167H, FcγRIIA167R and FcγRIIB contribution to phagocytosis was significantly modified and expanded to include all of the remaining FcγRs: FcγRI, FcγRIIIA176F, and FcγRIIIA176V. In clinical studies, therapeutic efficacy of antibodies correlated with their binding affinities to the allelic variant of FcγRIIIA[5,6]. By expanding the model to include all of the FcγR we can obtain a more complete representation of the driving force behind the phagocytosis results.

Our model represents the contact area of a tumor cell and a macrophage where phagocytosis is initiated (Figure 5-6a). In this system, antibody (Ab) can bind to the antigen (Ag) with an equilibrium constant of K_{Ab} to become bound antibody (B). Free FcγR (R_f) can diffuse into the contact volume to become R_{cv}, and only FcγR in the contact volume (R_{cv}) can bind to bound antibody (B) with an equilibrium constant of K_R to form complexes (C). Only complexes (C) can dimerize with an equilibrium constant of K_{cross} to form dimers (D). The amount of dimers formed allows us to determine which FcγR play the major roles in signaling for phagocytosis.

Normalized dimer concentrations were plotted as heat maps for each aglycosylated construct (Figure 5-6b). Heat maps demonstrate that FcγRI is the major receptor in driving phagocytosis in our system. Only wild-type, DTT-IYG, and DAT-IYG antibodies promote increased phagocytosis in GM-CSF derived macrophages, and their FcγRI:FcγRI dimer concentration is of the highest reading in contrast to all of the other aglycosylated antibodies. These three constructs also have the higher FcγRI:FcγRIIIA dimer concentrations as compared to SGTA, which has none and HAT-IYG and 299A-IYG which have normalized dimer concentrations a level below that of the three constructs that promote phagocytosis.

If we look at the constructs individually, it appears that the wild-type glycosylated antibody has an increase in all possible dimer formations. The FcγRI:FcγRI is by far the highest concentration, and then the remaining FcγRI:FcγRIIA, FcγRI:FcγRIIB, and FcγRI:FcγRIIIA concentrations are roughly equivalent. From the heat map, it appears that FcγRIIB dimers with other FcγRs are of lower concentration and therefore probably play a lesser role in driving biological activity. The N297Q construct has no dimerization of the low affinity FcγRs and very low dimerization levels of FcγRI. This agrees with the fact that N297Q is aglycosylated and loses all binding to FcγR. The SGTA construct was engineered to only regain binding to FcγRIIA and

FcγRIIB and not FcγRIIIA. Therefore, the majority of its dimer concentrations are of FcγRI in complex with FcγRI, FcγRIIA, or FcγRIIB. The FcγRIIA and FcγRIIB dimers with each other are at lower levels. The DTT-IYG aglycosylated construct also mainly forms FcγRI:FcγRI dimers in addition to slightly lower levels of FcγRI: FcγRIIA167R and FcγRI:FcγRIIIA dimers. There are very few FcγRIIA167H and FcγRIIB dimers, which would agree with the fact that the DTT-IYG construct has no detectable binding to those two receptors. There are some FcγRIIIA:FcγRIIIA dimers, but most likely the FcγRI dimers are driving phagocytosis with this construct. The DAT-IYG construct is also mostly driven by FcγRI dimers, but also shows some FcγRIIIA dimers. It has very few FcγRIIA167H dimers, since it also had no measureable binding to that receptor. The HAT-IYG construct mainly has FcγRI:FcγRI dimers and a lower level of FcγRI: FcγRIIIA and FcγRIIIA:FcγRIIIA dimers. HAT-IYG has no detectable binding to both the activating and inhibitory FcγRII. The 299A-IYG constuct is unique in that it has restored binding to all of the low affinity FcγR as shown in the heat map of all the low affinity receptors, but for some reason does not drive phagocytosis. When observing the FcγRI: FcγRI dimer concentration level, it is lower than that of the wild-type glycosylated antibody and the DTT-IYG and DAT-IYG constructs. This could be the explanation for why 299A-IYG does not drive phagocytosis, since FcγRI appears to be the main receptor for this biological activity.

Discussion

In this study, we further characterized the aglycosylated constructs isolated previously. The variable regions of the aglycosylated antibodies were first swapped to the melanoma antigen TRP-1 targeting TA99. The antibodies were run on a SDS-PAGE gel, through SEC, and DLS to confirm proper size and stability. All of the constructs appeared to run as expected on the SDS-PAGE gel, with the glycosylated antibody running higher and having less mobility as compared to the

aglycosylated constructs. All constructs appeared to have similar SEC runs with few aggregates. Hydrodynamic radii of the aglycosylated antibodies were similar to that of a normal antibody and percent of polydispersity of the constructs were on average fairly low and considered monodisperse. It was observed that some of the aglycosylated antibodies tended to aggregate over time, which suggested slight instability as compared to that of wild-type glycosylated antibodies.

Previous binding studies of the aglycosylated constructs were conducted with yeast titrations and tetramers of FcγR. Label free binding affinity was measured between the aglycosylated antibodies and FcγR using Biacore. Measurements confirmed aglycosylated N297Q had no binding to low affinity FcγR and decreased binding to FcγRI. This construct was considered the baseline of aglycosylated antibodies, and the remaining mutants restored/improved binding to the FcγR. All of the aglycosylated variants had different binding patterns to the FcγRs. Interestingly, 299A-IYG restored binding to all of the low affinity FcγR and was expected to behave most similarly to wild-type glycosylated antibody. Phagocytosis data showed that only the aglycosylated variants DTT-IYG and DAT-IYG promoted phagocytosis by macrophages. This seemed counter to expected results, since all of the aglycosylated variants except for N297Q restored binding to FcγR, so it would be assumed that all would promote some level of phagocytosis.

In order to understand the phagocytosis results better, a mathematical model of phagocytosis was modified to represent all of the FcγR. Quantified binding affinities were used as parameters in the model of phagocytosis. The model output suggested that FcγRI was the main driving force of phagocytosis. All three constructs that promoted phagocytosis had higher binding affinity to FcγRI as compared to N297Q. Other studies suggest that the other low affinity FcγRIIA and FcγRIIIA also play a role in phagocytosis, but in our studies we saw most of the biological

activity driven by FcγRI. Perhaps if binding affinities to these other FcγR were increased above that of wild-type, they would play a larger role.

Pharmacokinetic studies of the aglycosylated variants were conducted and all constructs have fairly long beta half-lives of above 50 hours. Preliminary *in vivo* studies in C57BL/6 transgenic for the human FcγRs were conducted with HAT-IYG and 299A-IYG demonstrated very little tumor control, which agrees with the phagocytosis results. Future studies with the DTT-IYG and DAT-IYG variants will be conducted in the human FcγR transgenic mice.

Materials and methods

Cell lines

HEK293F cells (Invitrogen) were cultured in Freestyle 293 expression medium (Invitrogen) in suspension. The murine melanoma cell line B16-F10 (ATCC) was cultured in DMEM (ATCC) with 10% heat inactivated FBS (Invitrogen) and 100 U/ml penicillin and 100 μg/ml streptomycin (Corning Cellgro). All cell lines were maintained at 37°C with 5% CO2. Cells were subcultured every 2-3 days and when necessary detached using 0.25% trypsin and 1mM EDTA (Invitrogen).

Proteins

DNA for transfection was obtained using a PureLink HiPure Plasmid FP Maxiprep Kit (Invitrogen). Proteins were obtained through transient transfection of HEK293F cells with DNA and 2 mg of polyethyleneimine per liter of culture per manufacturer's protocol. Supernatants were harvested and sterile filtered with a 0.2 μm filter one week after transfection. All antibodies were purified using Protein A resin (Genscript) per manufacturer's protocol. Proteins are all buffer exchanged and stored in 1x PBS.

Protein characterization

Proteins were run on a TSKgel G3000SWxl (Tosoh Bioscience) SEC-HPLC column in 50mM sodium phosophate, 150 mM NaCl pH 7.2 buffer. Dynamic light scattering (DLS) analysis was performed on a DynaPro NanoStar (Wyatt Technology). Readings were taken with UVette disposable cuvettes (Eppendorf).

Biacore characterization

Readings were taken on a Biacore T200 instrument (GE Healthcare Life Sciences). Anti-tetra HIS antibody was immobilized to a CM5 series S chip using amine chemistry to a level of 14,000 RU. HIS-tagged human FcγR were diluted in HBS-EP+ binding buffer (GE Healthcare Life Sciences) and captured on the chip. Aglycosylated antibodies were buffer exchanged into the HBS-EP+ buffer and injected into the instrument in serial dilutions at various concentrations to measure the binding. Chip surfaces were regenerated with 10 mM glycine pH 1.5. Binding affinities to FcγRI were determined using k_{on} and k_{off} rates determined by global fits with the Langmuir model. The remaining equilibrium binding constants to the low affinity FcγR were determined by plotting steady state binding affinities.

Phagocytosis assay

Monocytes were isolated from whole human blood using RosetteSep™ Human Monocyte Enrichment Cocktail (Stemcell Technologies). For phagocytosis with monocytes, cells were used as is. For differentiation into macrophages, monocytes were seeded into a 96-well tissue culture plate at $1x10^5$ cells per well and treated with 50 ng/ml of recombinant human GM-CSF (Biolegend) in RPMI (Corning Cellgro) with 10% heat-inactivated fetal bovine serum (Invitrogen) and 1X penicillin-streptomycin solution on days 0, 2 and 5 after harvest. Macrophages that were IFN-γ

activated were treated with 25 ng/ml of IFN-γ (Biolegend) on day 5 after harvest in addition to the GM-CSF treatment. Cells were ready to use on day 7 after harvest and treatment with GM-CSF.

Cell lines were detached with 0.25% trypsin and 1mM EDTA, and washed and resuspended with 1XPBS and 0.1% Bovine serum albumin (PBSA) at $5x10^6$ cells/ml. Cells were labeled with 5μM carboxyfluorescein succinimidyl ester (CFSE) for 10 minutes at room temperature in the dark. Cells were then quenched with excess PBSA and washed two more times with serum free DMEM. Cell lines were then incubated with 100 nM of TA99 hIgG1 WT, N297Q, SGTA, DTT-IYG, DAT-IYG, HAT-IYG, or 299A-IYG for 30 minutes at room temperature in the dark. Cells incubated in protein were then transferred to the 96-well plate the macrophages were seeded in previously. Plates were incubated at 37°C with 5% CO_2 for at least 3 hours to allow for phagocytosis.

After phagocytosis, plates were pelleted, supernatants removed, and incubated with Versene (Invitrogen) for 15 min at 37°C with 5% CO_2. Cells were transferred to a new plate and washed with excess PBSA before staining for 1 hour at 4°C with an anti-human CD14 Alexa Fluor 647 (Biolegend) antibody as a macrophage marker. Plates were analyzed on a FACSCalibur HTS instrument.

Microscopy

Imaging was performed on an Applied Precision DeltaVision (GE healthcare) deconvolution microscope. The phagocytosis assay was prepared as stated above with $3x10^5$ macrophages per well in an 8 well Lab-Tek Chambered Coverglass (Thermo Scientific). $1x10^5$ CFSE labeled B16F10 cells were incubated with the proteins and then added to the macrophages for at least 3 hours before imaging. Samples were stained with anti-human CD14 Alexa Fluor 647 antibody before imaging on the DeltaVision microscope. Images were recorded on the 20X lens and 60X oil lens.

Pharmacokinetic study

C57BL/6 mice were injected intraperitoneally with 100 μg of antibody labeled with IRDye® 800CW (LI-COR Biosciences). Time points are measured by taking samples of blood at the tip of the tail immediately after injection at 0 hour and then subsequent hours after at 1, 3, 5, 8, 12, 24, 25, 27,29, 32, 48, 72, 96, and 120 hrs after injection. Fluorescent readings are read on the Odyssey scanner (LI-COR Biosciences) and taken on serum only. All readings are normalized to the first reading and fit to: $C(t) = Ae^{-\alpha t} + Be^{-\beta t}$. All PK studies were conducted in triplicate with three separate mice. Because with an IP injection it takes a while for the antibody to distribute into the blood, the first 2 time points were ignored for the curve fit for SGTA, DAT-IYG, HAT-IYG, and 299A-IYG. For WT, N297Q, and DTT-IYG the first 3 time points were ignored for the curve fit.

Mathematical model

The mathematical model was modified from the one developed by Jung *et al.*[13] to model the phagocytosis of B16F10 melanoma cells by macrophages. In this system, free FcγR (R_f) can diffuse into the contact volume to become R_{cv}, where free FcγR is equivalent to the total FcγR (R_T) minus R_{cv}. Antibody (Ab) can bind to the antigen (Ag) with an equilibrium constant of K_{Ab} to become bound antibody (B). Only FcγR in the contact volume (R_{cv}) can bind to bound antibody (B) with an equilibrium constant of K_R to form complexes (C). Only complexes (C) can dimerize with an equilibrium constant of K_{cross} to form dimers (D).

$$R_f \xleftrightarrow{K_{diff}} R_{cv}$$
$$Ag + Ab \xleftrightarrow{K_{Ab}} B$$
$$B + R_{cv} \xleftrightarrow{K_R} C$$
$$C + C \xleftrightarrow{K_{cross}} D$$

Using the system of equations at steady state as follows:

$$[R_T - R_{cv}] = K_{diff}[R_{cv}]$$
$$[Ag][Ab] = K_{Ab}[B]$$
$$[B][R_{cv}] = K_R[C]$$
$$[C][C] = K_{cross}[D]$$

Several of the parameters, given in Table 5-2, were taken from Jung *et al.*[13] including tumor cell diameter, macrophage diameter, and the method of calculating contact area and K_{diff}. Antibody concentration used in the model was the same used in the phagocytosis assays of 100 nM. The antigen expression number of TRP-1 on B16F10s was measured using Quantum Simply Cellular anti-mouse beads (Bangs Laboratories). The total FcγR level was taken from literature[14]. Kcross was calculated by using the dimer cross-linking rate constant k_{onx} and the dimer dissociation rate constant k_{offx}. The k_{offx} was taken from Wofsy *et al.* to be $1x10^{-5}$ s^{-1} and the k_{onx} was calculated to be kx_1R_o/R_o, where the R_o was the initial cell surface FcγR expression[14]. This system of equations was expanded to include all combinations of FcγR dimers and was solved in MATLAB using fsolve to obtain the concentrations of the dimers. MATLAB code is included in Appendix B. The data was normalized the highest dimer value, wild-type glycosylated antibody FcγRI:FcγRI dimer. In order to plot the data as heat maps, the $\log_{10}$ was taken of the matrices and 11 was added to the data to center the range around 0 with +/-11. This allows all of the data to be compared under the same scale.

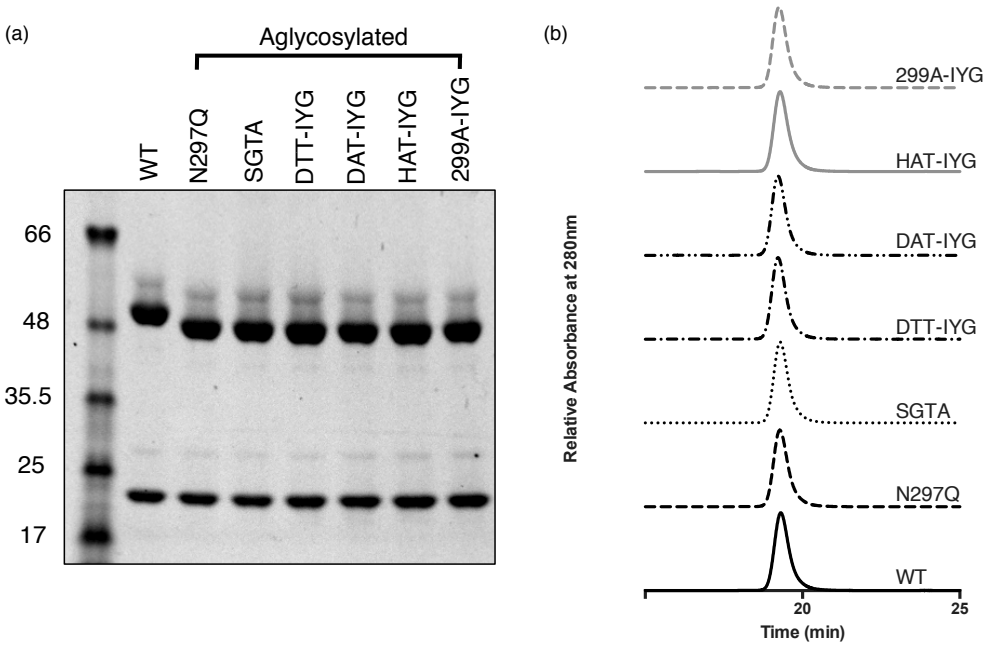

(c)

2 days after purification

Sample	Radius (nm)	% Polydispersity
WT	5.21	18.5
N297Q	5.253	16.6
SGTA	5.16	24.7
DTT-IYG	5.552	11.7
DAT-IYG	5.35	13.4
HAT-IYG	5.423	11.9
299A-IYG	5.162	18.1

2 weeks after purification

Sample	Radius (nm)	% Polydispersity
WT	5.55	11.9
N297Q	5.507	13.2
SGTA	5.337	18.9
DTT-IYG	5.415	18.7
DAT-IYG	5.2	24.4
HAT-IYG	5.154	22.9
299A-IYG	5.256	18.3

% Polydispersity < 20% = monodisperse
20% < % Polydispersity < 30% = medium disperse
% Polydispersity > 30% = polydisperse

Figure 5-1: Characterization of Aglycosylated Antibodies

(a) SDS-PAGE gel of reduced antibodies. Aglycosylated heavy chains demonstrate higher mobility on the gel because of the lack of the large glycosylation group (b) SEC-HPLC profiles of aglycosylated constructs. All run similarly to wild-type antibody. (c) Aglycosylated constructs measured with DLS at 1 mg/ml in 1xPBS buffer. Hydrodynamic radii fall within the normal antibody range of 5-6nm. % Polydispersity varies upon protein preparation and length of storage at 4°C. Two different batches for proteins were used for the two different measurement times. SEC-HPLC data was collected by Julie Bird from the laboratory of Huawei Qiu.

Table 5-1

Sample	FcγRI Kinetic K_D (nM)	FcγRIIA 167H Steady State K_D (nM)	FcγRIIA 167R Steady State K_D (nM)	FcγRIIB Steady State K_D (nM)	FcγRIIIA 176F Steady State K_D (nM)	FcγRIIIA 176V Steady State K_D (nM)
WT	3	1148	8015	3516	4538	1703
N297Q	295	n.d.	n.d.	n.d.	n.d.	n.d.
SGTA	222	996	> 10,000	6447	n.d.	n.d.
DTT-IYG	5	n.d.	2730	n.d.	1807	1040
DAT-IYG	29	n.d.	> 10,000	4169	2227	1051
HAT-IYG	216	n.d.	n.d.	n.d.	1680	1793
299A-IYG	243	605	2494	2101	1244	452
hIgG1	3	1095	5160	6499	710	348

Biacore data was collected by Julie Bird from the laboratory of Huawei Qiu.

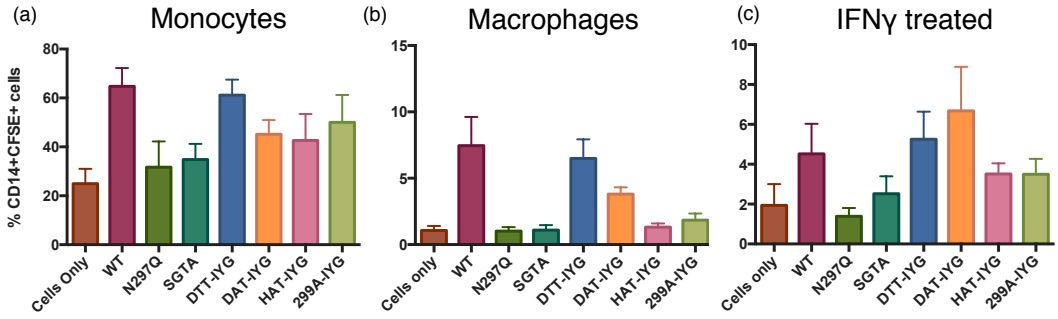

Figure 5-2: Phagocytosis of Tumor Cells Driven by Aglycosylated Antibodies

Phagocytosis assays were conducted to demonstrate biological activity of the aglycosylated antibody mutants that have productive engagement with human FcγR. The negative control of "cells only" combine monocytes/macrophages with B16F10 tumor cells, which leads to a basal level of phagocytosis. Wild-type glycosylated antibody serves as the positive control. N297Q aglycosylated antibody serves as a second negative control. Monocytes/macrophages are stained as CD14+ cells and B16F10 tumor cells as CFSE+. (a) Initial studies conducted with freshly harvested monocytes from whole human blood (b) Phagocytosis assay conducted from macrophages that were derived from monocytes harvested from whole human blood and matured with human GM-CSF. (c) Phagocytosis assay conducted from macrophages that were derived from monocytes harvested from whole human blood and matured with human GM-CSF and treated with IFN-γ.

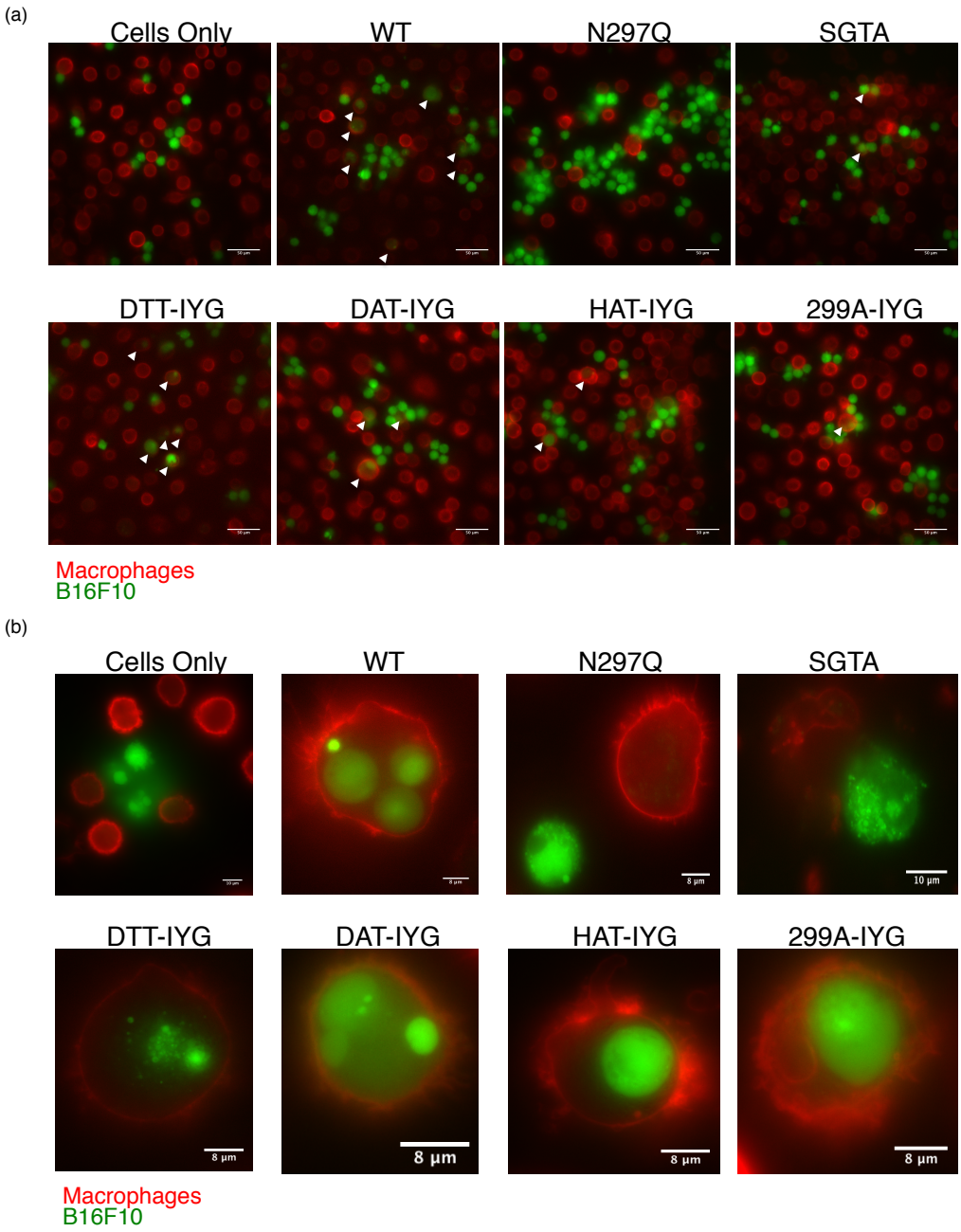

Figure 5-3: Microscopy Confirmation of Phagocytosis

(a) Microscopy images of phagocytosis of CFSE+ B16F10 cells (green) by CD14+ macrophages (red) at 20X. Arrows point to phagocytosis events. Scale bars at 50 µm (b) Microscopy images of phagocytosis at higher magnification of 60X. Scale bars at 10 µm or 8 µm as noted.

(a)

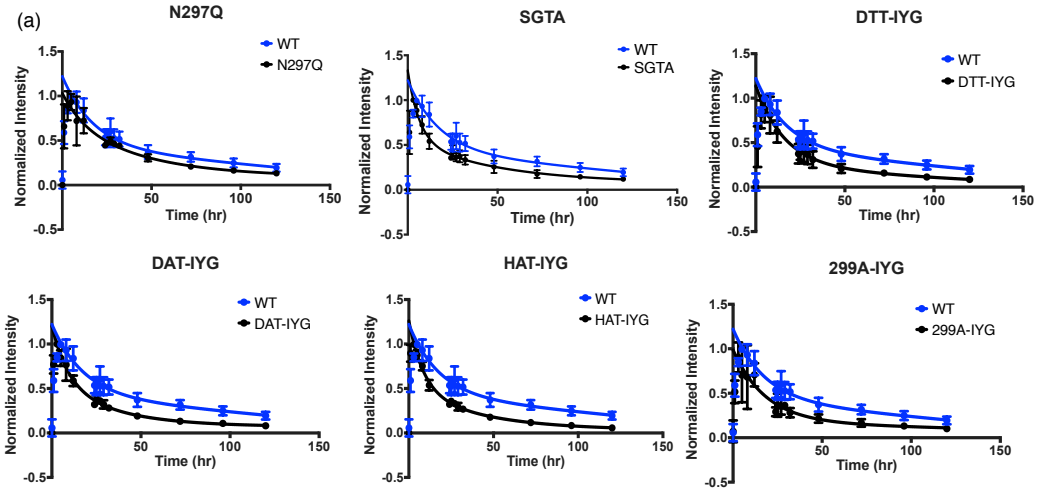

(b)

	WT	N297Q	SGTA	DTT-IYG	DAT-IYG	HAT-IYG	299A-IYG
$t_{1/2}$,α (hrs)	17.48	15.55	10.32	13.00	12.01	10.69	9.20
$t_{1/2}$,β (hrs)	108.28	89.67	81.66	77.99	89.43	53.89	76.78

Figure 5-4: Pharmacokinetics of Aglycosylated antibodies

(a) Pharmacokinetic curves of each aglycosylated antibody in comparison to the wild-type glycosylated antibody. Each study was done in triplicate. (b) Table of alpha half-lives and beta half-lives of each aglycosylated antibody.

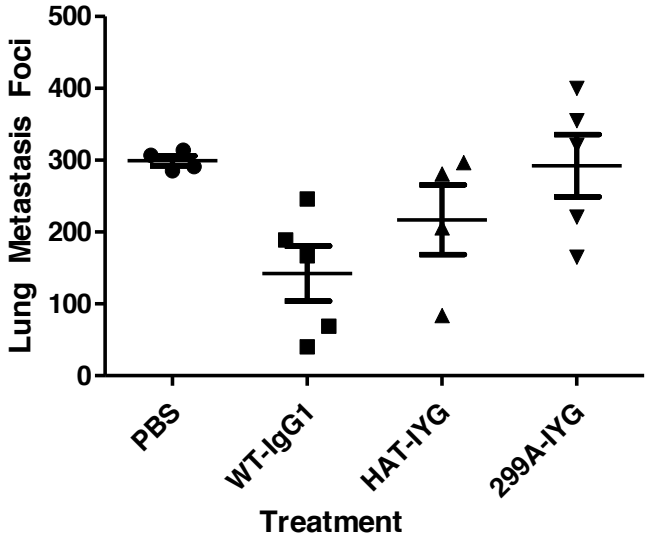

Figure 5-5: Lung Metastasis Study

Select aglycosylated antibodies HAT-IYG and 299A-IYG were used to treat B16F10 lung metastases. Neither construct demonstrates efficacy to the extent of the wild-type glycosylated IgG1. Both aglycosylated antibody treated groups have a few mice that respond positively to treatment. HAT-IYG has slightly better control of lung metastases as compared to 299A-IYG treated mice. Five mice were used per group. Data was collected by David Dilillo from the laboratory of Jeffrey Ravetch.

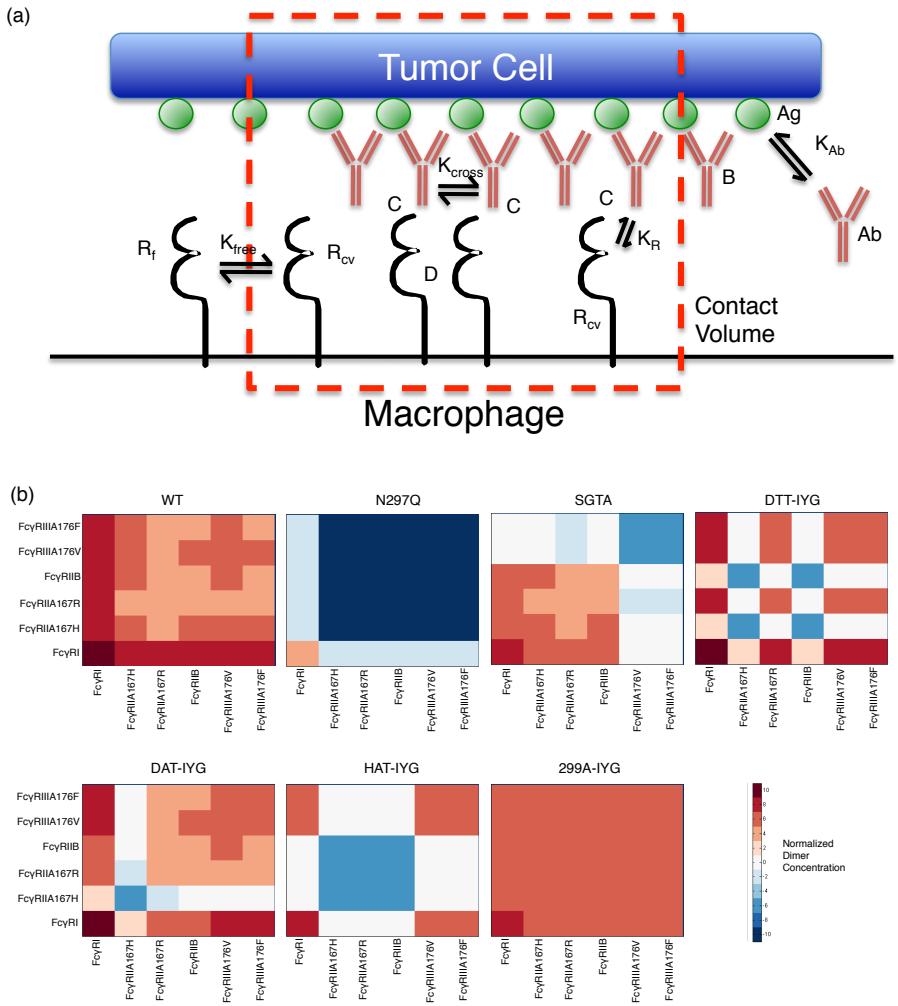

Figure 5-6: Mathematical Model of Phagocytosis

(a) Diagram of phagocytosis where the red dotted outline represents the contact volume between tumor cell (top) and macrophage (bottom). Antibody "Ab" can bind to the antigen "Ag" with an equilibrium constant of K_{Ab} to become bound antibody "B". Free FcγR "R_f" can diffuse into the contact volume (red dotted line) to become R_{cv}, and only FcγR in the contact volume "R_{cv}" can bind to bound antibody "B" with an equilibrium constant of K_R to form complexes "C". Only complexes "C" can dimerize with an equilibrium constant of K_{cross} to form dimers "D". (b) Heat maps of normalized dimer concentrations based on the mathematical model. Red signals an increase in concentration and blue a decrease in concentration.

Table 5-2

Parameters	Value	Description
Physical paramters		
B16_dia	10 μm	Diameter of B16F10 cell
Mac_dia	21 μm	Diameter of macrophage
Cell_gap	12 nm	Distance between tumor cell and macrophage
contact_area	104.7 μm^2	Calculated contact area of cells
Expression level parameters		
B16_TRP1	33904	TRP1 (tumor antigen) expression level on B16F10
Mac_FcR	$3x10^5$	Total FcγR per cell
Ab	0.1 μM	Antibody concentration
Affinity parameters		
K_{offx}	$1x10^{-5}$ s^{-1}	Dimer dissociation rate constant
Kd_{ab}	$6.1x10^4$ μM	Antibody binding affinity to antigen

References

1. Weiner, L. M., Surana, R. & Wang, S. Monoclonal antibodies: versatile platforms for cancer immunotherapy. *Nat. Rev. Immunol.* **10,** 317–327 (2010).
2. Adams, G. P. & Weiner, L. M. Monoclonal antibody therapy of cancer. *Nat. Biotechnol.* **23,** 1147–1157 (2005).
3. Carter, P. Improving the efficacy of antibody-based cancer therapies. *Nat. Rev. Cancer* **1,** 118–129 (2001).
4. Desjarlais, J. R., Lazar, G. A., Zhukovsky, E. A. & Chu, S. Y. Optimizing engagement of the immune system by anti-tumor antibodies: an engineer's perspective. *Drug Discov. Today* **12,** 898–910 (2007).
5. Weng, W.-K. & Levy, R. Two immunoglobulin G fragment C receptor polymorphisms independently predict response to rituximab in patients with follicular lymphoma. *J. Clin. Oncol. Off. J. Am. Soc. Clin. Oncol.* **21,** 3940–3947 (2003).
6. Cartron, G. *et al.* Therapeutic activity of humanized anti-CD20 monoclonal antibody and polymorphism in IgG Fc receptor FcγRIIIa gene. *Blood* **99,** 754–758 (2002).
7. Musolino, A. *et al.* Immunoglobulin G fragment C receptor polymorphisms and clinical efficacy of trastuzumab-based therapy in patients with HER-2/neu-positive metastatic breast cancer. *J. Clin. Oncol. Off. J. Am. Soc. Clin. Oncol.* **26,** 1789–1796 (2008).
8. Shields, R. L. *et al.* High resolution mapping of the binding site on human IgG1 for Fc gamma RI, Fc gamma RII, Fc gamma RIII, and FcRn and design of IgG1 variants with improved binding to the Fc gamma R. *J. Biol. Chem.* **276,** 6591–6604 (2001).
9. Tao, M. H. & Morrison, S. L. Studies of aglycosylated chimeric mouse-human IgG. Role of carbohydrate in the structure and effector functions mediated by the human IgG constant region. *J. Immunol. Baltim. Md 1950* **143,** 2595–2601 (1989).
10. Sazinsky, S. L. *et al.* Aglycosylated immunoglobulin G1 variants productively engage activating Fc receptors. *Proc. Natl. Acad. Sci. U. S. A.* **105,** 20167–20172 (2008).
11. Strome, S. E., Sausville, E. A. & Mann, D. A mechanistic perspective of monoclonal antibodies in cancer therapy beyond target-related effects. *The oncologist* **12,** 1084–1095 (2007).
12. Bethea, D. *et al.* Mechanisms of self-association of a human monoclonal antibody CNTO607. *Protein Eng. Des. Sel. PEDS* **25,** 531–537 (2012).
13. Jung, S. T. *et al.* Effective phagocytosis of low Her2 tumor cell lines with engineered, aglycosylated IgG displaying high FcγRIIa affinity and selectivity. *ACS Chem. Biol.* **8,** 368–375 (2013).
14. Wofsy, C., Torigoe, C., Kent, U. M., Metzger, H. & Goldstein, B. Exploiting the difference between intrinsic and extrinsic kinases: implications for regulation of signaling by immunoreceptors. *J. Immunol. Baltim. Md 1950* **159,** 5984–5992 (1997).

CHAPTER 6: CONCLUSIONS AND FUTURE DIRECTIONS

A current major focus in antibody therapeutic development is to drive greater therapeutic efficacy by engineering interactions with FcγRs. Much of the previous work aimed at understanding FcγR contributions have been conducted with knock-out mice, but unfortunately knock-out mice have been shown to change FcγR expression patterns to compensate for the lack of certain FcγRs.[1] Instead, by studying these interactions through modifying the protein interaction, we can invoke innate immune responses that utilize only individual FcγRs within a wild-type immune system.

In this work, we engineered individual Fn3 using yeast display of the Fn3 scaffold to bind with specificity to murine FcγRI, FcγRIIB, FcγRIII, and FcγRIV. In this process, we outline two different sorting methods: 1) sequential enrichments and depletions and 2) two-color sorting that allow us to engineer binders to be able to differentiate between proteins that share a large percentage of homology to each other. Two separate sorts were conducted against FcγRIV because previous literature suggests its importance for tumor clearance, and we wanted to increase the variety of binders engineered against this receptor. We selected the Fn3 clones that bound their target FcγR with the highest affinity and had the highest expression on yeast for further study.

This panel of Fn3 binders to individual FcγRs named: I, II, III, IV1, and IV2 against murine FcγRI, FcγRIIB, FcγRIII, and FcγRIV, respectively, was engineered for high specificity and higher affinity than that of the wild-type antibody Fc to their target FcγR. The yeast display titrations show very little cross-reactivity of the Fn3 binders to other mFcγR. Competition studies suggested that clones III and IV1 competed with the Fc binding epitope on the FcγR, whereas clone II did not compete with the Fc binding epitope. Clones I and IV2 showed slight decrease in binding to their respective FcγRs in the presence of antibody, which suggests possible steric hindrance caused by the antibody. Clones IV1 and IV2 were epitope mapped on FcγRIV using a single point mutation yeast

display library of the FcγRIV. Results confirmed that the clone IV1 epitope overlaps with that of the Fc binding epitope, whereas IV2 binds to an epitope on domain 1, which is distinct from the Fc binding epitope. Future studies could include epitope maps of the other Fn3 binders to their respective FcγR. Past studies showed slight conformational instability of the other FcγR displayed on yeast, but a single point mutation library would allow for selection of more stable clones.

The five Fn3 clones: I, II, III, IV1, and IV2 show specificity to their target FcγR based on binding studies in the dsSSMSA-Fn3 format. At high concentrations, using a non-label-free method of detection, proteins can become stickier and therefore slight cross-reactivity is detected at high concentrations. Although the binding affinities of these Fn3 binders are not higher than that of the wild-type antibody with the mIgG2a isotype for each mFcγR, the ratio of binding to the activating receptors versus inhibitory receptors, (known as the A/I ratio[2]) is dramatically larger because of their specificity. These binders to the activating receptors have several hundred to thousand fold higher A/I ratios compared to that of the wild-type antibody Fc.

The dsSSMSA-Fn3 construct functionally, if not structurally, mimics an antibody except with monospecific FcγR binding. Antigen-binding, FcRn-mediated lifetime extension, and FcγR engagement are all present in these constructs, which are very modular allowing the scFv to be switched out to target other antigens. The Fn3s are also easily swapped out to target different FcγRs. The MSA extends *in vivo* serum half-life and increases protein expression yields. The engineered dsSSMSA-Fn3 constructs show specificity of the scFv to the target antigen, CEA, and demonstrates that they can simultaneously bind cells and FcγR.

The phagocytosis assays demonstrate that our dsSSMSA-Fn3 constructs can drive biological activity *in vitro*. Macrophages were used for this biological assay because they are known to express all four mFcγR.[3] The constructs that were engineered to bind to the activating receptors: mFcγRI, mFcγRIII, and mFcγRIV all drive increased phagocytosis when compared to antigen-negative cells

or the construct with the control L Fn3. The construct with the II Fn3 specific for inhibitory mFcγRIIB showed no phagocytosis, which is consistent with the fact that mFcγRIIB sends inhibitory signals when cross-linked and therefore would not drive phagocytosis. This assay also demonstrates that our constructs can bridge two types of cells together, tumor cells and macrophages. Future studies could include combinations of the various binders and to observe how cross-linking multiple different activating FcγR can effect phagocytosis along with dimerizing activating and inhibitory FcγRs.

We have shown that it is possible to engineer Fn3-based binders specific to each individual mFcγR. This allows us to parse out the individual contribution of each mFcγR from the protein level. By engineering binders instead of altering the Fc portion of an antibody, this allows us to bypass allelic restrictions. Our current construct is also designed to be optimal for *in vivo* work with the presence of the serum albumin, which would provide an extended half-life. The Fn3 binders also provide a powerful toolkit that can be used to study many different ailments ranging from cancer to autoimmune diseases.

In order to test the *in vivo* stability of our engineered constructs, we performed initial pharmacokinetic studies in wild-type C56BL/6 mice. The constructs had reasonable serum half-lives and had detectable protein in the blood even on the fifth day after injection. These results convinced us to move forward with *in vivo* biodistribution studies. The biodistribution studies were conducted in albino C56BL/6 mice that were inoculated with antigen positive and antigen negative MC38 tumor cell lines. Both the cell lines and mice were chosen for ease of imaging since melanin pigments in wild-type C56BL/6 mice and the B16F10 melanoma cell line interfere with fluorescence imaging. It appears that the constructs are cleared from the organs when imaged on the IVIS and accumulate within the tumors after 24 hours. Most of the accumulation is probably due to the enhanced permeability and retention (EPR) effect, where the constructs accumulate passively in the

tumors because of the lack of lymphatic drainage. When quantified and calculated by percent-injected dose per gram, results indicate that the constructs have higher accumulation in the antigen positive tumor.

These results allowed us to move forward in attempting tumor control experiments. The initial experiment with the MC38-CEA tumor model in CEA.Tg mice showed no difference between treatments with the PBS vehicle versus dsSSMSA-Fn3 constructs that only interacted with mFcγRI and mFcγRIV. Although the fact that our constructs failed to control tumor growth was disappointing, the positive control with the sm3E mIgG2a antibody monotherapy also failed to control tumor growth. This suggested that our model was not a good representation of determining efficacy of mFcγR driven tumor control. The study was also ended early at only 14 days after tumor inoculation, which is standard for lung metastasis models, but perhaps too early for subcutaneous models. It is possible that if the study was extended, we would have observed more of a difference in tumor control with our constructs and sm3E mIgG2a compared to the PBS treated mice. Tumors were analyzed and blood samples were taken to detect immunoediting or specific anti-CEA antibodies. Results show that CEA levels have not gone down on the MC38-CEA tumors and no detectable anti-CEA antibodies are in the serum. Since this study is so short, it would make sense that a robust B-cell response has not occurred yet to produce the anti-CEA antibodies. Another explanation would be that since this study was conducted in CEA.Tg mice, the mice are already tolerized to CEA as a self-antigen and therefore would not produce anti-CEA antibodies. Another possibility for the model failure could be that the antigen, CEA, is being shed and therefore not a good target for ADCC.

Previous mouse models used to demonstrate mFcγR driven tumor control were conducted with B16F10 melanoma cells in a lung metastasis model. Therefore, the mouse model was switched to B16F10 cell lines that were made to stably express CEA inoculated via tail vein for lung

metastases. The lung metastasis model has a greater discrepancy in outcomes between treatment options and was useful for optimization of tumor models and treatments. Preliminary studies with the three different B16CEA cell lines suggested that B16CEA F metastasized to the lung most similarly to B16F10s whereas B16CEA B and D were less fit. Unfortunately, B16CEA F lung metastases that were treated with antibody monotherapies of either sm3E mIgG2a or TA99 mIgG2a, which both bind to the cell line, were not controlled in stark contrast to normal B16F10s when treated with TA99 mIgG2a[2]. When B16CEA F lung metastases were treated with Fc/IL-2 or the combination therapy of Fc/IL-2 and sm3E mIgG2a, there was a decrease of lung metastases compared to the PBS controls. These results suggested that combination therapy of antibody with Fc/IL-2 or a long serum half-life IL-2 molecule would be able to demonstrate slowed tumor growth.

The tumor model was switched to a subcutaneous model since all previous antibody combination treatments with long serum half-life IL-2 molecules were conducted in this format. The subcutaneous models showed that the B16CEA F cell line was incredibly difficult to control even with the combination treatment, but the B16CEA B cell line demonstrated some efficacy. Replicates of the combination treatment on B16CEA B with the dsSSMSA-Fn3 suggested that some dsSSMSA-I, dsSSMSA-IV1, and dsSSMSA-IV2 treated mice had significantly delayed or controlled tumor growth. Interestingly, combination treatment with dsSSMSA-II also appeared to have a few controlled tumors, along with the MSA/IL-2 only treatment. The combination therapy with MSA/IL-2 confounded much of the results since MSA/IL-2 only demonstrated efficacy and therefore efficacy from the combinations could just be due to the addition of MSA/IL-2 and not the dsSSMSA-Fn3 constructs.

In order to work with a simpler model, monotherapies in very aggressive dosages were given to mice inoculated subcutaneously with B16CEA B tumors. In this case, all tumors are expected to grow out, except at different rates. When treated with sm3E mIgG2a antibody only, tumor growth is

delayed as compared to the PBS negative control. The dsSSMSA-Fn3 constructs that bind to the activating receptors dsSSMSA-I, dsSSMSA-III, dsSSMSA-IV1, and dsSSMSA-IV2 all seemed to delay tumor growth as compared to the vehicle control, PBS, and the negative control, dsSSMSA-L. The dsSSMSA-II monotherapy does not control tumor growth since it binds to the inhibitory receptor. All of the treatments that showed efficacy appear to behave similarly except for dsSSMSA-III which decreased tumor growth compared to the controls but did not work as well as the others. This could be due to the fact that the Fn3 binder has a lower binding affinity to the mFcγRIII. Technically all of the Fn3 binders to the activating receptors have very high A/I ratios, since they do not cross-react with the inhibitory receptor. This appears to agree with the A/I ratio hypothesis in that as long as there is decreased binding to the inhibitory receptor, interaction with any of the activating receptors can drive tumor control. The data from the tumor control studies with the monotherapy suggests that all of the activating mFcγRs behave in a similar fashion regarding tumor control, which also agrees with the phagocytosis data.

Although the prophylactic treatment of subcutaneous tumors with sm3E mIgG2a antibody or the dsSSMSA-Fn3 constructs demonstrated decrease in tumor growth, the results were not as drastic as previous published TA99 mIgG2a antibody treatment[4]. Multiple factors could explain the differences in results, one of which could be that the tumor inocula for our study is one order of magnitude larger ($5x10^5$ B16CEA B cells) than the amount that Nimmerjahn *et al.* used ($5x10^4$ B16F10 cells). We used this higher number because the B16CEA B cells were less fit than the B16F10 and were harder to establish even in CEA.Tg mice. Another factor could be that since we were using CEA.Tg mice, the endogenous CEA was acting as a sink by binding a large percentage of our constructs before they could reach the tumor. Performing pharmacokinetic studies in the CEA.Tg mice with our constructs tested this hypothesis. Preliminary studies suggested that our constructs clear faster in CEA.Tg mice as compared to C56BL/6 mice. This could also be due to the

fact that CEA is known to be shed, which could also act as another sink for our therapeutics[5]. Our mouse model demonstrated the potential of our constructs to drive tumor control, but suggests that CEA as a target antigen is not the best at promoting anti-tumor responses driven by mFcγR. Pharmacokinetic studies with the dsSSMSA-Fn3 constructs will have to be redone in CEA.Tg mice to obtain more accurate clearance values. Biodistribution of the dsSSMSA-Fn3 constructs will also allow us to understand if the constructs are accumulating in any specific organs (i.e. liver or kidney). Specific time points of measuring biodistribution will have to be optimized based on the pharmacokinetic studies, otherwise it is possible that all of the construct will have cleared by the time organs are harvested. Future work would also include combination therapies of different dsSSMSA-Fn3 constructs. Combinations of two activating receptor binders (i.e. I and IV1 or IV2) might show more efficacy as compared to binding a single activating receptor.

We also further characterized the aglycosylated constructs isolated previously. The variable regions of the aglycosylated antibodies were first swapped to the melanoma antigen TRP-1 targeting TA99. The antibodies were run on a SDS-PAGE gel, through SEC, and DLS to confirm proper size and stability. All of the constructs appeared to run as expected on the SDS-PAGE gel, with the glycosylated antibody running higher and having less mobility as compared to the aglycosylated constructs. All constructs appeared to have similar SEC runs with few aggregates. Hydrodynamic radii of the aglycosylated antibodies were similar to that of a normal antibody and percent of polydispersity of the constructs were on average fairly low and considered monodisperse. It was observed that some of the aglycosylated antibodies tended to aggregate over time, which suggested slight instability as compared to that of wild-type glycosylated antibodies.

Previous binding studies of the aglycosylated constructs were conducted with yeast titrations and tetramers of FcγR. Label free binding affinity was measured between the aglycosylated antibodies and FcγR using Biacore. Measurements confirmed that aglycosylated N297Q had no

binding to low affinity FcγR and decreased binding to FcγRI. This construct was considered the baseline of aglycosylated antibodies, and the remaining mutants restored/improved binding to the FcγR. All of the aglycosylated variants had different binding patterns to the FcγRs. Interestingly, 299A-IYG restored binding to all of the low affinity FcγR and was expected to behave most similarly to wild-type glycosylated antibody. Phagocytosis data showed that only the aglycosylated variants DTT-IYG and DAT-IYG promoted phagocytosis by macrophages. This seemed counter to expected results, since all of the engineered aglycosylated variants restored binding to FcγR, it would be assumed that all would promote some level of phagocytosis.

In order to understand the phagocytosis results better, a mathematical model of phagocytosis was modified to represent all of the FcγR. Quantified binding affinities were used as parameters in the model of phagocytosis. The model output suggested that FcγRI was the main driving force of phagocytosis. All three constructs that promoted phagocytosis had higher binding affinity to FcγRI as compared to N297Q. Other studies suggest that the other low affinity FcγRIIA and FcγRIIIA also play a role in phagocytosis, but in our studies we saw most of the biological activity driven by FcγRI. Perhaps if binding affinities to these other FcγR were increased above that of wild-type, they would play a larger role.

Pharmacokinetic studies of the aglycosylated variants were conducted and all constructs have fairly long beta half-lives of above 50 hours. Preliminary *in vivo* studies in C57BL/6 transgenic for the human FcγRs were conducted with HAT-IYG and 299A-IYG and demonstrated very little tumor control, which agrees with the phagocytosis results. Future studies with the DTT-IYG and DAT-IYG variants will be conducted in the human FcγR transgenic mice.

This work was focused on targeting and optimizing FcγR interaction with anti-tumor therapies. The role of murine FcγR interaction in therapeutic efficacy was further investigated with

Fn3 binders that were highly specific for the individual FcγR. As expected, the murine inhibitory receptor FcγRII did not show any anti-tumor activity within the *in vitro* phagocytosis model or the *in vivo* subcutaneous tumor model. Interestingly, although previous literature suggested that FcγRIV was the key receptor in tumor control[2], this work demonstrated that as long as any activating FcγR is targeted in the absence of targeting the inhibitory receptor, all constructs controlled tumor growth to a certain extent. Data suggests that targeting FcγRI and FcγRIV results in similar levels of control, with slightly more tumor delay than targeting FcγRIII. Future combination therapies of various FcγRI and FcγRIV binders might result in increased tumor control as compared to typical monoclonal antibody therapy.

The aglycosylated antibodies have much potential in the industrial setting since they can be made in practically any expression system. In this study, we characterized previously engineered aglycosylated constructs that regained binding function to FcγRIIIA along with binding to FcγRIIA and FcγRI. From the *in vitro* biological studies, the DTT-IYG and DAT-IYG constructs behaved the most similar to wild-type glycosylated antibody. These two constructs could potentially be used in tumor control studies.

References

1. Bruhns, P. Properties of mouse and human IgG receptors and their contribution to disease models. *Blood* **119,** 5640–5649 (2012).
2. Nimmerjahn, F. & Ravetch, J. V. Divergent Immunoglobulin G Subclass Activity Through Selective Fc Receptor Binding. *Science* **310,** 1510–1512 (2005).
3. Nimmerjahn, F. & Ravetch, J. V. Fcγ receptors as regulators of immune responses. *Nat. Rev. Immunol.* **8,** 34–47 (2008).
4. Nimmerjahn, F. *et al.* FcγRIV deletion reveals its central role for IgG2a and IgG2b activity in vivo. *Proc. Natl. Acad. Sci. U. S. A.* **107,** 19396–19401 (2010).
5. Watson, S. A. *et al.* Inhibition of tumour growth by marimastat in a human xenograft model of gastric cancer: relationship with levels of circulating CEA. *Br. J. Cancer* **81,** 19–23 (1999).

APPENDIX A: SEQUENCES

Fn3 sequences

Fn3s that bind FcγR are in both the pCT vector and the pEThk vector. The sequences below are the originally isolated sequences from pCT. When converted to other fusions and moved to other vectors, some framework mutations at the beginning and end of the Fn3 were converted back to the wild-type. These reversions back to wild-type did not affect binding and efficacy of the Fn3s.

L

```
GTTTCTGATGTTCCGAGGGACCTGGAAGTTGTTGCTGCGACCTCCACCAGCCTACTGATCAGTTGGCGCGGCTACCC
CTGGGCTACCTATTATGGGATCATTTACGGAGAAACGGGAGGAAATAGCCTTGTCCAGGAGTTCACTATGCCTGGGG
TTACCAATGCTACCATCAGCGGCCTTAAACCTGGAGTTGATTATACCATCACTGTGTATGCTGTCACTCGCGTGGGG
CGGACGTTTGACACGCCGGGCCCAATCTCCATTAATTACCGAACAGAAATTGACAAACCATCCCAGGGATCC
```

I

```
GTTTCCGATGTTCCGAGGGACCTGGAAGTTGTTGCTGCGACCCCCACCAGCCTACTGATCAGCTGGCATTTGCCCTA
CCACGCGATCTTTTACAGGATCACTTACGGAGAAACAGGAGGAAATAGCCCTGCCCAGGAGTTCACTGTGCCTTGGT
CTTATACCTCGGCTACCATCAGCGGCCTTAAACCTGGAGTTGACTATACCATCACTGTGTATGCTGTCACTTACAAC
GGCCCCCCCTTTTTTTATCCAACTTCCATTAATTACCGGACAGAAATTGGCAAACCATCCCAG
```

II

```
CTTTCTGACGTTCCGAGGGTCCTGGAAGTTGTTACTGCGACCCCCACCAGCCTACTGATCAGCTGGTTTCCTCTTCA
CGATGAGCATGCGGACTATTTCAGGATCACTTACGGAGAAACAGGAGGAAATAGCCCTGTCCAGGAGTTCACTGTGC
CTGGGTGGATGTTGGCGGCTCCCATCAGCGGCCTTAAACCTGGAGTTGATTATACCATCACTGTGTATGCTGTCACT
TCCAACGACTCCTACTCTAATCCACTCTCCATTAATTACCGAACAGAAATTGACAAACCACCCCAG
```

III

```
GTTTCTGATGTTCCGAGGGACCTGGAAGTTGTTGCTGCGACCCCCACCAGCCTACTGATCAGCTGGCATTGTCCCTA
CTGTGATTCGGACTCTTACAGGATCACTTACGGAGAAACAGGAGGAAATAGCCCTGTCCAGGAGTTCACTGTGCCTT
ATTGGAGGTTTTCGGCTACCATCAGCGGCCTTAAACCTGGAATTGATTATACCATCACTATGTATGCCGTCACTGGC
AGGTACTGGTCTGAGCCAATTTCCATTAATTACCGAACAGAAACTGACAAACCATCCCAG
```

IV1

```
GTTCCTGATGTTCCGAGGGACCTGGAAGTTGTTGCTGCGACCCCCACCAGCCTACTGATCAGCTGGGACGATCCGAG
TGGCATGGCCCCCTACAGGATCACTTACGGAGAAACAGGAGGAAATAGCCCTGTCCAGGAGTTCACTGTGCCTGAAC
ACGTATGGATGGCTACCATCAGCGGCCTTAAACCTGGAGTTGATTATACCATCACTGTGTATGCTGTCACTGACCAG
GGTTCTTCTCACCCAATTTCTATTAATTACCGAACAGAAATTGACAAACCATCCCAGGGATCC
```

IV2

```
GTTTCTGATGTTCCGGGGGACCTGGAAGTTGTCGCTGCGACCCCCACCAGCCTACTGATCAGCTGGGATATTCCTGC
TGGTGATTATTTGGATTATTACAAGATCACTTACGGAGAAACAGGAGGAAATAGCCCTGTCCAGAAGTTCGCTGTGC
CTTGGTCTATTCATACTGCTACCATCAGCGGCCTTAAACCTGGAGTTGATTATACCATCACTGTGTATGCTGTCACT
TGGAAGGGCCCTTCTCCTAAGCCAATTTCCATTAATTACCGAACAGAAATTGACAAACCATCCCAG
```

dsSSMSA-Fn3 sequences

All sequences were in the gWiz vector. These constructs use the sm3E scFv as a tumor-targeting agent. The scFv is disulfide-stabilized in order to increase the stability of the protein for *in vivo* studies.

dsSSMSA-L

HUMAN LC LEADER – DS(SM3E SCFV) – GGGGS - MOUSE SERUM ALBUMIN – GGGS – L – HHHHHHH – STOP

w/o propeptide

ds(sm3E ScFv) = Vh – (Gly4Ser)3 – Vl

Yellow: Forward Sequence Primer

Light Blue: Reverse Sequence Primer

ATGAGGGTCCCCGCTCAGCTCCTGGGGCTCCTGCTGCTCTGGCTCCCAGGTGCACGATGTCAAGTTAAACTGGAACA
GTCCGGTGCTGAAGTTGTCAAACCAGGTGCTTCCGTGAAGTTGTCCTGTAAAGCCTCTGGTTTTAACATCAAGGATT
CGTATATGCATTGGTTGAGACAAGGGCCAGGACAATGTTTGGAATGGATTGGCTGGATTGATCCAGAGAATGGTGAT
ACCGAGTACGCTCCTAAATTTCAGGGAAAGGCTACTTTTACTACCGACACTTCCGCTAATACCGCATACTTGGGCTT
ATCTTCCTTGAGACCAGAGGACACTGCCGTATACTACTGCAACGAAGGGACACCAACTGGTCCTTACTATTTCGACT
ACTGGGGACAAGGTACCTTAGTTACTGTCTCTAGCGGTGGCGGAGGTTCAGGCGGTGGAGGGTCTGGAGGTGGCGGT
AGTGAAAATGTGCTGACCCAATCTCCAAGCTCCATGTCTGTTTCTGTTGGCGATAGAGTAACCATCGCTTGTAGCGC
ATCCTCTAGTGTCCCATATATGCACTGGCTTCAACAGAAGCCAGGTAAAAGCCCAAAGTTGTTGATTTATTTGACAT
CCAACTTGGCTTCTGGAGTGCCTTCAAGGTTTTCTGGTTCCGGCTCAGGAACCGATTATAGTTTGACTATTAGCTCA
GTGCAGCCAGAGGATGCTGCAACCTACTATTGCCAGCAAAGGTCCTCATATCCACTGACTTTCGGGTGTGGAACGAA
GTTGGAAATCAAGGGTGGAGGCGGTTCAGAAGCACACAAGAGTGAGATCGCCCATCGGTATAATGATTTGGGAGAAC
AACATTTCAAAGGCCTAGTCCTGATTGCCTTTTCCCAGTATCTCCAGAAATGCTCATACGATGAGCATGCCAAATTA
GTGCAGGAAGTAACAGACTTTGCAAAGACGTGTGTTGCCGATGAGTCTGCCGCCAACTGTGACAAATCCCTTCACAC
TCTTTTTGGAGATAAGTTGTGTGCCATTCCAAACCTCCGTGAAAACTATGGTGAACTGGCTGACTGCTGTACAAAAC
AAGAGCCCGAAAGAAACGAATGTTTCCTGCAACACAAAGATGACAACCCCAGCCTGCCACCATTTGAAAGGCCAGAG
GCTGAGGCCATGTGCACCTCCTTTAAGGAAAACCCAACCACCTTTATGGGACACTATTTGCATGAAGTTGCCAGAAG
ACATCCTTATTTCTATGCCCCAGAACTTCTTTACTATGCTGAGCAGTACAATGAGATTCTGACCCAGTGTTGTGCAG
AGGCTGACAAGGAAAGCTGCCTGACCCCGAAGCTTGATGGTGTGAAGGAGAAAGCATTGGTCTCATCTGTCCGTCAG
AGAATGAAGTGCTCCAGTATGCAGAAGTTTGGAGAGAGAGCTTTTAAAGCATGGGCAGTAGCTCGTCTGAGCCAGAC
ATTCCCCAATGCTGACTTTGCAGAAATCACCAAATTGGCAACAGACCTGACCAAAGTCAACAAGGAGTGCTGCCATG
GTGACCTGCTGGAATGCGCAGATGACAGGGCGGAACTTGCCAAGTACATGTGTGAAAACCAGGCGACTATCTCCAGC
AAACTGCAGACTTGCTGCGATAAACCACTGTTGAAGAAAGCCCACTGTCTTAGTGAGGTGGAGCATGACACCATGCC
TGCTGATCTGCCTGCCATTGCTGCTGATTTTGTTGAGGACCAGGAAGTGTGCAAGAACTATGCTGAGGCCAAGGATG
TCTTCCTGGGCACGTTCTTGTATGAATATTCAAGAAGACACCCTGATTACTCTGTATCCCTGTTGCTGAGACTTGCT
AAGAAATATGAAGCCACTCTGGAAAAGTGCTGCGCTGAAGCCAATCCTCCCGCATGCTACGGCACAGTGCTTGCTGA
ATTTCAGCCTCTTGTAGAAGAGCCTAAGAACTTGGTCAAAACCAACTGTGATCTTTACGAGAAGCTTGGAGAATATG
GATTCCAAAATGCCATTCTAGTTCGCTACACCCAGAAAGCACCTCAGGTGTCAACCCCAACTCTCGTGGAGGCTGCA
AGAAACCTAGGAAGAGTGGGCACCAAGTGTTGTACACTTCCTGAAGATCAGAGACTGCCTTGTGTGGAAGACTATCT
GTCTGCAATCCTGAACCGTGTGTGTCTGCTGCATGAGAAGACCCCAGTGAGTGAGCATGTTACCAAGTGCTGTAGTG
GATCCCTGGTGGAAAGGCGGCCATGCTTCTCTGCTCTGACAGTTGATGAAACATATGTCCCCAAAGAGTTTAAAGCT
GAGACCTTCACCTTCCACTCTGATATCTGCACACTTCCAGAGAAGGAGAAGCAGATTAAGAAACAAACGGCTCTTGC
TGAGCTGGTGAAGCACAAGCCCAAGGCTACAGCGGAGCAACTGAAGACTGTCATGGATGACTTTGCACAGTTCCTGG
ATACATGTTGCAAGGCTGCTGACAAGGACACCTGCTTCTCGACTGAGGGTCCAAACCTTGTCACTAGATGCAAAGAC
GCCTTAGCCGGAGGGGGCTCCGTTTCTGATGTCCCGAGGGACCTGGAAGTTGTTGCTGCGACCTCCACCAGCCTACT
GATCAGTTGGCGCGGCTACCCCTGGGCTACCTATTATGGGATCATTTACGGAGAAACGGGAGGAAATAGCCTTGTCC
AGGAGTTCACTATGCCTGGGGTTACCAATGCTACCATCAGCGGCCTTAAACCTGGAGTTGATTATACCATCACTGTG
TATGCTGTCACTCGCGTGGGGCGGACGTTTGACACGCCGGGCCCAATCTCCATTAATTACCGAACAGAAATTGACAA
ACCATCCCAGCACCATCACCACCATCACTGATAA

dsSSMSA-I

HUMAN LC LEADER – DS(SM3E SCFV) – GGGGS - MOUSE SERUM ALBUMIN – GGGS – I –

HHHHHHH – STOP
w/o propeptide
ds(sm3E ScFv) = Vh – (Gly4Ser)3 – Vl
Yellow: Forward Sequence Primer
Light Blue: Reverse Sequence Primer

ATGAGGGTCCCCGCTCAGCTCCTGGGGCTCCTGCTGCTCTGGCTCCCAGGTGCACGATGTCAAGTTAAACTGGAACA
GTCCGGTGCTGAAGTTGTCAAACCAGGTGCTTCCGTGAAGTTGTCCTGTAAAGCCTCTGGTTTTAACATCAAGGATT
CGTATATGCATTGGTTGAGACAAGGGCCAGGACAATGTTTGGAATGGATTGGCTGGATTGATCCAGAGAATGGTGAT
ACCGAGTACGCTCCTAAATTTCAGGGAAAGGCTACTTTTACTACCGACACTTCCGCTAATACCGCATACTTGGGCTT
ATCTTCCTTGAGACCAGAGGACACTGCCGTATACTACTGCAACGAAGGGACACCAACTGGTCCTTACTATTTCGACT
ACTGGGGACAAGGTACCTTAGTTACTGTCTCTAGCGGTGGCGGAGGTTCAGGCGGTGGAGGGTCTGGAGGTGGCGGT
AGTGAAAATGTGCTGACCCAATCTCCAAGCTCCATGTCTGTTTCTGTTGGCGATAGAGTAACCATCGCTTGTAGCGC
ATCCTCTAGTGTCCCATATATGCACTGGCTTCAACAGAAGCCAGGTAAAAGCCCAAAGTTGTTGATTTATTTGACAT
CCAACTTGGCTTCTGGAGTGCCTTCAAGGTTTTCTGGTTCCGGCTCAGGAACCGATTATAGTTTGACTATTAGCTCA
GTGCAGCCAGAGGATGCTGCAACCTACTATTGCCAGCAAAGGTCCTCATATCCACTGACTTTCGGGTGTGGAACGAA
GTTGGAAATCAAGGGTGGAGGCGGTTCAGAAGCACACAAGAGTGAGATCGCCCATCGGTATAATGATTTGGGAGAAC
AACATTTCAAAGGCCTAGTCCTGATTGCCTTTTCCCAGTATCTCCAGAAATGCTCATACGATGAGCATGCCAAATTA
GTGCAGGAAGTAACAGACTTTGCAAAGACGTGTGTTGCCGATGAGTCTGCCGCCAACTGTGACAAATCCCTTCACAC
TCTTTTTGGAGATAAGTTGTGTGCCATTCCAAACCTCCGTGAAAACTATGGTGAACTGGCTGACTGCTGTACAAAAC
AAGAGCCCGAAAGAAACGAATGTTTCCTGCAACACAAAGATGACAACCCCAGCCTGCCACCATTTGAAAGGCCAGAG
GCTGAGGCCATGTGCACCTCCTTTAAGGAAAACCCAACCACCTTTATGGGACACTATTTGCATGAAGTTGCCAGAAG
ACATCCTTATTTCTATGCCCCAGAACTTCTTTACTATGCTGAGCAGTACAATGAGATTCTGACCCAGTGTTGTGCAG
AGGCTGACAAGGAAAGCTGCCTGACCCCGAAGCTTGATGGTGTGAAGGAGAAAGCATTGGTCTCATCTGTCCGTCAG
AGAATGAAGTGCTCCAGTATGCAGAAGTTTGGAGAGAGAGCTTTTAAAGCATGGGCAGTAGCTCGTCTGAGCCAGAC
ATTCCCCAATGCTGACTTTGCAGAAATCACCAAATTGGCAACAGACCTGACCAAAGTCAACAAGGAGTGCTGCCATG
GTGACCTGCTGGAATGCGCAGATGACAGGGCGGAACTTGCCAAGTACATGTGTGAAAACCAGGCGACTATCTCCAGC
AAACTGCAGACTTGCTGCGATAAACCACTGTTGAAGAAAGCCCACTGTCTTAGTGAGGTGGAGCATGACACCATGCC
TGCTGATCTGCCTGCCATTGCTGCTGATTTTGTTGAGGACCAGGAAGTGTGCAAGAACTATGCTGAGGCCAAGGATG
TCTTCCTGGGCACGTTCTTGTATGAATATTCAAGAAGACACCCTGATTACTCTGTATCCCTGTTGCTGAGACTTGCT
AAGAAATATGAAGCCACTCTGGAAAAGTGCTGCGCTGAAGCCAATCCTCCCGCATGCTACGGCACAGTGCTTGCTGA
ATTTCAGCCTCTTGTAGAAGAGCCTAAGAACTTGGTCAAAACCAACTGTGATCTTTACGAGAAGCTTGGAGAATATG
GATTCCAAAATGCCATTCTAGTTCGCTACACCCAGAAAGCACCTCAGGTGTCAACCCCAACTCTCGTGGAGGCTGCA
AGAAACCTAGGAAGAGTGGGCACCAAGTGTTGTACACTTCCTGAAGATCAGAGACTGCCTTGTGTGGAAGACTATCT
GTCTGCAATCCTGAACCGTGTGTGTCTGCTGCATGAGAAGACCCCAGTGAGTGAGCATGTTACCAAGTGCTGTAGTG
GATCCCTGGTGGAAAGGCGGCCATGCTTCTCTGCTCTGACAGTTGATGAAACATATGTCCCCAAAGAGTTTAAAGCT
GAGACCTTCACCTTCCACTCTGATATCTGCACACTTCCAGAGAAGGAGAAGCAGATTAAGAAACAAACGGCTCTTGC
TGAGCTGGTGAAGCACAAGCCCAAGGCTACAGCGGAGCAACTGAAGACTGTCATGGATGACTTTGCACAGTTCCTGG
ATACATGTTGCAAGGCTGCTGACAAGGACACCTGCTTCTCGACTGAGGGTCCAAACCTTGTCACTAGATGCAAAGAC
GCCTTAGCCGGAGGGGGCTCCGTTTCTGATGTCCCGAGGGACCTGGAAGTTGTTGCTGCGACCCCCACCAGCCTACT
GATCAGCTGGCATTTGCCCTACCACGCGATCTTTTACAGGATCACTTACGGAGAAACAGGAGGAAATAGCCCTGCCC
AGGAGTTCACTGTGCCTTGGTCTTATACCTCGGCTACCATCAGCGGCCTTAAACCTGGAGTTGACTATACCATCACT
GTGTATGCTGTCACTTACAACGGCCCCCCCTTTTTTTATCCAACTTCCATTAATTACCGGACAGAAATTGACAAACC
ATCCCAGCACCATCACCACCATCACTGATAA

dsSSMSA-II
HUMAN LC LEADER – DS(SM3E SCFV) – GGGGS - MOUSE SERUM ALBUMIN – GGGS – II – HHHHHHH – STOP
w/o propeptide
ds(sm3E ScFv) = Vh – (Gly4Ser)3 – Vl
Yellow: Forward Sequence Primer
Light Blue: Reverse Sequence Primer

ATGAGGGTCCCCGCTCAGCTCCTGGGGCTCCTGCTGCTCTGGCTCCCAGGTGCACGATGTCAAGTTAAACTGGAACA
GTCCGGTGCTGAAGTTGTCAAACCAGGTGCTTCCGTGAAGTTGTCCTGTAAAGCCTCTGGTTTTAACATCAAGGATT
CGTATATGCATTGGTTGAGACAAGGGCCAGGACAATGTTTGGAATGGATTGGCTGGATTGATCCAGAGAATGGTGAT
ACCGAGTACGCTCCTAAATTTCAGGGAAAGGCTACTTTTACTACCGACACTTCCGCTAATACCGCATACTTGGGCTT
ATCTTCCTTGAGACCAGAGGACACTGCCGTATACTACTGCAACGAAGGGACACCAACTGGTCCTTACTATTTCGACT
ACTGGGGACAAGGTACCTTAGTTACTGTCTCTAGCGGTGGCGGAGGTTCAGGCGGTGGAGGGTCTGGAGGTGGCGGT
AGTGAAAATGTGCTGACCCAATCTCCAAGCTCCATGTCTGTTTCTGTTGGCGATAGAGTAACCATCGCTTGTAGCGC
ATCCTCTAGTGTCCCATATATGCACTGGCTTCAACAGAAGCCAGGTAAAAGCCCAAAGTTGTTGATTTATTTGACAT
CCAACTTGGCTTCTGGAGTGCCTTCAAGGTTTTCTGGTTCCGGCTCAGGAACCGATTATAGTTTGACTATTAGCTCA
GTGCAGCCAGAGGATGCTGCAACCTACTATTGCCAGCAAAGGTCCTCATATCCACTGACTTTCGGGTGTGGAACGAA
GTTGGAAATCAAGGGTGGAGGCGGTTCAGAAGCACACAAGAGTGAGATCGCCCATCGGTATAATGATTTGGGAGAAC
AACATTTCAAAGGCCTAGTCCTGATTGCCTTTTCCCAGTATCTCCAGAAATGCTCATACGATGAGCATGCCAAATTA
GTGCAGGAAGTAACAGACTTTGCAAAGACGTGTGTTGCCGATGAGTCTGCCGCCAACTGTGACAAATCCCTTCACAC
TCTTTTTGGAGATAAGTTGTGTGCCATTCCAAACCTCCGTGAAAACTATGGTGAACTGGCTGACTGCTGTACAAAAC
AAGAGCCCGAAAGAAACGAATGTTTCCTGCAACACAAAGATGACAACCCCAGCCTGCCACCATTTGAAAGGCCAGAG
GCTGAGGCCATGTGCACCTCCTTTAAGGAAAACCCAACCACCTTTATGGGACACTATTTGCATGAAGTTGCCAGAAG
ACATCCTTATTTCTATGCCCCAGAACTTCTTTACTATGCTGAGCAGTACAATGAGATTCTGACCCAGTGTTGTGCAG
AGGCTGACAAGGAAAGCTGCCTGACCCCGAAGCTTGATGGTGTGAAGGAGAAAGCATTGGTCTCATCTGTCCGTCAG
AGAATGAAGTGCTCCAGTATGCAGAAGTTTGGAGAGAGAGCTTTTAAAGCATGGGCAGTAGCTCGTCTGAGCCAGAC
ATTCCCCAATGCTGACTTTGCAGAAATCACCAAATTGGCAACAGACCTGACCAAAGTCAACAAGGAGTGCTGCCATG
GTGACCTGCTGGAATGCGCAGATGACAGGGCGGAACTTGCCAAGTACATGTGTGAAAACCAGGCGACTATCTCCAGC
AAACTGCAGACTTGCTGCGATAAACCACTGTTGAAGAAAGCCCACTGTCTTAGTGAGGTGGAGCATGACACCATGCC
TGCTGATCTGCCTGCCATTGCTGCTGATTTTGTTGAGGACCAGGAAGTGTGCAAGAACTATGCTGAGGCCAAGGATG
TCTTCCTGGGCACGTTCTTGTATGAATATTCAAGAAGACACCCTGATTACTCTGTATCCCTGTTGCTGAGACTTGCT
AAGAAATATGAAGCCACTCTGGAAAAGTGCTGCGCTGAAGCCAATCCTCCCGCATGCTACGGCACAGTGCTTGCTGA
ATTTCAGCCTCTTGTAGAAGAGCCTAAGAACTTGGTCAAAACCAACTGTGATCTTTACGAGAAGCTTGGAGAATATG
GATTCCAAAATGCCATTCTAGTTCGCTACACCCAGAAAGCACCTCAGGTGTCAACCCCAACTCTCGTGGAGGCTGCA
AGAAACCTAGGAAGAGTGGGCACCAAGTGTTGTACACTTCCTGAAGATCAGAGACTGCCTTGTGTGGAAGACTATCT
GTCTGCAATCCTGAACCGTGTGTGTCTGCTGCATGAGAAGACCCCAGTGAGTGAGCATGTTACCAAGTGCTGTAGTG
GATCCCTGGTGGAAAGGCGGCCATGCTTCTCTGCTCTGACAGTTGATGAAACATATGTCCCCAAAGAGTTTAAAGCT
GAGACCTTCACCTTCCACTCTGATATCTGCACACTTCCAGAGAAGGAGAAGCAGATTAAGAAACAAACGGCTCTTGC
TGAGCTGGTGAAGCACAAGCCCAAGGCTACAGCGGAGCAACTGAAGACTGTCATGGATGACTTTGCACAGTTCCTGG
ATACATGTTGCAAGGCTGCTGACAAGGACACCTGCTTCTCGACTGAGGGTCCAAACCTTGTCACTAGATGCAAAGAC
GCCTTAGCCGGAGGGGGCTCCGTTTCTGACGTTCCGAGGGTCCTGGAAGTTGTTACTGCGACCCCCACCAGCCTACT
GATCAGCTGGTTTCCTCTTCACGATGAGCATGCGGACTATTTCAGGATCACTTACGGAGAAACAGGAGGAAATAGCC
CTGTCCAGGAGTTCACTGTGCCTGGGTGGATGTTGGCGGCTCCCATCAGCGGCCTTAAACCTGGAGTTGATTATACC
ATCACTGTGTATGCTGTCACTTCCAACGACTCCTACTCTAATCCACTCTCCATTAATTACCGAACAGAAATTGACAA
ACCATCCCAGCACCATCACCACCATCACTGATAA

dsSSMSA-III

HUMAN LC LEADER – DS(SM3E SCFV) – GGGGS - MOUSE SERUM ALBUMIN – GGGS – III – HHHHHH – STOP

w/o propeptide

ds(sm3E ScFv) = Vh – (Gly4Ser)3 – Vl

Yellow: Forward Sequence Primer

Light Blue: Reverse Sequence Primer

ATGAGGGTCCCCGCTCAGCTCCTGGGGCTCCTGCTGCTCTGGCTCCCAGGTGCACGATGTCAAGTTAAACTGGAACA
GTCCGGTGCTGAAGTTGTCAAACCAGGTGCTTCCGTGAAGTTGTCCTGTAAAGCCTCTGGTTTTAACATCAAGGATT
CGTATATGCATTGGTTGAGACAAGGGCCAGGACAATGTTTGGAATGGATTGGCTGGATTGATCCAGAGAATGGTGAT
ACCGAGTACGCTCCTAAATTTCAGGGAAAGGCTACTTTTACTACCGACACTTCCGCTAATACCGCATACTTGGGCTT
ATCTTCCTTGAGACCAGAGGACACTGCCGTATACTACTGCAACGAAGGGACACCAACTGGTCCTTACTATTTCGACT
ACTGGGGACAAGGTACCTTAGTTACTGTCTCTAGCGGTGGCGGAGGTTCAGGCGGTGGAGGGTCTGGAGGTGGCGGT
AGTGAAAATGTGCTGACCCAATCTCCAAGCTCCATGTCTGTTTCTGTTGGCGATAGAGTAACCATCGCTTGTAGCGC
ATCCTCTAGTGTCCCATATATGCACTGGCTTCAACAGAAGCCAGGTAAAAGCCCAAAGTTGTTGATTTATTTGACAT

CCAACTTGGCTTCTGGAGTGCCTTCAAGGTTTTCTGGTTCCGGCTCAGGAACCGATTATAGTTTGACTATTAGCTCA
GTGCAGCCAGAGGATGCTGCAACCTACTATTGCCAGCAAAGGTCCTCATATCCACTGACTTTCGGGTGTGGAACGAA
GTTGGAAATCAAGGGTGGAGGCGGTTCAGAAGCACACAAGAGTGAGATCGCCCATCGGTATAATGATTTGGGAGAAC
AACATTTCAAAGGCCTAGTCCTGATTGCCTTTTCCCAGTATCTCCAGAAATGCTCATACGATGAGCATGCCAAATTA
GTGCAGGAAGTAACAGACTTTGCAAAGACGTGTGTTGCCGATGAGTCTGCCGCCAACTGTGACAAATCCCTTCACAC
TCTTTTTGGAGATAAGTTGTGTGCCATTCCAAACCTCCGTGAAAACTATGGTGAACTGGCTGACTGCTGTACAAAAC
AAGAGCCCGAAAGAAACGAATGTTTCCTGCAACACAAAGATGACAACCCCAGCCTGCCACCATTTGAAAGGCCAGAG
GCTGAGGCCATGTGCACCTCCTTTAAGGAAAACCCAACCACCTTTATGGGACACTATTTGCATGAAGTTGCCAGAAG
ACATCCTTATTTCTATGCCCCAGAACTTCTTTACTATGCTGAGCAGTACAATGAGATTCTGACCCAGTGTTGTGCAG
AGGCTGACAAGGAAAGCTGCCTGACCCCGAAGCTTGATGGTGTGAAGGAGAAAGCATTGGTCTCATCTGTCCGTCAG
AGAATGAAGTGCTCCAGTATGCAGAAGTTTGGAGAGAGAGCTTTTAAAGCATGGGCAGTAGCTCGTCTGAGCCAGAC
ATTCCCCAATGCTGACTTTGCAGAAATCACCAAATTGGCAACAGACCTGACCAAAGTCAACAAGGAGTGCTGCCATG
GTGACCTGCTGGAATGCGCAGATGACAGGGCGGAACTTGCCAAGTACATGTGTGAAAACCAGGCGACTATCTCCAGC
AAACTGCAGACTTGCTGCGATAAACCACTGTTGAAGAAAGCCCACTGTCTTAGTGAGGTGGAGCATGACACCATGCC
TGCTGATCTGCCTGCCATTGCTGCTGATTTTGTTGAGGACCAGGAAGTGTGCAAGAACTATGCTGAGGCCAAGGATG
TCTTCCTGGGCACGTTCTTGTATGAATATTCAAGAAGACACCCTGATTACTCTGTATCCCTGTTGCTGAGACTTGCT
AAGAAATATGAAGCCACTCTGGAAAAGTGCTGCGCTGAAGCCAATCCTCCCGCATGCTACGGCACAGTGCTTGCTGA
ATTTCAGCCTCTTGTAGAAGAGCCTAAGAACTTGGTCAAAACCAACTGTGATCTTTACGAGAAGCTTGGAGAATATG
GATTCCAAAATGCCATTCTAGTTCGCTACACCCAGAAAGCACCTCAGGTGTCAACCCCAACTCTCGTGGAGGCTGCA
AGAAACCTAGGAAGAGTGGGCACCAAGTGTTGTACACTTCCTGAAGATCAGAGACTGCCTTGTGTGGAAGACTATCT
GTCTGCAATCCTGAACCGTGTGTGTCTGCTGCATGAGAAGACCCCAGTGAGTGAGCATGTTACCAAGTGCTGTAGTG
GATCCCTGGTGGAAAGGCGGCCATGCTTCTCTGCTCTGACAGTTGATGAAACATATGTCCCCAAAGAGTTTAAAGCT
GAGACCTTCACCTTCCACTCTGATATCTGCACACTTCCAGAGAAGGAGAAGCAGATTAAGAAACAAACGGCTCTTGC
TGAGCTGGTGAAGCACAAGCCCAAGGCTACAGCGGAGCAACTGAAGACTGTCATGGATGACTTTGCACAGTTCCTGG
ATACATGTTGCAAGGCTGCTGACAAGGACACCTGCTTCTCGACTGAGGGTCCAAACCTTGTCACTAGATGCAAAGAC
GCCTTAGCCGGAGGGGGCTCCGTTTCTGATGTTCCGAGGGACCTGGAAGTTGTTGCTGCGACCCCCACCAGCCTACT
GATCAGCTGGCATTGTCCCTACTGTGATTCGGACTCTTACAGGATCACTTACGGAGAAACAGGAGGAAATAGCCCTG
TCCAGGAGTTCACTGTGCCTTATTGGAGGTTTTCGGCTACCATCAGCGGCCTTAAACCTGGAATTGATTATACCATC
ACTATGTATGCCGTCACTGGCAGGTACTGGTCTGAGCCAATTTCCATTAATTACCGAACAGAAATTGACAAACCATC
CCAGCACCATCACCACCATCACTGATAA

dsSSMSA-IV1

HUMAN LC LEADER – DS(SM3E SCFV) – GGGGS - MOUSE SERUM ALBUMIN – GGGS – IV1 – HHHHHH – STOP

w/o propeptide

ds(sm3E ScFv) = Vh – (Gly4Ser)3 – Vl

Yellow: Forward Sequence Primer

Light Blue: Reverse Sequence Primer

ATGAGGGTCCCCGCTCAGCTCCTGGGGCTCCTGCTGCTCTGGCTCCCAGGTGCACGATGTCAAGTTAAACTGGAACA
GTCCGGTGCTGAAGTTGTCAAACCAGGTGCTTCCGTGAAGTTGTCCTGTAAAGCCTCTGGTTTTAACATCAAGGATT
CGTATATGCATTGGTTGAGACAAGGGCCAGGACAATGTTTGGAATGGATTGGCTGGATTGATCCAGAGAATGGTGAT
ACCGAGTACGCTCCTAAATTTCAGGGAAAGGCTACTTTTACTACCGACACTTCCGCTAATACCGCATACTTGGGCTT
ATCTTCCTTGAGACCAGAGGACACTGCCGTATACTACTGCAACGAAGGGACACCAACTGGTCCTTACTATTTCGACT
ACTGGGGACAAGGTACCTTAGTTACTGTCTCTAGCGGTGGCGGAGGTTCAGGCGGTGGAGGGTCTGGAGGTGGCGGT
AGTGAAAATGTGCTGACCCAATCTCCAAGCTCCATGTCTGTTTCTGTTGGCGATAGAGTAACCATCGCTTGTAGCGC
ATCCTCTAGTGTCCCATATATGCACTGGCTTCAACAGAAGCCAGGTAAAAGCCCAAAGTTGTTGATTTATTTGACAT
CCAACTTGGCTTCTGGAGTGCCTTCAAGGTTTTCTGGTTCCGGCTCAGGAACCGATTATAGTTTGACTATTAGCTCA
GTGCAGCCAGAGGATGCTGCAACCTACTATTGCCAGCAAAGGTCCTCATATCCACTGACTTTCGGGTGTGGAACGAA
GTTGGAAATCAAGGGTGGAGGCGGTTCAGAAGCACACAAGAGTGAGATCGCCCATCGGTATAATGATTTGGGAGAAC
AACATTTCAAAGGCCTAGTCCTGATTGCCTTTTCCCAGTATCTCCAGAAATGCTCATACGATGAGCATGCCAAATTA
GTGCAGGAAGTAACAGACTTTGCAAAGACGTGTGTTGCCGATGAGTCTGCCGCCAACTGTGACAAATCCCTTCACAC
TCTTTTTGGAGATAAGTTGTGTGCCATTCCAAACCTCCGTGAAAACTATGGTGAACTGGCTGACTGCTGTACAAAAC
AAGAGCCCGAAAGAAACGAATGTTTCCTGCAACACAAAGATGACAACCCCAGCCTGCCACCATTTGAAAGGCCAGAG
GCTGAGGCCATGTGCACCTCCTTTAAGGAAAACCCAACCACCTTTATGGGACACTATTTGCATGAAGTTGCCAGAAG

ACATCCTTATTTCTATGCCCCAGAACTTCTTTACTATGCTGAGCAGTACAATGAGATTCTGACCCAGTGTTGTGCAG
AGGCTGACAAGGAAAGCTGCCTGACCCCGAAGCTTGATGGTGTGAAGGAGAAAGCATTGGTCTCATCTGTCCGTCAG
AGAATGAAGTGCTCCAGTATGCAGAAGTTTGGAGAGAGAGCTTTTAAAGCATGGGCAGTAGCTCGTCTGAGCCAGAC
ATTCCCCAATGCTGACTTTGCAGAAATCACCAAATTGGCAACAGACCTGACCAAAGTCAACAAGGAGTGCTGCCATG
GTGACCTGCTGGAATGCGCAGATGACAGGGCGGAACTTGCCAAGTACATGTGTGAAAACCAGGCGACTATCTCCAGC
AAACTGCAGACTTGCTGCGATAAACCACTGTTGAAGAAAGCCCACTGTCTTAGTGAGGTGGAGCATGACACCATGCC
TGCTGATCTGCCTGCCATTGCTGCTGATTTTGTTGAGGACCAGGAAGTGTGCAAGAACTATGCTGAGGCCAAGGATG
TCTTCCTGGGCACGTTCTTGTATGAATATTCAAGAAGACACCCTGATTACTCTGTATCCCTGTTGCTGAGACTTGCT
AAGAAATATGAAGCCACTCTGGAAAAGTGCTGCGCTGAAGCCAATCCTCCCGCATGCTACGGCACAGTGCTTGCTGA
ATTTCAGCCTCTTGTAGAAGAGCCTAAGAACTTGGTCAAAACCAACTGTGATCTTTACGAGAAGCTTGGAGAATATG
GATTCCAAAATGCCATTCTAGTTCGCTACACCCAGAAAGCACCTCAGGTGTCAACCCCAACTCTCGTGGAGGCTGCA
AGAAACCTAGGAAGAGTGGGCACCAAGTGTTGTACACTTCCTGAAGATCAGAGACTGCCTTGTGTGGAAGACTATCT
GTCTGCAATCCTGAACCGTGTGTGTCTGCTGCATGAGAAGACCCCAGTGAGTGAGCATGTTACCAAGTGCTGTAGTG
GATCCCTGGTGGAAAGGCGGCCATGCTTCTCTGCTCTGACAGTTGATGAAACATATGTCCCCAAAGAGTTTAAAGCT
GAGACCTTCACCTTCCACTCTGATATCTGCACACTTCCAGAGAAGGAGAAGCAGATTAAGAAACAAACGGCTCTTGC
TGAGCTGGTGAAGCACAAGCCCAAGGCTACAGCGGAGCAACTGAAGACTGTCATGGATGACTTTGCACAGTTCCTGG
ATACATGTTGCAAGGCTGCTGACAAGGACACCTGCTTCTCGACTGAGGGTCCAAACCTTGTCACTAGATGCAAAGAC
GCCTTAGCCGGAGGGGGCTCCGTTTCTGATGTTCCGAGGGACCTGGAAGTTGTTGCTGCGACCCCCACCAGCCTACT
GATCAGCTGGGACGATCCGAGTGGCATGGCCCCCTACAGGATCACTTACGGAGAAACAGGAGGAAATAGCCCTGTCC
AGGAGTTCACTGTGCCTGAACACGTATGGATGGCTACCATCAGCGGCCTTAAACCTGGAGTTGATTATACCATCACT
GTGTATGCTGTCACTGACCAGGGTTCTTCTCACCCAATTTCTATTAATTACCGAACAGAAATTGACAAACCATCCCA
GCACCATCACCACCATCACTGATAA

dsSSMSA-IV2

HUMAN LC LEADER – DS(SM3E SCFV) – GGGGS - MOUSE SERUM ALBUMIN – GGGS – IV2 – HHHHHHH – STOP

w/o propeptide

ds(sm3E ScFv) = Vh – (Gly4Ser)3 – Vl

Yellow: Forward Sequence Primer

Light Blue: Reverse Sequence Primer

ATGAGGGTCCCCGCTCAGCTCCTGGGGCTCCTGCTGCTCTGGCTCCCAGGTGCACGATGTCAAGTTAAACTGGAACA
GTCCGGTGCTGAAGTTGTCAAACCAGGTGCTTCCGTGAAGTTGTCCTGTAAAGCCTCTGGTTTTAACATCAAGGATT
CGTATATGCATTGGTTGAGACAAGGGCCAGGACAATGTTTGGAATGGATTGGCTGGATTGATCCAGAGAATGGTGAT
ACCGAGTACGCTCCTAAATTTCAGGGAAAGGCTACTTTTACTACCGACACTTCCGCTAATACCGCATACTTGGGCTT
ATCTTCCTTGAGACCAGAGGACACTGCCGTATACTACTGCAACGAAGGGACACCAACTGGTCCTTACTATTTCGACT
ACTGGGGACAAGGTACCTTAGTTACTGTCTCTAGCGGTGGCGGAGGTTCAGGCGGTGGAGGGTCTGGAGGTGGCGGT
AGTGAAAATGTGCTGACCCAATCTCCAAGCTCCATGTCTGTTTCTGTTGGCGATAGAGTAACCATCGCTTGTAGCGC
ATCCTCTAGTGTCCCATATATGCACTGGCTTCAACAGAAGCCAGGTAAAAGCCCAAAGTTGTTGATTTATTTGACAT
CCAACTTGGCTTCTGGAGTGCCTTCAAGGTTTTCTGGTTCCGGCTCAGGAACCGATTATAGTTTGACTATTAGCTCA
GTGCAGCCAGAGGATGCTGCAACCTACTATTGCCAGCAAAGGTCCTCATATCCACTGACTTTCGGGTGTGGAACGAA
GTTGGAAATCAAGGGTGGAGGCGGTTCAGAAGCACACAAGAGTGAGATCGCCCATCGGTATAATGATTTGGGAGAAC
AACATTTCAAAGGCCTAGTCCTGATTGCCTTTTCCCAGTATCTCCAGAAATGCTCATACGATGAGCATGCCAAATTA
GTGCAGGAAGTAACAGACTTTGCAAAGACGTGTGTTGCCGATGAGTCTGCCGCCAACTGTGACAAATCCCTTCACAC
TCTTTTTGGAGATAAGTTGTGTGCCATTCCAAACCTCCGTGAAAACTATGGTGAACTGGCTGACTGCTGTACAAAAC
AAGAGCCCGAAAGAAACGAATGTTTCCTGCAACACAAAGATGACAACCCCAGCCTGCCACCATTTGAAAGGCCAGAG
GCTGAGGCCATGTGCACCTCCTTTAAGGAAAACCCAACCACCTTTATGGGACACTATTTGCATGAAGTTGCCAGAAG
ACATCCTTATTTCTATGCCCCAGAACTTCTTTACTATGCTGAGCAGTACAATGAGATTCTGACCCAGTGTTGTGCAG
AGGCTGACAAGGAAAGCTGCCTGACCCCGAAGCTTGATGGTGTGAAGGAGAAAGCATTGGTCTCATCTGTCCGTCAG
AGAATGAAGTGCTCCAGTATGCAGAAGTTTGGAGAGAGAGCTTTTAAAGCATGGGCAGTAGCTCGTCTGAGCCAGAC
ATTCCCCAATGCTGACTTTGCAGAAATCACCAAATTGGCAACAGACCTGACCAAAGTCAACAAGGAGTGCTGCCATG
GTGACCTGCTGGAATGCGCAGATGACAGGGCGGAACTTGCCAAGTACATGTGTGAAAACCAGGCGACTATCTCCAGC
AAACTGCAGACTTGCTGCGATAAACCACTGTTGAAGAAAGCCCACTGTCTTAGTGAGGTGGAGCATGACACCATGCC
TGCTGATCTGCCTGCCATTGCTGCTGATTTTGTTGAGGACCAGGAAGTGTGCAAGAACTATGCTGAGGCCAAGGATG
TCTTCCTGGGCACGTTCTTGTATGAATATTCAAGAAGACACCCTGATTACTCTGTATCCCTGTTGCTGAGACTTGCT

AAGAAATATGAAGCCACTCTGGAAAAGTGCTGCGCTGAAGCCAATCCTCCCGCATGCTACGGCACAGTGCTTGCTGA
ATTTCAGCCTCTTGTAGAAGAGCCTAAGAACTTGGTCAAAACCAACTGTGATCTTTACGAGAAGCTTGGAGAATATG
GATTCCAAAATGCCATTCTAGTTCGCTACACCCAGAAAGCACCTCAGGTGTCAACCCCAACTCTCGTGGAGGCTGCA
AGAAACCTAGGAAGAGTGGGCACCAAGTGTTGTACACTTCCTGAAGATCAGAGACTGCCTTGTGTGGAAGACTATCT
GTCTGCAATCCTGAACCGTGTGTGTCTGCTGCATGAGAAGACCCCAGTGAGTGAGCATGTTACCAAGTGCTGTAGTG
GATCCCTGGTGGAAAGGCGGCCATGCTTCTCTGCTCTGACAGTTGATGAAACATATGTCCCCAAAGAGTTTAAAGCT
GAGACCTTCACCTTCCACTCTGATATCTGCACACTTCCAGAGAAGGAGAAGCAGATTAAGAAACAAACGGCTCTTGC
TGAGCTGGTGAAGCACAAGCCCAAGGCTACAGCGGAGCAACTGAAGACTGTCATGGATGACTTTGCACAGTTCCTGG
ATACATGTTGCAAGGCTGCTGACAAGGACACCTGCTTCTCGACTGAGGGTCCAAACCTTGTCACTAGATGCAAAGAC
GCCTTAGCCGGAGGGGGCTCCGTTTCTGATGTTCCGAGGGACCTGGAAGTTGTCGCTGCGACCCCCACCAGCCTACT
GATCAGCTGGGATATTCCTGCTGGTGATTATTTGGATTATTACAAGATCACTTACGGAGAAACAGGAGGAAATAGCC
CTGTCCAGAAGTTCGCTGTGCCTTGGTCTATTCATACTGCTACCATCAGCGGCCTTAAACCTGGAGTTGATTATACC
ATCACTGTGTATGCTGTCACTTGGAAGGGCCCTTCTCCTAAGCCAATTTCCATTAATTACCGAACAGAAATTGACAA
ACCATCCCAGCACCATCACCACCATCACTGATAA

Fn3 fusion sequences

Several alternate Fn3 fusions were made but not mentioned in the thesis compilation. The sequences are outlined below for future use if needed.

Fn3-Fc fusions in jWiz vector

Fn3s were fused the a mIgG2a Fc, which can be made into a bivalent molecule. Outlined below are the sequences in the jWiz vector, which is an alternate form of the gWiz vector with the NheI and BamHI restriction cut sites inserted to flank the gene of interest. Two versions were made, one with the wild-type Fc and another as the FcKO mutation that includes two point mutations (G236R/L328R) that knocks out binding to the FcγRs. Only the wild-type Fc sequences are shown.

L mFc

PstI –LEADER – NheI – L mFc – BamHI – STOP
leader: human heavy chain
Fn3: L (HEL binder)
HC**:** hinge, C_H2, and C_H3 (IgG2a)

CTGCAGATGGGTTGGAGCCTCATCTTGCTCTTCCTTGTCGCTGTTGCTGCTAGCGTTTCTGATGTTCCGAGGGACCT
GGAAGTTGTTGCTGCGACCTCCACCAGCCTACTGATCAGTTGGCGCGGCTACCCCTGGGCTACCTATTATGGGATCA
TTTACGGAGAAACGGGAGGAAATAGCCTTGTCCAGGAGTTCACTATGCCTGGGGTTACCAATGCTACCATCAGCGGC
CTTAAACCTGGAGTTGATTATACCATCACTGTGTATGCTGTCACTCGCGTGGGGCGGACGTTTGACACGCCGGGCCC
AATCTCCATTAATTACCGAACAGAAATTGACAAACCATCCCAGGAGCCCAGAGTGCCCATAACACAGAACCCCTGTC
CTCCACTCAAAGAGTGTCCCCCATGCGCAGCTCCAGACCTCTTGGGTGGACCATCCGTCTTCATCTTCCCTCCAAAG
ATCAAGGATGTACTCATGATCTCCCTGAGCCCCATGGTCACATGTGTGGTGGTGGATGTGAGCGAGGATGACCCAGA
CGTCCAGATCAGCTGGTTTGTGAACAACGTGGAAGTACACACAGCTCAGACACAAACCCATAGAGAGGATTACAACA
GTACTCTCCGGGTGGTCAGTGCCCTCCCCATCCAGCACCAGGACTGGATGAGTGGCAAGGAGTTCAAATGCAAGGTC
AACAACAGAGCCCTCCCATCCCCCATCGAGAAAACCATCTCAAAACCCAGAGGGCCAGTAAGAGCTCCACAGGTATA
TGTCTTGCCTCCACCAGCAGAAGAGATGACTAAGAAAGAGTTCAGTCTGACCTGCATGATCACAGGCTTCTTACCTG
CCGAAATTGCTGTGGACTGGACCAGCAATGGGCGTACAGAGCAAAACTACAAGAACACCGCAACAGTCCTGGACTCT
GATGGTTCTTACTTCATGTACAGCAAGCTCAGAGTACAAAAGAGCACTTGGGAAAGAGGAAGTCTTTTCGCCTGCTC
AGTGGTCCACGAGGGTCTGCACAATCACCTTACGACTAAGACCATCTCCCGGTCTCTGGGTAAAGGATCCTGATAA

I mFc

PstI –LEADER – NheI – I mFc – BamHI - STOP
leader: human heavy chain
Fn3: I (mFcγRI binder)
HC: hinge, C_H2, and C_H3 (IgG2a)

CTGCAGATGGGTTGGAGCCTCATCTTGCTCTTCCTTGTCGCTGTTGCTGCTAGCGTTTCTGATGTTCCGAGGGACCT
GGAAGTTGTTGCTGCGACCCCCACCAGCCTACTGATCAGCTGGCATTTGCCCTACCACGCGATCTTTTACAGGATCA
CTTACGGAGAAACAGGAGGAAATAGCCCTGCCCAGGAGTTCACTGTGCCTTGGTCTTATACCTCGGCTACCATCAGC
GGCCTTAAACCTGGAGTTGACTATACCATCACTGTGTATGCTGTCACTTACAACGGCCCCCCCTTTTTTTATCCAAC
TTCCATTAATTACCGAACAGAAATTGACAAACCATCCCAGGAGCCCAGAGTGCCCATAACACAGAACCCCTGTCCTC
CACTCAAAGAGTGTCCCCCATGCGCAGCTCCAGACCTCTTGGGTGGACCATCCGTCTTCATCTTCCCTCCAAAGATC
AAGGATGTACTCATGATCTCCCTGAGCCCCATGGTCACATGTGTGGTGGTGGATGTGAGCGAGGATGACCCAGACGT
CCAGATCAGCTGGTTTGTGAACAACGTGGAAGTACACACAGCTCAGACACAAACCCATAGAGAGGATTACAACAGTA
CTCTCCGGGTGGTCAGTGCCCTCCCCATCCAGCACCAGGACTGGATGAGTGGCAAGGAGTTCAAATGCAAGGTCAAC
AACAGAGCCCTCCCATCCCCCATCGAGAAAACCATCTCAAAACCCAGAGGGCCAGTAAGAGCTCCACAGGTATATGT
CTTGCCTCCACCAGCAGAAGAGATGACTAAGAAAGAGTTCAGTCTGACCTGCATGATCACAGGCTTCTTACCTGCCG
AAATTGCTGTGGACTGGACCAGCAATGGGCGTACAGAGCAAAACTACAAGAACACCGCAACAGTCCTGGACTCTGAT
GGTTCTTACTTCATGTACAGCAAGCTCAGAGTACAAAAGAGCACTTGGGAAAGAGGAAGTCTTTTCGCCTGCTCAGT
GGTCCACGAGGGTCTGCACAATCACCTTACGACTAAGACCATCTCCCGGTCTCTGGGTAAAGGATCCTGATAA

II mFc

PstI –LEADER – NheI – II mFc – BamHI - STOP

leader: human heavy chain
Fn3: II (mFcγRII binder)
HC: hinge, C_H2, and C_H3 (IgG2a)

CTGCAGATGGGTTGGAGCCTCATCTTGCTCTTCCTTGTCGCTGTTGCTGCTAGCGTTTCTGATGTTCCGAGGGACCT
GGAAGTTGTTACTGCGACCCCCACCAGCCTACTGATCAGCTGGTTTCCTCTTCACGATGAGCATGCGGACTATTTCA
GGATCACTTACGGAGAAACAGGAGGAAATAGCCCTGTCCAGGAGTTCACTGTGCCTGGGTGGATGTTGGCGGCTCCC
ATCAGCGGCCTTAAACCTGGAGTTGATTATACCATCACTGTGTATGCTGTCACTTCCAACGACTCCTACTCTAATCC
ACTCTCCATTAATTACCGAACAGAAATTGACAAACCATCCCAGGAGCCCAGAGTGCCCATAACACAGAACCCCTGTC
CTCCACTCAAAGAGTGTCCCCCATGCGCAGCTCCAGACCTCTTGGGTGGACCATCCGTCTTCATCTTCCCTCCAAAG
ATCAAGGATGTACTCATGATCTCCCTGAGCCCCATGGTCACATGTGTGGTGGTGGATGTGAGCGAGGATGACCCAGA
CGTCCAGATCAGCTGGTTTGTGAACAACGTGGAAGTACACACAGCTCAGACACAAACCCATAGAGAGGATTACAACA
GTACTCTCCGGGTGGTCAGTGCCCTCCCCATCCAGCACCAGGACTGGATGAGTGGCAAGGAGTTCAAATGCAAGGTC
AACAACAGAGCCCTCCCATCCCCCATCGAGAAAACCATCTCAAAACCCAGAGGGCCAGTAAGAGCTCCACAGGTATA
TGTCTTGCCTCCACCAGCAGAAGAGATGACTAAGAAAGAGTTCAGTCTGACCTGCATGATCACAGGCTTCTTACCTG
CCGAAATTGCTGTGGACTGGACCAGCAATGGGCGTACAGAGCAAAACTACAAGAACACCGCAACAGTCCTGGACTCT
GATGGTTCTTACTTCATGTACAGCAAGCTCAGAGTACAAAAGAGCACTTGGGAAAGAGGAAGTCTTTTCGCCTGCTC
AGTGGTCCACGAGGGTCTGCACAATCACCTTACGACTAAGACCATCTCCCGGTCTCTGGGTAAAGGATCCTGATAA

III mFc

PstI –LEADER – NheI – III mFc – BamHI - STOP

leader: human heavy chain
Fn3: III (mFcγRIII binder)
HC**:** hinge, C_H2, and C_H3 (IgG2a)

CTGCAGATGGGTTGGAGCCTCATCTTGCTCTTCCTTGTCGCTGTTGCTGCTAGCGTTTCTGATGTTCCGAGGGACCT
GGAAGTTGTTGCTGCGACCCCCACCAGCCTACTGATCAGCTGGCATTGTCCCTACTGTGATTCGGACTCTTACAGGA
TCACTTACGGAGAAACAGGAGGAAATAGCCCTGTCCAGGAGTTCACTGTGCCTTATTGGAGGTTTTCGGCTACCATC
AGCGGCCTTAAACCTGGAATTGATTATACCATCACTATGTATGCCGTCACTGGCAGGTACTGGTCTGAGCCAATTTC
CATTAATTACCGAACAGAAATTGACAAACCATCCCAGGAGCCCAGAGTGCCCATAACACAGAACCCCTGTCCTCCAC
TCAAAGAGTGTCCCCCATGCGCAGCTCCAGACCTCTTGGGTGGACCATCCGTCTTCATCTTCCCTCCAAAGATCAAG
GATGTACTCATGATCTCCCTGAGCCCCATGGTCACATGTGTGGTGGTGGATGTGAGCGAGGATGACCCAGACGTCCA
GATCAGCTGGTTTGTGAACAACGTGGAAGTACACACAGCTCAGACACAAACCCATAGAGAGGATTACAACAGTACTC
TCCGGGTGGTCAGTGCCCTCCCCATCCAGCACCAGGACTGGATGAGTGGCAAGGAGTTCAAATGCAAGGTCAACAAC
AGAGCCCTCCCATCCCCCATCGAGAAAACCATCTCAAAACCCAGAGGGCCAGTAAGAGCTCCACAGGTATATGTCTT
GCCTCCACCAGCAGAAGAGATGACTAAGAAAGAGTTCAGTCTGACCTGCATGATCACAGGCTTCTTACCTGCCGAAA
TTGCTGTGGACTGGACCAGCAATGGGCGTACAGAGCAAAACTACAAGAACACCGCAACAGTCCTGGACTCTGATGGT

TCTTACTTCATGTACAGCAAGCTCAGAGTACAAAAGAGCACTTGGGAAAGAGGAAGTCTTTTCGCCTGCTCAGTGGT
CCACGAGGGTCTGCACAATCACCTTACGACTAAGACCATCTCCCGGTCTCTGGGTAAAGGATCCTGATAA

IV1 mFc

PstI –LEADER – NheI – IV1 mFc – BamHI - STOP

leader: human heavy chain
Fn3: IV1 (mFcγRIV binder)
HC: hinge, C_H2, and C_H3 (IgG2a)

CTGCAGATGGGTTGGAGCCTCATCTTGCTCTTCCTTGTCGCTGTTGCTGCTAGCGTTTCTGATGTTCCGAGGGACCT
GGAAGTTGTTGCTGCGACCCCCACCAGCCTACTGATCAGCTGGGACGATCCGAGTGGCATGGCCCCCTACAGGATCA
CTTACGGAGAAACAGGAGGAAATAGCCCTGTCCAGGAGTTCACTGTGCCTGAACACGTATGGATGGCTACCATCAGC
GGCCTTAAACCTGGAGTTGATTATACCATCACTGTGTATGCTGTCACTGACCAGGGTTCTTCTCACCCAATTTCTAT
TAATTACCGAACAGAAATTGACAAACCATCCCAGGAGCCCAGAGTGCCCATAACACAGAACCCCTGTCCTCCACTCA
AAGAGTGTCCCCCATGCGCAGCTCCAGACCTCTTGGGTGGACCATCCGTCTTCATCTTCCCTCCAAAGATCAAGGAT
GTACTCATGATCTCCCTGAGCCCCATGGTCACATGTGTGGTGGTGGATGTGAGCGAGGATGACCCAGACGTCCAGAT
CAGCTGGTTTGTGAACAACGTGGAAGTACACACAGCTCAGACACAAACCCATAGAGAGGATTACAACAGTACTCTCC
GGGTGGTCAGTGCCCTCCCCATCCAGCACCAGGACTGGATGAGTGGCAAGGAGTTCAAATGCAAGGTCAACAACAGA
GCCCTCCCATCCCCCATCGAGAAAACCATCTCAAAACCCAGAGGGCCAGTAAGAGCTCCACAGGTATATGTCTTGCC
TCCACCAGCAGAAGAGATGACTAAGAAAGAGTTCAGTCTGACCTGCATGATCACAGGCTTCTTACCTGCCGAAATTG
CTGTGGACTGGACCAGCAATGGGCGTACAGAGCAAAACTACAAGAACACCGCAACAGTCCTGGACTCTGATGGTTCT
TACTTCATGTACAGCAAGCTCAGAGTACAAAAGAGCACTTGGGAAAGAGGAAGTCTTTTCGCCTGCTCAGTGGTCCA
CGAGGGTCTGCACAATCACCTTACGACTAAGACCATCTCCCGGTCTCTGGGTAAAGGATCCTGATAA

IV2 mFc

PstI –LEADER – NheI – IV2 mFc – BamHI - STOP

leader: human heavy chain
Fn3: IV2 (mFcγRIV binder)
HC: hinge, C_H2, and C_H3 (IgG2a)

CTGCAGATGGGTTGGAGCCTCATCTTGCTCTTCCTTGTCGCTGTTGCTGCTAGCGTTTCTGATGTTCCGAGGGACCT
GGAAGTTGTCGCTGCGACCCCCACCAGCCTACTGATCAGCTGGGATATTCCTGCTGGTGATTATTTGGATTATTACA
AGATCACTTACGGAGAAACAGGAGGAAATAGCCCTGTCCAGAAGTTCGCTGTGCCTTGGTCTATTCATACTGCTACC
ATCAGCGGCCTTAAACCTGGAGTTGATTATACCATCACTGTGTATGCTGTCACTTGGAAGGGCCCTTCTCCTAAGCC
AATTTCCATTAATTACCGAACAGAAATTGACAAACCATCCCAGGAGCCCAGAGTGCCCATAACACAGAACCCCTGTC
CTCCACTCAAAGAGTGTCCCCCATGCGCAGCTCCAGACCTCTTGGGTGGACCATCCGTCTTCATCTTCCCTCCAAAG
ATCAAGGATGTACTCATGATCTCCCTGAGCCCCATGGTCACATGTGTGGTGGTGGATGTGAGCGAGGATGACCCAGA
CGTCCAGATCAGCTGGTTTGTGAACAACGTGGAAGTACACACAGCTCAGACACAAACCCATAGAGAGGATTACAACA
GTACTCTCCGGGTGGTCAGTGCCCTCCCCATCCAGCACCAGGACTGGATGAGTGGCAAGGAGTTCAAATGCAAGGTC
AACAACAGAGCCCTCCCATCCCCCATCGAGAAAACCATCTCAAAACCCAGAGGGCCAGTAAGAGCTCCACAGGTATA
TGTCTTGCCTCCACCAGCAGAAGAGATGACTAAGAAAGAGTTCAGTCTGACCTGCATGATCACAGGCTTCTTACCTG
CCGAAATTGCTGTGGACTGGACCAGCAATGGGCGTACAGAGCAAAACTACAAGAACACCGCAACAGTCCTGGACTCT
GATGGTTCTTACTTCATGTACAGCAAGCTCAGAGTACAAAAGAGCACTTGGGAAAGAGGAAGTCTTTTCGCCTGCTC
AGTGGTCCACGAGGGTCTGCACAATCACCTTACGACTAAGACCATCTCCCGGTCTCTGGGTAAAGGATCCTGATAA

2.5F-MSA-Fn3 fusions in gWiz vector

2.5F is a knottin peptide that binds to three integrins $\alpha_v\beta_3$, $\alpha_v\beta_5$, and $\alpha_5\beta_1$. We used 2.5F as an alternative tumor-targeting agent for our Fn3 constructs.

2.5FMSA-L

HUMAN LC LEADER – 2.5F – GGGGS - MOUSE SERUM ALBUMIN – GGGS – L – HHHHHH – STOP
w/o propeptide

Yellow: Forward Sequence Primer
Light Blue: Reverse Sequence Primer

ATGAGGGTCCCCGCTCAGCTCCTGGGGCTCCTGCTGCTCTGGCTCCCAGGTGCACGATGTGGTTGTCCAAGACCAAG
AGGTGATAATCCACCATTGACTTGTTCTCAAGATTCTGATTGTTTGGCTGGTTGTGTTTGTGGTCCAAATGGTTTTT
GTGGTGGTGGAGGCGGTTCAGAAGCACACAAGAGTGAGATCGCCCATCGGTATAATGATTTGGGAGAACAACATTTC
AAAGGCCTAGTCCTGATTGCCTTTTCCCAGTATCTCCAGAAATGCTCATACGATGAGCATGCCAAATTAGTGCAGGA
AGTAACAGACTTTGCAAAGACGTGTGTTGCCGATGAGTCTGCCGCCAACTGTGACAAATCCCTTCACACTCTTTTTG
GAGATAAGTTGTGTGCCATTCCAAACCTCCGTGAAAACTATGGTGAACTGGCTGACTGCTGTACAAAACAAGAGCCC
GAAAGAAACGAATGTTTCCTGCAACACAAAGATGACAACCCCAGCCTGCCACCATTTGAAAGGCCAGAGGCTGAGGC
CATGTGCACCTCCTTTAAGGAAAACCCAACCACCTTTATGGGACACTATTTGCATGAAGTTGCCAGAAGACATCCTT
ATTTCTATGCCCCAGAACTTCTTTACTATGCTGAGCAGTACAATGAGATTCTGACCCAGTGTTGTGCAGAGGCTGAC
AAGGAAAGCTGCCTGACCCCGAAGCTTGATGGTGTGAAGGAGAAAGCATTGGTCTCATCTGTCCGTCAGAGAATGAA
GTGCTCCAGTATGCAGAAGTTTGGAGAGAGAGCTTTTAAAGCATGGGCAGTAGCTCGTCTGAGCCAGACATTCCCCA
ATGCTGACTTTGCAGAAATCACCAAATTGGCAACAGACCTGACCAAAGTCAACAAGGAGTGCTGCCATGGTGACCTG
CTGGAATGCGCAGATGACAGGGCGGAACTTGCCAAGTACATGTGTGAAAACCAGGCGACTATCTCCAGCAAACTGCA
GACTTGCTGCGATAAACCACTGTTGAAGAAAGCCCACTGTCTTAGTGAGGTGGAGCATGACACCATGCCTGCTGATC
TGCCTGCCATTGCTGCTGATTTTGTTGAGGACCAGGAAGTGTGCAAGAACTATGCTGAGGCCAAGGATGTCTTCCTG
GGCACGTTCTTGTATGAATATTCAAGAAGACACCCTGATTACTCTGTATCCCTGTTGCTGAGACTTGCTAAGAAATA
TGAAGCCACTCTGGAAAAGTGCTGCGCTGAAGCCAATCCTCCCGCATGCTACGGCACAGTGCTTGCTGAATTTCAGC
CTCTTGTAGAAGAGCCTAAGAACTTGGTCAAAACCAACTGTGATCTTTACGAGAAGCTTGGAGAATATGGATTCCAA
AATGCCATTCTAGTTCGCTACACCCAGAAAGCACCTCAGGTGTCAACCCCAACTCTCGTGGAGGCTGCAAGAAACCT
AGGAAGAGTGGGCACCAAGTGTTGTACACTTCCTGAAGATCAGAGACTGCCTTGTGTGGAAGACTATCTGTCTGCAA
TCCTGAACCGTGTGTGTCTGCTGCATGAGAAGACCCCAGTGAGTGAGCATGTTACCAAGTGCTGTAGTGGATCCCTG
GTGGAAAGGCGGCCATGCTTCTCTGCTCTGACAGTTGATGAAACATATGTCCCCAAAGAGTTTAAAGCTGAGACCTT
CACCTTCCACTCTGATATCTGCACACTTCCAGAGAAGGAGAAGCAGATTAAGAAACAAACGGCTCTTGCTGAGCTGG
TGAAGCACAAGCCCAAGGCTACAGCGGAGCAACTGAAGACTGTCATGGATGACTTTGCACAGTTCCTGGATACATGT
TGCAAGGCTGCTGACAAGGACACCTGCTTCTCGACTGAGGGTCCAAACCTTGTCACTAGATGCAAAGACGCCTTAGC
CGGAGGGGGCTCCGTTTCTGATGTCCCGAGGGACCTGGAAGTTGTTGCTGCGACCTCCACCAGCCTACTGATCAGTT
GGCGCGGCTACCCCTGGGCTACCTATTATGGGATCATTTACGGAGAAACGGGAGGAAATAGCCTTGTCCAGGAGTTC
ACTATGCCTGGGGTTACCAATGCTACCATCAGCGGCCTTAAACCTGGAGTTGATTATACCATCACTGTGTATGCTGT
CACTCGCGTGGGGCGGACGTTTGACACGCCGGGCCCAATCTCCATTAATTACCGAACAGAAATTGACAAACCATCCC
AGCACCATCACCACCATCACTGATAA

2.5FMSA-I
HUMAN LC LEADER – 2.5F – GGGGS - MOUSE SERUM ALBUMIN – GGGS – I – HHHHHH – STOP
w/o propeptide
Yellow: Forward Sequence Primer
Light Blue: Reverse Sequence Primer

ATGAGGGTCCCCGCTCAGCTCCTGGGGCTCCTGCTGCTCTGGCTCCCAGGTGCACGATGTGGTTGTCCAAGACCAAG
AGGTGATAATCCACCATTGACTTGTTCTCAAGATTCTGATTGTTTGGCTGGTTGTGTTTGTGGTCCAAATGGTTTTT
GTGGTGGTGGAGGCGGTTCAGAAGCACACAAGAGTGAGATCGCCCATCGGTATAATGATTTGGGAGAACAACATTTC
AAAGGCCTAGTCCTGATTGCCTTTTCCCAGTATCTCCAGAAATGCTCATACGATGAGCATGCCAAATTAGTGCAGGA
AGTAACAGACTTTGCAAAGACGTGTGTTGCCGATGAGTCTGCCGCCAACTGTGACAAATCCCTTCACACTCTTTTTG
GAGATAAGTTGTGTGCCATTCCAAACCTCCGTGAAAACTATGGTGAACTGGCTGACTGCTGTACAAAACAAGAGCCC
GAAAGAAACGAATGTTTCCTGCAACACAAAGATGACAACCCCAGCCTGCCACCATTTGAAAGGCCAGAGGCTGAGGC
CATGTGCACCTCCTTTAAGGAAAACCCAACCACCTTTATGGGACACTATTTGCATGAAGTTGCCAGAAGACATCCTT
ATTTCTATGCCCCAGAACTTCTTTACTATGCTGAGCAGTACAATGAGATTCTGACCCAGTGTTGTGCAGAGGCTGAC
AAGGAAAGCTGCCTGACCCCGAAGCTTGATGGTGTGAAGGAGAAAGCATTGGTCTCATCTGTCCGTCAGAGAATGAA
GTGCTCCAGTATGCAGAAGTTTGGAGAGAGAGCTTTTAAAGCATGGGCAGTAGCTCGTCTGAGCCAGACATTCCCCA
ATGCTGACTTTGCAGAAATCACCAAATTGGCAACAGACCTGACCAAAGTCAACAAGGAGTGCTGCCATGGTGACCTG
CTGGAATGCGCAGATGACAGGGCGGAACTTGCCAAGTACATGTGTGAAAACCAGGCGACTATCTCCAGCAAACTGCA
GACTTGCTGCGATAAACCACTGTTGAAGAAAGCCCACTGTCTTAGTGAGGTGGAGCATGACACCATGCCTGCTGATC
TGCCTGCCATTGCTGCTGATTTTGTTGAGGACCAGGAAGTGTGCAAGAACTATGCTGAGGCCAAGGATGTCTTCCTG

GGCACGTTCTTGTATGAATATTCAAGAAGACACCCTGATTACTCTGTATCCCTGTTGCTGAGACTTGCTAAGAAATA
TGAAGCCACTCTGGAAAAGTGCTGCGCTGAAGCCAATCCTCCCGCATGCTACGGCACAGTGCTTGCTGAATTTCAGC
CTCTTGTAGAAGAGCCTAAGAACTTGGTCAAAACCAACTGTGATCTTTACGAGAAGCTTGGAGAATATGGATTCCAA
AATGCCATTCTAGTTCGCTACACCCAGAAAGCACCTCAGGTGTCAACCCCAACTCTCGTGGAGGCTGCAAGAAACCT
AGGAAGAGTGGGCACCAAGTGTTGTACACTTCCTGAAGATCAGAGACTGCCTTGTGTGGAAGACTATCTGTCTGCAA
TCCTGAACCGTGTGTGTCTGCTGCATGAGAAGACCCCAGTGAGTGAGCATGTTACCAAGTGCTGTAGTGGATCCCTG
GTGGAAAGGCGGCCATGCTTCTCTGCTCTGACAGTTGATGAAACATATGTCCCCAAAGAGTTTAAAGCTGAGACCTT
CACCTTCCACTCTGATATCTGCACACTTCCAGAGAAGGAGAAGCAGATTAAGAAACAAACGGCTCTTGCTGAGCTGG
TGAAGCACAAGCCCAAGGCTACAGCGGAGCAACTGAAGACTGTCATGGATGACTTTGCACAGTTCCTGGATACATGT
TGCAAGGCTGCTGACAAGGACACCTGCTTCTCGACTGAGGGTCCAAACCTTGTCACTAGATGCAAAGACGCCTTAGC
CGGAGGGGGCTCCGTTTCTGATGTCCCGAGGGACCTGGAAGTTGTTGCTGCGACCCCCACCAGCCTACTGATCAGCT
GGCATTTGCCCTACCACGCGATCTTTTACAGGATCACTTACGGAGAAACAGGAGGAAATAGCCCTGCCCAGGAGTTC
ACTGTGCCTTGGTCTTATACCTCGGCTACCATCAGCGGCCTTAAACCTGGAGTTGACTATACCATCACTGTGTATGC
TGTCACTTACAACGGCCCCCCCTTTTTTTATCCAACTTCCATTAATTACCGGACAGAAATTGACAAACCATCCCAGC
ACCATCACCACCATCACTGATAA

2.5FMSA-II

HUMAN LC LEADER – 2.5F – GGGGS - MOUSE SERUM ALBUMIN – GGGS – II – HHHHHH – STOP

w/o propeptide

Yellow: Forward Sequence Primer

Light Blue: Reverse Sequence Primer

ATGAGGGTCCCCGCTCAGCTCCTGGGGCTCCTGCTGCTCTGGCTCCCAGGTGCACGATGTGGTTGTCCAAGACCAAG
AGGTGATAATCCACCATTGACTTGTTCTCAAGATTCTGATTGTTTGGCTGGTTGTGTTTGTGGTCCAAATGGTTTTT
GTGGTGGTGGAGGCGGTTCAGAAGCACACAAGAGTGAGATCGCCCATCGGTATAATGATTTGGGAGAACAACATTTC
AAAGGCCTAGTCCTGATTGCCTTTTCCCAGTATCTCCAGAAATGCTCATACGATGAGCATGCCAAATTAGTGCAGGA
AGTAACAGACTTTGCAAAGACGTGTGTTGCCGATGAGTCTGCCGCCAACTGTGACAAATCCCTTCACACTCTTTTTG
GAGATAAGTTGTGTGCCATTCCAAACCTCCGTGAAAACTATGGTGAACTGGCTGACTGCTGTACAAAACAAGAGCCC
GAAAGAAACGAATGTTTCCTGCAACACAAAGATGACAACCCCAGCCTGCCACCATTTGAAAGGCCAGAGGCTGAGGC
CATGTGCACCTCCTTTAAGGAAAACCCAACCACCTTTATGGGACACTATTTGCATGAAGTTGCCAGAAGACATCCTT
ATTTCTATGCCCCAGAACTTCTTTACTATGCTGAGCAGTACAATGAGATTCTGACCCAGTGTTGTGCAGAGGCTGAC
AAGGAAAGCTGCCTGACCCCGAAGCTTGATGGTGTGAAGGAGAAAGCATTGGTCTCATCTGTCCGTCAGAGAATGAA
GTGCTCCAGTATGCAGAAGTTTGGAGAGAGAGCTTTTAAAGCATGGGCAGTAGCTCGTCTGAGCCAGACATTCCCCA
ATGCTGACTTTGCAGAAATCACCAAATTGGCAACAGACCTGACCAAAGTCAACAAGGAGTGCTGCCATGGTGACCTG
CTGGAATGCGCAGATGACAGGGCGGAACTTGCCAAGTACATGTGTGAAAACCAGGCGACTATCTCCAGCAAACTGCA
GACTTGCTGCGATAAACCACTGTTGAAGAAAGCCCACTGTCTTAGTGAGGTGGAGCATGACACCATGCCTGCTGATC
TGCCTGCCATTGCTGCTGATTTTGTTGAGGACCAGGAAGTGTGCAAGAACTATGCTGAGGCCAAGGATGTCTTCCTG
GGCACGTTCTTGTATGAATATTCAAGAAGACACCCTGATTACTCTGTATCCCTGTTGCTGAGACTTGCTAAGAAATA
TGAAGCCACTCTGGAAAAGTGCTGCGCTGAAGCCAATCCTCCCGCATGCTACGGCACAGTGCTTGCTGAATTTCAGC
CTCTTGTAGAAGAGCCTAAGAACTTGGTCAAAACCAACTGTGATCTTTACGAGAAGCTTGGAGAATATGGATTCCAA
AATGCCATTCTAGTTCGCTACACCCAGAAAGCACCTCAGGTGTCAACCCCAACTCTCGTGGAGGCTGCAAGAAACCT
AGGAAGAGTGGGCACCAAGTGTTGTACACTTCCTGAAGATCAGAGACTGCCTTGTGTGGAAGACTATCTGTCTGCAA
TCCTGAACCGTGTGTGTCTGCTGCATGAGAAGACCCCAGTGAGTGAGCATGTTACCAAGTGCTGTAGTGGATCCCTG
GTGGAAAGGCGGCCATGCTTCTCTGCTCTGACAGTTGATGAAACATATGTCCCCAAAGAGTTTAAAGCTGAGACCTT
CACCTTCCACTCTGATATCTGCACACTTCCAGAGAAGGAGAAGCAGATTAAGAAACAAACGGCTCTTGCTGAGCTGG
TGAAGCACAAGCCCAAGGCTACAGCGGAGCAACTGAAGACTGTCATGGATGACTTTGCACAGTTCCTGGATACATGT
TGCAAGGCTGCTGACAAGGACACCTGCTTCTCGACTGAGGGTCCAAACCTTGTCACTAGATGCAAAGACGCCTTAGC
CGGAGGGGGCTCCGTTTCTGACGTTCCGAGGGTCCTGGAAGTTGTTACTGCGACCCCCACCAGCCTACTGATCAGCT
GGTTTCCTCTTCACGATGAGCATGCGGACTATTTCAGGATCACTTACGGAGAAACAGGAGGAAATAGCCCTGTCCAG
GAGTTCACTGTGCCTGGGTGGATGTTGGCGGCTCCCATCAGCGGCCTTAAACCTGGAGTTGATTATACCATCACTGT
GTATGCTGTCACTTCCAACGACTCCTACTCTAATCCACTCTCCATTAATTACCGAACAGAAATTGACAAACCATCCC
AGCACCATCACCACCATCACTGATAA

2.5FMSA-III

HUMAN LC LEADER – 2.5F – GGGGS - MOUSE SERUM ALBUMIN – GGGS – III – HHHHHHH – STOP
w/o propeptide
Yellow: Forward Sequence Primer
Light Blue: Reverse Sequence Primer

ATGAGGGTCCCCGCTCAGCTCCTGGGGCTCCTGCTGCTCTGGCTCCCAGGTGCACGATGTGGTTGTCCAAGACCAAG
AGGTGATAATCCACCATTGACTTGTTCTCAAGATTCTGATTGTTTGGCTGGTTGTGTTTGTGGTCCAAATGGTTTTT
GTGGTGGTGGAGGCGGTTCAGAAGCACACAAGAGTGAGATCGCCCATCGGTATAATGATTTGGGAGAACAACATTTC
AAAGGCCTAGTCCTGATTGCCTTTTCCCAGTATCTCCAGAAATGCTCATACGATGAGCATGCCAAATTAGTGCAGGA
AGTAACAGACTTTGCAAAGACGTGTGTTGCCGATGAGTCTGCCGCCAACTGTGACAAATCCCTTCACACTCTTTTTG
GAGATAAGTTGTGTGCCATTCCAAACCTCCGTGAAAACTATGGTGAACTGGCTGACTGCTGTACAAAACAAGAGCCC
GAAAGAAACGAATGTTTCCTGCAACACAAAGATGACAACCCCAGCCTGCCACCATTTGAAAGGCCAGAGGCTGAGGC
CATGTGCACCTCCTTTAAGGAAAACCCAACCACCTTTATGGGACACTATTTGCATGAAGTTGCCAGAAGACATCCTT
ATTTCTATGCCCCAGAACTTCTTTACTATGCTGAGCAGTACAATGAGATTCTGACCCAGTGTTGTGCAGAGGCTGAC
AAGGAAAGCTGCCTGACCCCGAAGCTTGATGGTGTGAAGGAGAAAGCATTGGTCTCATCTGTCCGTCAGAGAATGAA
GTGCTCCAGTATGCAGAAGTTTGGAGAGAGAGCTTTTAAAGCATGGGCAGTAGCTCGTCTGAGCCAGACATTCCCCA
ATGCTGACTTTGCAGAAATCACCAAATTGGCAACAGACCTGACCAAAGTCAACAAGGAGTGCTGCCATGGTGACCTG
CTGGAATGCGCAGATGACAGGGCGGAACTTGCCAAGTACATGTGTGAAAACCAGGCGACTATCTCCAGCAAACTGCA
GACTTGCTGCGATAAACCACTGTTGAAGAAAGCCCACTGTCTTAGTGAGGTGGAGCATGACACCATGCCTGCTGATC
TGCCTGCCATTGCTGCTGATTTTGTTGAGGACCAGGAAGTGTGCAAGAACTATGCTGAGGCCAAGGATGTCTTCCTG
GGCACGTTCTTGTATGAATATTCAAGAAGACACCCTGATTACTCTGTATCCCTGTTGCTGAGACTTGCTAAGAAATA
TGAAGCCACTCTGGAAAAGTGCTGCGCTGAAGCCAATCCTCCCGCATGCTACGGCACAGTGCTTGCTGAATTTCAGC
CTCTTGTAGAAGAGCCTAAGAACTTGGTCAAAACCAACTGTGATCTTTACGAGAAGCTTGGAGAATATGGATTCCAA
AATGCCATTCTAGTTCGCTACACCCAGAAAGCACCTCAGGTGTCAACCCCAACTCTCGTGGAGGCTGCAAGAAACCT
AGGAAGAGTGGGCACCAAGTGTTGTACACTTCCTGAAGATCAGAGACTGCCTTGTGTGGAAGACTATCTGTCTGCAA
TCCTGAACCGTGTGTGTCTGCTGCATGAGAAGACCCCAGTGAGTGAGCATGTTACCAAGTGCTGTAGTGGATCCCTG
GTGGAAAGGCGGCCATGCTTCTCTGCTCTGACAGTTGATGAAACATATGTCCCCAAAGAGTTTAAAGCTGAGACCTT
CACCTTCCACTCTGATATCTGCACACTTCCAGAGAAGGAGAAGCAGATTAAGAAACAAACGGCTCTTGCTGAGCTGG
TGAAGCACAAGCCCAAGGCTACAGCGGAGCAACTGAAGACTGTCATGGATGACTTTGCACAGTTCCTGGATACATGT
TGCAAGGCTGCTGACAAGGACACCTGCTTCTCGACTGAGGGTCCAAACCTTGTCACTAGATGCAAAGACGCCTTAGC
CGGAGGGGGCTCCGTTTCTGATGTTCCGAGGGACCTGGAAGTTGTTGCTGCGACCCCCACCAGCCTACTGATCAGCT
GGCATTGTCCCTACTGTGATTCGGACTCTTACAGGATCACTTACGGAGAAACAGGAGGAAATAGCCCTGTCCAGGAG
TTCACTGTGCCTTATTGGAGGTTTTCGGCTACCATCAGCGGCCTTAAACCTGGAATTGATTATACCATCACTATGTA
TGCCGTCACTGGCAGGTACTGGTCTGAGCCAATTTCCATTAATTACCGAACAGAAATTGACAAACCATCCCAGCACC
ATCACCACCATCACTGATAA

2.5FMSA-IV1
HUMAN LC LEADER – 2.5F – GGGGS - MOUSE SERUM ALBUMIN – GGGS – IV1 – HHHHHHH – STOP
w/o propeptide
Yellow: Forward Sequence Primer
Light Blue: Reverse Sequence Primer

ATGAGGGTCCCCGCTCAGCTCCTGGGGCTCCTGCTGCTCTGGCTCCCAGGTGCACGATGTGGTTGTCCAAGACCAAG
AGGTGATAATCCACCATTGACTTGTTCTCAAGATTCTGATTGTTTGGCTGGTTGTGTTTGTGGTCCAAATGGTTTTT
GTGGTGGTGGAGGCGGTTCAGAAGCACACAAGAGTGAGATCGCCCATCGGTATAATGATTTGGGAGAACAACATTTC
AAAGGCCTAGTCCTGATTGCCTTTTCCCAGTATCTCCAGAAATGCTCATACGATGAGCATGCCAAATTAGTGCAGGA
AGTAACAGACTTTGCAAAGACGTGTGTTGCCGATGAGTCTGCCGCCAACTGTGACAAATCCCTTCACACTCTTTTTG
GAGATAAGTTGTGTGCCATTCCAAACCTCCGTGAAAACTATGGTGAACTGGCTGACTGCTGTACAAAACAAGAGCCC
GAAAGAAACGAATGTTTCCTGCAACACAAAGATGACAACCCCAGCCTGCCACCATTTGAAAGGCCAGAGGCTGAGGC
CATGTGCACCTCCTTTAAGGAAAACCCAACCACCTTTATGGGACACTATTTGCATGAAGTTGCCAGAAGACATCCTT
ATTTCTATGCCCCAGAACTTCTTTACTATGCTGAGCAGTACAATGAGATTCTGACCCAGTGTTGTGCAGAGGCTGAC
AAGGAAAGCTGCCTGACCCCGAAGCTTGATGGTGTGAAGGAGAAAGCATTGGTCTCATCTGTCCGTCAGAGAATGAA

GTGCTCCAGTATGCAGAAGTTTGGAGAGAGAGCTTTTAAAGCATGGGCAGTAGCTCGTCTGAGCCAGACATTCCCCA
ATGCTGACTTTGCAGAAATCACCAAATTGGCAACAGACCTGACCAAAGTCAACAAGGAGTGCTGCCATGGTGACCTG
CTGGAATGCGCAGATGACAGGGCGGAACTTGCCAAGTACATGTGTGAAAACCAGGCGACTATCTCCAGCAAACTGCA
GACTTGCTGCGATAAACCACTGTTGAAGAAAGCCCACTGTCTTAGTGAGGTGGAGCATGACACCATGCCTGCTGATC
TGCCTGCCATTGCTGCTGATTTTGTTGAGGACCAGGAAGTGTGCAAGAACTATGCTGAGGCCAAGGATGTCTTCCTG
GGCACGTTCTTGTATGAATATTCAAGAAGACACCCTGATTACTCTGTATCCCTGTTGCTGAGACTTGCTAAGAAATA
TGAAGCCACTCTGGAAAAGTGCTGCGCTGAAGCCAATCCTCCCGCATGCTACGGCACAGTGCTTGCTGAATTTCAGC
CTCTTGTAGAAGAGCCTAAGAACTTGGTCAAAACCAACTGTGATCTTTACGAGAAGCTTGGAGAATATGGATTCCAA
AATGCCATTCTAGTTCGCTACACCCAGAAAGCACCTCAGGTGTCAACCCCAACTCTCGTGGAGGCTGCAAGAAACCT
AGGAAGAGTGGGCACCAAGTGTTGTACACTTCCTGAAGATCAGAGACTGCCTTGTGTGGAAGACTATCTGTCTGCAA
TCCTGAACCGTGTGTGTCTGCTGCATGAGAAGACCCCAGTGAGTGAGCATGTTACCAAGTGCTGTAGTGGATCCCTG
GTGGAAAGGCGGCCATGCTTCTCTGCTCTGACAGTTGATGAAACATATGTCCCCAAAGAGTTTAAAGCTGAGACCTT
CACCTTCCACTCTGATATCTGCACACTTCCAGAGAAGGAGAAGCAGATTAAGAAACAAACGGCTCTTGCTGAGCTGG
TGAAGCACAAGCCCAAGGCTACAGCGGAGCAACTGAAGACTGTCATGGATGACTTTGCACAGTTCCTGGATACATGT
TGCAAGGCTGCTGACAAGGACACCTGCTTCTCGACTGAGGGTCCAAACCTTGTCACTAGATGCAAAGACGCCTTAGC
CGGAGGGGGCTCCGTTTCTGATGTTCCGAGGGACCTGGAAGTTGTTGCTGCGACCCCCACCAGCCTACTGATCAGCT
GGGACGATCCGAGTGGCATGGCCCCCTACAGGATCACTTACGGAGAAACAGGAGGAAATAGCCCTGTCCAGGAGTTC
ACTGTGCCTGAACACGTATGGATGGCTACCATCAGCGGCCTTAAACCTGGAGTTGATTATACCATCACTGTGTATGC
TGTCACTGACCAGGGTTCTTCTCACCCAATTTCTATTAATTACCGAACAGAAATTGACAAACCATCCCAGCACCATC
ACCACCATCACTGATAA

2.5FMSA-IV2

HUMAN LC LEADER – 2.5F – GGGGS - MOUSE SERUM ALBUMIN – GGGS – IV2 – HHHHHH – STOP

w/o propeptide

Yellow: Forward Sequence Primer

Light Blue: Reverse Sequence Primer

ATGAGGGTCCCCGCTCAGCTCCTGGGGCTCCTGCTGCTCTGGCTCCCAGGTGCACGATGTGGTTGTCCAAGACCAAG
AGGTGATAATCCACCATTGACTTGTTCTCAAGATTCTGATTGTTTGGCTGGTTGTGTTTGTGGTCCAAATGGTTTTT
GTGGTGGTGGAGGCGGTTCAGAAGCACACAAGAGTGAGATCGCCCATCGGTATAATGATTTGGGAGAACAACATTTC
AAAGGCCTAGTCCTGATTGCCTTTTCCCAGTATCTCCAGAAATGCTCATACGATGAGCATGCCAAATTAGTGCAGGA
AGTAACAGACTTTGCAAAGACGTGTGTTGCCGATGAGTCTGCCGCCAACTGTGACAAATCCCTTCACACTCTTTTTG
GAGATAAGTTGTGTGCCATTCCAAACCTCCGTGAAAACTATGGTGAACTGGCTGACTGCTGTACAAAACAAGAGCCC
GAAAGAAACGAATGTTTCCTGCAACACAAAGATGACAACCCCAGCCTGCCACCATTTGAAAGGCCAGAGGCTGAGGC
CATGTGCACCTCCTTTAAGGAAAACCCAACCACCTTTATGGGACACTATTTGCATGAAGTTGCCAGAAGACATCCTT
ATTTCTATGCCCCAGAACTTCTTTACTATGCTGAGCAGTACAATGAGATTCTGACCCAGTGTTGTGCAGAGGCTGAC
AAGGAAAGCTGCCTGACCCCGAAGCTTGATGGTGTGAAGGAGAAAGCATTGGTCTCATCTGTCCGTCAGAGAATGAA
GTGCTCCAGTATGCAGAAGTTTGGAGAGAGAGCTTTTAAAGCATGGGCAGTAGCTCGTCTGAGCCAGACATTCCCCA
ATGCTGACTTTGCAGAAATCACCAAATTGGCAACAGACCTGACCAAAGTCAACAAGGAGTGCTGCCATGGTGACCTG
CTGGAATGCGCAGATGACAGGGCGGAACTTGCCAAGTACATGTGTGAAAACCAGGCGACTATCTCCAGCAAACTGCA
GACTTGCTGCGATAAACCACTGTTGAAGAAAGCCCACTGTCTTAGTGAGGTGGAGCATGACACCATGCCTGCTGATC
TGCCTGCCATTGCTGCTGATTTTGTTGAGGACCAGGAAGTGTGCAAGAACTATGCTGAGGCCAAGGATGTCTTCCTG
GGCACGTTCTTGTATGAATATTCAAGAAGACACCCTGATTACTCTGTATCCCTGTTGCTGAGACTTGCTAAGAAATA
TGAAGCCACTCTGGAAAAGTGCTGCGCTGAAGCCAATCCTCCCGCATGCTACGGCACAGTGCTTGCTGAATTTCAGC
CTCTTGTAGAAGAGCCTAAGAACTTGGTCAAAACCAACTGTGATCTTTACGAGAAGCTTGGAGAATATGGATTCCAA
AATGCCATTCTAGTTCGCTACACCCAGAAAGCACCTCAGGTGTCAACCCCAACTCTCGTGGAGGCTGCAAGAAACCT
AGGAAGAGTGGGCACCAAGTGTTGTACACTTCCTGAAGATCAGAGACTGCCTTGTGTGGAAGACTATCTGTCTGCAA
TCCTGAACCGTGTGTGTCTGCTGCATGAGAAGACCCCAGTGAGTGAGCATGTTACCAAGTGCTGTAGTGGATCCCTG
GTGGAAAGGCGGCCATGCTTCTCTGCTCTGACAGTTGATGAAACATATGTCCCCAAAGAGTTTAAAGCTGAGACCTT
CACCTTCCACTCTGATATCTGCACACTTCCAGAGAAGGAGAAGCAGATTAAGAAACAAACGGCTCTTGCTGAGCTGG
TGAAGCACAAGCCCAAGGCTACAGCGGAGCAACTGAAGACTGTCATGGATGACTTTGCACAGTTCCTGGATACATGT
TGCAAGGCTGCTGACAAGGACACCTGCTTCTCGACTGAGGGTCCAAACCTTGTCACTAGATGCAAAGACGCCTTAGC
CGGAGGGGGCTCCGTTTCTGATGTTCCGAGGGACCTGGAAGTTGTCGCTGCGACCCCCACCAGCCTACTGATCAGCT
GGGATATTCCTGCTGGTGATTATTTGGATTATTACAAGATCACTTACGGAGAAACAGGAGGAAATAGCCCTGTCCAG

AAGTTCGCTGTGCCTTGGTCTATTCATACTGCTACCATCAGCGGCCTTAAACCTGGAGTTGATTATACCATCACTGT
GTATGCTGTCACTTGGAAGGGCCCTTCTCCTAAGCCAATTTCCATTAATTACCGAACAGAAATTGACAAACCATCCC
AGCACCATCACCACCATCACTGATAA

Antibody sequences

Mouse sm3E antibody in gWiz vector

sm3E mIgG2a (Heavy Chain)

PSTI – SM3E LEADER – SM3E MIGG2A – STOP - SALI

leader: mouse Sm3e heavy chain

HC: sm3EV$_H$ C$_H$1, hinge, C$_H$2, and C$_H$3 (IgG2a)

CTGCAGATGGGTTGGAGCCTCATCTTGCTCTTCCTTGTCGCTGTTGCTACGACGCGTCAAGTTAAACTGGAACAGTC
CGGTGCTGAAGTTGTCAAACCAGGTGCTTCCGTGAAGTTGTCCTGTAAAGCCTCTGGTTTTAACATCAAGGATTCGT
ATATGCATTGGTTGAGACAAGGGCCAGGACAAAGATTGGAATGGATTGGCTGGATTGATCCAGAGAATGGTGATACC
GAGTACGCTCCTAAATTTCAGGGAAAGGCTACTTTTACTACCGACACTTCCGCTAATACCGCATACTTGGGCTTATC
TTCCTTGAGACCAGAGGACACTGCCGTATACTACTGCAACGAAGGGACACCAACTGGTCCTTACTATTTCGACTACT
GGGGACAAGGTACCTTAGTTACTGTCTCTAGCGCTAGCGCCAAAACAACAGCCCCATCGGTCTATCCACTGGCCCCT
GTGTGTGGAGGTACAACTGGCTCCTCGGTGACTCTAGGATGCCTGGTCAAGGGTTATTTCCCTGAGCCAGTGACCTT
GACCTGGAACTCTGGCTCACTGTCCAGTGGTGTGCACACCTTCCCAGCTCTCCTCCAATCTGGCCTCTACACCCTCA
GCAGCTCAGTGACTGTAACCTCGAACACCTGGCCCAGCCAGACCATCACCTGCAATGTGGCCCACCCGGCAAGCAGC
ACCAAAGTGGACAAGAAAATTGAGCCCAGAGTGCCCATAACACAGAACCCCTGTCCTCCACTCAAAGAGTGTCCCCC
ATGCGCAGCTCCAGACCTCTTGGGTGGACCATCCGTCTTCATCTTCCCTCCAAAGATCAAGGATGTACTCATGATCT
CCCTGAGCCCCATGGTCACATGTGTGGTGGTGGATGTGAGCGAGGATGACCCAGACGTCCAGATCAGCTGGTTTGTG
AACAACGTGGAAGTACACACAGCTCAGACACAAACCCATAGAGAGGATTACAACAGTACTCTCCGGGTGGTCAGTGC
CCTCCCCATCCAGCACCAGGACTGGATGAGTGGCAAGGAGTTCAAATGCAAGGTCAACAACAGAGCCCTCCCATCCC
CCATCGAGAAAACCATCTCAAAACCCAGAGGGCCAGTAAGAGCTCCACAGGTATATGTCTTGCCTCCACCAGCAGAA
GAGATGACTAAGAAAGAGTTCAGTCTGACCTGCATGATCACAGGCTTCTTACCTGCCGAAATTGCTGTGGACTGGAC
CAGCAATGGGCGTACAGAGCAAAACTACAAGAACACCGCAACAGTCCTGGACTCTGATGGTTCTTACTTCATGTACA
GCAAGCTCAGAGTACAAAAGAGCACTTGGGAAAGAGGAAGTCTTTTCGCCTGCTCAGTGGTCCACGAGGGTCTGCAC
AATCACCTTACGACTAAGACCATCTCCCGGTCTCTGGGTAAATGATAAGTCGAC

LQMGWSLILLFLVAVATTRQVKLEQSGAEVVKPGASVKLSCKASGFNIKDSYMHWLRQGPGQRLEWIGWIDPENGDT
EYAPKFQGKATFTTDTSANTAYLGLSSLRPEDTAVYYCNEGTPTGPYYFDYWGQGTLVTVSSASAKTTAPSVYPLAP
VCGGTTGSSVTLGCLVKGYFPEPVTLTWNSGSLSSGVHTFPALLQSGLYTLSSSVTVTSNTWPSQTITCNVAHPASS
TKVDKKIEPRVPITQNPCPPLKECPPCAAPDLLGGPSVFIFPPKIKDVLMISLSPMVTCVVVDVSEDDPDVQISWFV
NNVEVHTAQTQTHREDYNSTLRVVSALPIQHQDWMSGKEFKCKVNNRALPSPIEKTISKPRGPVRAPQVYVLPPPAE
EMTKKEFSLTCMITGFLPAEIAVDWTSNGRTEQNYKNTATVLDSDGSYFMYSKLRVQKSTWERGSLFACSVVHEGLH
NHLTTKTISRSLGK**VD

sm3E mLC (Light Chain)

PSTI – LEADER – FLAG TAG - SM3E MLC – STOP - SALI

leader: mouse Sm3e light chain

LC: sm3E V$_L$ C$_{kappa}$

CTGCAGATGAGGGTCCCCGCTCAGCTCCTGGGGCTCCTGCTGCTCTGGCTCCCAGGTGCACGATGTCTCTTTGACTA
CAAGGACGACGATGACAAGCCTAGGGAAAATGTGCTGACCCAATCTCCAAGCTCCATGTCTGTTTCTGTTGGCGATA
GAGTAACCATCGCTTGTAGCGCATCCTCTAGTGTCCCATATATGCACTGGCTTCAACAGAAGCCAGGTAAAAGCCCA
AAGTTGTTGATTTATTTGACATCCAACTTGGCTTCTGGAGTGCCTTCAAGGTTTTCTGGTTCCGGCTCAGGAACCGA
TTATAGTTTGACTATTAGCTCAGTGCAGCCAGAGGATGCTGCAACCTACTATTGCCAGCAAAGGTCCTCATATCCAC
TGACTTTCGGGGGTGGAACGAAGTTGGAAATCAAGCGTACGCGGGCTGATGCTGCACCAACTGTATCCATCTTCCCA

CCATCCAGTGAGCAGTTAACATCTGGAGGTGCCTCAGTCGTGTGCTTCTTGAACAACTTCTACCCCAAAGACATCAA
TGTCAAGTGGAAGATTGATGGCAGTGAACGACAAAATGGCGTCCTGAACAGTTGGACTGATCAGGACAGCAAAGACA
GCACCTACAGCATGAGCAGCACCCTCACGTTGACCAAGGACGAGTATGAACGACATAACAGCTATACCTGTGAGGCC
ACTCACAAGACATCAACTTCACCCATTGTCAAGAGCTTCAACAGGAATGAGTGTTAATAGGTCGAC

LQMRVPAQLLGLLLLWLPGARCLFDYKDDDDKPRENVLTQSPSSMSVSVGDRVTIACSASSSVPYMHWLQQKPGKSP
KLLIYLTSNLASGVPSRFSGSGSGTDYSLTISSVQPEDAATYYCQQRSSYPLTFGGGTKLEIKRTRADAAPTVSIFP
PSSEQLTSGGASVVCFLNNFYPKDINVKWKIDGSERQNGVLNSWTDQDSKDSTYSMSSTLTLTKDEYERHNSYTCEA
THKTSTSPIVKSFNRNEC**VD

Mouse TA99 antibody in gWiz vector

TA99 mIgG2a (Heavy Chain)

PstI – TA99 leader – TA99 mIgG2a – STOP - SalI

leader: mouse TA99 heavy chain

HC: TA99V_H C_H1, hinge, C_H2, and C_H3 (IgG2a)

CTGCAGatgAAATGGAGCTGGGTCTTTCTCTTCCTGATGGCAATGGTTACAGGGGTCAATTCAGAGGTTCAGCTCCA
ACAGTCTGGGGCTGAGCTTGTGAGGCCAGGGGCCTTGGTCAAGTTGTCCTGCAAAACTTCTGGCTTCAACATTAAAG
ACTACTTTTTACACTGGGTGAGACAGAGGCCTGACCAGGGCCTGGAGTGGATTGGATGGATTAATCCTGATAATGGT
AATACTGTTTATGACCCGAAGTTTCAGGGCACGGCCAGTTTAACAGCAGACACATCCTCCAACACAGTCTACTTGCA
GCTCAGCGGCCTGACATCTGAGGACACTGCCGTCTATTTCTGTACTCGGAGGGACTATACTTATGAAAAGGCTGCTC
TGGACTACTGGGGTCAGGGAGCCTCAGTCATCGTCTCCTCAGCCAAAACAACAGCCCCATCGGTCTATCCACTGGCC
CCTGTGTGTGGAGGTACAACTGGCTCCTCGGTGACTCTAGGATGCCTGGTCAAGGGTTATTTCCCTGAGCCAGTGAC
CTTGACCTGGAACTCTGGCTCACTGTCCAGTGGTGTGCACACCTTCCCAGCTCTCCTCCAATCTGGCCTCTACACCC
TCAGCAGCTCAGTGACTGTAACCTCGAACACCTGGCCCAGCCAGACCATCACCTGCAATGTGGCCCACCCGGCAAGC
AGCACCAAAGTGGACAAGAAAATTGAGCCCAGAGTGCCCATAACACAGAACCCCTGTCCTCCACTCAAAGAGTGTCC
CCCATGCGCAGCTCCAGACCTCTTGGGTGGACCATCCGTCTTCATCTTCCCTCCAAAGATCAAGGATGTACTCATGA
TCTCCCTGAGCCCCATGGTCACATGTGTGGTGGTGGATGTGAGCGAGGATGACCCAGACGTCCAGATCAGCTGGTTT
GTGAACAACGTGGAAGTACACACAGCTCAGACACAAACCCATAGAGAGGATTACAACAGTACTCTCCGGGTGGTCAG
TGCCCTCCCCATCCAGCACCAGGACTGGATGAGTGGCAAGGAGTTCAAATGCAAGGTCAACAACAGAGCCCTCCCAT
CCCCCATCGAGAAAACCATCTCAAAACCCAGAGGGCCAGTAAGAGCTCCACAGGTATATGTCTTGCCTCCACCAGCA
GAAGAGATGACTAAGAAAGAGTTCAGTCTGACCTGCATGATCACAGGCTTCTTACCTGCCGAAATTGCTGTGGACTG
GACCAGCAATGGGCGTACAGAGCAAAACTACAAGAACACCGCAACAGTCCTGGACTCTGATGGTTCTTACTTCATGT
ACAGCAAGCTCAGAGTACAAAAGAGCACTTGGGAAAGAGGAAGTCTTTTCGCCTGCTCAGTGGTCCACGAGGGTCTG
CACAATCACCTTACGACTAAGACCATCTCCCGGTCTCTGGGTAAATGATAAGTCGAC

LQMKWSWVFLFLMAMVTGVNSEVQLQQSGAELVRPGALVKLSCKTSGFNIKDYFLHWVRQRPDQGLEWIGWINPDNG
NTVYDPKFQGTASLTADTSSNTVYLQLSGLTSEDTAVYFCTRRDYTYEKAALDYWGQGASVIVSSAKTTAPSVYPLA
PVCGGTTGSSVTLGCLVKGYFPEPVTLTWNSGSLSSGVHTFPALLQSGLYTLSSSVTVTSNTWPSQTITCNVAHPAS
STKVDKKIEPRVPITQNPCPPLKECPPCAAPDLLGGPSVFIFPPKIKDVLMISLSPMVTCVVVDVSEDDPDVQISWF
VNNVEVHTAQTQTHREDYNSTLRVVSALPIQHQDWMSGKEFKCKVNNRALPSPIEKTISKPRGPVRAPQVYVLPPPA
EEMTKKEFSLTCMITGFLPAEIAVDWTSNGRTEQNYKNTATVLDSDGSYFMYSKLRVQKSTWERGSLFACSVVHEGL
HNHLTTKTISRSLGK**VD

TA99 mLC (Light Chain)

PstI – leader – TA99 mLC – STOP - SalI

leader: mouse TA99 light chain

LC: TA99V_L C_{kappa}

CTGCAGatgAGTGTGCTCACTCAGGTCCTGGCGTTGCTGCTGCTGTGGCTTACAGGTGCCAGATGTGCCATCCAGAT
GTCTCAGTCTCCAGCCTCCCTATCTGCATCTGTGGGAGAAACTGTCACCATCACATGTCGAGCAAGTGGAAATATTT
ACAATTATTTAGCATGGTATCAGCAGAAACAGGGAAAATCTCCTCACCTCCTGGTCTATGATGCAAAAACCTTAGCA
GATGGTGTGCCATCAAGGTTCAGTGGCAGTGGCTCAGGGACACAATATTCTCTCAAGATTAGCAGCCTGCAGACTGA
AGATTCTGGGAATTATTACTGTCAACATTTTTGGAGTCTTCCATTCACGTTCGGCTCGGGGACAAAGTTGGAAATAA

AACGGGCTGATGCTGCACCAACTGTATCCATCTTCCCACCATCCAGTGAGCAGTTAACATCTGGAGGTGCCTCAGTC
GTGTGCTTCTTGAACAACTTCTACCCCAAAGACATCAATGTCAAGTGGAAGATTGATGGCAGTGAACGACAAAATGG
CGTCCTGAACAGTTGGACTGATCAGGACAGCAAAGACAGCACCTACAGCATGAGCAGCACCCTCACGTTGACCAAGG
ACGAGTATGAACGACATAACAGCTATACCTGTGAGGCCACTCACAAGACATCAACTTCACCCATTGTCAAGAGCTTC
AACAGGAATGAGTGTTAATAGGTCGAC

LQMSVLTQVLALLLLWLTGARCAIQMSQSPASLSASVGETVTITCRASGNIYNYLAWYQQKQGKSPHLLVYDAKTLA
DGVPSRFSGSGSGTQYSLKISSLQTEDSGNYYCQHFWSLPFTFGSGTKLEIKRADAAPTVSIFPPSSEQLTSGGASV
VCFLNNFYPKDINVKWKIDGSERQNGVLNSWTDQDSKDSTYSMSSTLTLTKDEYERHNSYTCEATHKTSTSPIVKSF
NRNEC**VD

Mouse FcγR sequences

Full FcγR in gWiz vector

mFcgRI

GWIZ –PSTI – SIGNAL SEQ – FCGR – STOP – SALI – GWIZ

CTGCAGATGATTCTTACCAGCTTTGGAGATGACATGTGGCTTCTAACAACTCTGCTACTTTGGGTTCCAGTCGGTGG
GGAAGTGGTTAATGCCACCAAGGCTGTGATCACCTTGCAGCCTCCATGGGTCAGTATTTTCCAGAAGGAAAATGTCA
CTTTATGGTGTGAGGGGCCTCACCTGCCTGGAGACAGTTCCACACAATGGTTTATCAACGGAACAGCCGTTCAGATC
TCCACGCCTAGTTATAGCATCCCAGAGGCCAGTTTTCAGGACAGTGGCGAATACAGGTGTCAGATAGGTTCCTCAAT
GCCAAGTGACCCTGTGCAGTTGCAAATCCACAATGATTGGCTGCTACTCCAGGCCTCCCGCAGAGTCCTCACAGAAG
GAGAACCCCTGGCCTTGAGGTGTCACGGATGGAAGAATAAACTGGTGTACAATGTGGTTTTCTATAGAAATGGAAAA
TCCTTTCAGTTTTCTTCAGATTCGGAGGTCGCCATTCTGAAAACCAACCTGAGTCACAGCGGCATCTACCACTGCTC
AGGCACGGGAAGACACCGCTACACATCTGCAGGAGTGTCCATCACGGTGAAAGAGCTGTTTACCACGCCAGTGCTGA
GAGCATCCGTGTCATCTCCCTTCCCGGAGGGGAGTCTGGTCACCCTGAACTGTGAGACGAATTTGCTCCTGCAGAGA
CCCGGCTTACAGCTTCACTTCTCCTTCTACGTGGGCAGCAAGATCCTGGAGTACAGGAACACATCCTCAGAGTACCA
TATAGCAAGGGCGGAAAGAGAAGATGCTGGATTCTACTGGTGTGAGGTAGCCACGGAGGACAGCAGTGTCCTTAAGC
GCAGCCCTGAGTTGGAGCTCCAAGTGCTTGGTCCCCAGTCATCAGCTCCTGTCTGGTTTCACATCCTGTTTTATCTG
TCAGTGGGAATAATGTTTTCGTTGAACACGGTTCTCTATGTGAAAATACACAGGCTGCAGAGAGAGAAGAAATACAA
CTTATAATAGGTCGAC

LQMILTSFGDDMWLLTTLLLWVPVGGEVVNATKAVITLQPPWVSIFQKENVTLWCEGPHLPGDSSTQWFINGTAVQI
STPSYSIPEASFQDSGEYRCQIGSSMPSDPVQLQIHNDWLLLQASRRVLTEGEPLALRCHGWKNKLVYNVVFYRNGK
SFQFSSDSEVAILKTNLSHSGIYHCSGTGRHRYTSAGVSITVKELFTTPVLRASVSSPFPEGSLVTLNCETNLLLQR
PGLQLHFSFYVGSKILEYRNTSSEYHIARAEREDAGFYWCEVATEDSSVLKRSPELELQVLGPQSSAPVWFHILFYL
SVGIMFSLNTVLYVKIHRLQREKKYNL**VD

mFcgRII

GWIZ –PSTI – SIGNAL SEQ – FCGR – STOP – SALI – GWIZ

CTGCAGATGGAGAGCAACTGGACTGTCCATGTGTTCTCACGGACTTTGTGCCATATGCTACTGTGGACAGCCGTGCT
AAATCTTGCTGCTGGGACTCATGATCTTCCAAAGGCTGTGGTCAAACTCGAGCCCCCGTGGATCCAGGTGCTCAAGG
AAGACACGGTGACACTGACATGCGAAGGGACCCACAACCCTGGGAACTCTTCTACCCAGTGGTTCCACAATGGGAGG
TCCATCCGGAGCCAGGTCCAAGCCAGCTACACGTTTAAGGCCACAGTCAATGACAGTGGAGAATATCGGTGTCAAAT
GGAGCAGACCCGCCTCAGCGACCCTGTAGATCTGGGAGTGATTTCTGACTGGCTGCTGCTCCAGACCCCTCAGCTGG
TGTTTCTGGAAGGGGAAACCATCACGCTAAGGTGCCATAGCTGGAGGAACAAACTACTGAACAGGATCTCGTTCTTC
CATAATGAAAAATCCGTGAGGTATCATCACTACAGTAGTAATTTCTCTATCCCAAAAGCCAACCACAGTCACAGTGG
GGACTACTACTGCAAAGGAAGTCTAGGAAGGACACTGCACCAGTCCAAGCCTGTCACCATCACTGTCCAAGGGCCCA
AGTCCAGCAGGTCTTTACCAGTATTGACAATTGTGGCTGCTGTCACTGGGATTGCTGTCGCAGCCATTGTTATTATC
CTAGTATCCTTGGTCTATCTCAAGAAAAAGCAGGTTCCAGACAATCCTCCTGATCTGGAAGAAGCTGCCAAAACTGA

GGCTGAGAATACGATCACCTACTCACTTCTCAAGCATCCCGAAGCCCTGGATGAAGAAACAGAGCATGATTACCAGA
ACCACATTTAATAGGTCGA

LQMESNWTVHVFSRTLCHMLLWTAVLNLAAGTHDLPKAVVKLEPPWIQVLKEDTVTLTCEGTHNPGNSSTQWFHNGR
SIRSQVQASYTFKATVNDSGEYRCQMEQTRLSDPVDLGVISDWLLLQTPQLVFLEGETITLRCHSWRNKLLNRISFF
HNEKSVRYHHYSSNFSIPKANHSHSGDYYCKGSLGRTLHQSKPVTITVQGPKSSRSLPVLTIVAAVTGIAVAAIVII
LVSLVYLKKKQVPDNPPDLEEAAKTEAENTITYSLLKHPEALDEETEHDYQNHI**VD

mFcgRIII

GWIZ –PSTI – SIGNAL SEQ – FCGR – STOP – SALI – GWIZ

CTGCAGATGTTTCAGAATGCACACTCTGGAAGCCAATGGCTACTTCCACCACTGACAATTCTGCTGCTGTTTGCTTT
TGCAGACAGGCAGAGTGCTCTTCCGAAGGCTGTGGTGAAACTGGACCCCCCATGGATCCAGGTGCTCAAGGAAGACA
TGGTGACACTGATGTGCGAAGGGACCCACAACCCTGGGAACTCTTCTACCCAGTGGTTCCACAACGGGAGGTCCATC
CGGAGCCAGGTCCAAGCCAGTTACACGTTTAAGGCCACAGTCAATGACAGTGGAGAATATCGGTGTCAAATGGAGCA
GACCCGCCTCAGCGACCCTGTAGATCTGGGAGTGATTTCTGACTGGCTGCTGCTCCAGACCCCTCAGCGGGTGTTTC
TGGAAGGGGAAACCATCACGCTAAGGTGCCATAGCTGGAGGAACAAACTACTGAACAGGATCTCATTCTTCCATAAT
GAAAAATCCGTGAGGTATCATCACTACAAAAGTAATTTCTCTATCCCAAAAGCCAACCACAGTCACAGTGGGGACTA
CTACTGCAAAGGAAGTCTAGGAAGTACACAGCACCAGTCCAAGCCTGTCACCATCACTGTCCAAGATCCAGCAACTA
CATCCTCCATCTCTCTAGTCTGGTACCACACTGCTTTCTCCCTAGTGATGTGCCTCCTGTTTGCAGTGGACACGGGC
CTTTATTTCTACGTACGGAGAAATCTTCAAACCCCGAGGGAGTACTGGAGGAAGTCCCTGTCAATCAGAAAGCGCCA
GGCTCCTCAAGATAAGTAATAGGTCGAC

LQMFQNAHSGSQWLLPPLTILLLFAFADRQSALPKAVVKLDPPWIQVLKEDMVTLMCEGTHNPGNSSTQWFHNGRSI
RSQVQASYTFKATVNDSGEYRCQMEQTRLSDPVDLGVISDWLLLQTPQRVFLEGETITLRCHSWRNKLLNRISFFHN
EKSVRYHHYKSNFSIPKANHSHSGDYYCKGSLGSTQHQSKPVTITVQDPATTSSISLVWYHTAFSLVMCLLFAVDTG
LYFYVRRNLQTPREYWRKSLSIRKRQAPQDK**VD

Polymorphism: V81I

mFcgRIV

GWIZ –PSTI – SIGNAL SEQ – FCGR – STOP – SALI – GWIZ

CTGCAGATGTGGCAGCTACTACTACCAACAGCTCTGGTACTTACAGCTTTCTCTGGCATTCAAGCTGGTCTCCAAAA
GGCTGTGGTGAACCTAGACCCCAAGTGGGTCAGGGTGCTTGAGGAAGACAGCGTGACCCTCAGATGCCAAGGCACTT
TCTCCCCCGAGGACAATTCTATCAAGTGGTTCCATAACGAAAGCCTCATCCCACACCAGGATGCCAACTATGTCATC
CAAAGTGCCAGAGTTAAGGACAGTGGAATGTACAGGTGCCAGACAGCCCTCTCCACGATCAGTGACCCAGTGCAACT
AGAGGTCCATATGGGCTGGCTATTGCTTCAGACCACTAAGTGGCTGTTCCAGGAGGGGGACCCCATTCATCTGAGAT
GCCACAGTTGGCAAAACAGACCTGTACGGAAGGTCACCTATTTACAGAACGGCAAAGGCAAGAAGTATTTCCATGAA
AATTCTGAATTACTCATTCCAAAAGCTACACACAATGACAGTGGCTCCTACTTCTGCAGAGGGCTCATTGGACACAA
CAACAAATCTTCAGCATCCTTTCGTATAAGCCTAGGCGATCCAGGGTCTCCATCCATGTTTCCACCGTGGCATCAAA
TCACATTCTGCCTGCTGATAGGACTCTTGTTTGCAATAGACACAGTGCTGTATTTCTCTGTGCGGAGGGGTCTTCAA
AGTCCTGTGGCTGACTATGAGGAACCCAAGATTCAATGGAGCAAGGAACCTCAGGACAAGTAATAGGTCGAC

LQMWQLLLPTALVLTAFSGIQAGLQKAVVNLDPKWVRVLEEDSVTLRCQGTFSPEDNSIKWFHNESLIPHQDANYVI
QSARVKDSGMYRCQTALSTISDPVQLEVHMGWLLLQTTKWLFQEGDPIHLRCHSWQNRPVRKVTYLQNGKGKKYFHE
NSELLIPKATHNDSGSYFCRGLIGHNNKSSASFRISLGDPGSPSMFPPWHQITFCLLIGLLFAIDTVLYFSVRRGLQ
SPVADYEEPKIQWSKEPQDK**VD

common gamma chain

GWIZ –PSTI – SIGNAL SEQ – COMMON GAMMA CHAIN – STOP – SALI – GWIZ

CTGCAGATGATCTCAGCCGTGATCTTGTTCTTGCTCCTTTTGGTGGAACAAGCAGCCGCCCTGGGAGAGCCGCAGCT
CTGCTATATCCTGGATGCTGTCCTGTTTTTGTATGGTATTGTCCTTACCCTACTCTACTGTCGACTCAAGATCCAGG

TCCGAAAGGCAGCTATAGCCAGCCGTGAGAAAGCAGATGCTGTCTACACGGGCCTGAACACCCGGAGCCAGGAGACA
TATGAGACTCTGAAGCATGAGAAACCACCCCAGTAGTAATAGGTCGAC

LQMISAVILFLLLLVEQAAALGEPQLCYILDAVLFLYGIVLTLLYCRLKIQVRKAAIASREKADAVYTGLNTRSQET
YETLKHEKPPQ***VD

FcγR ectodomains in gWiz vector

mFcγRI (CD64) ectodomain

GAAGTGGTTAATGCCACCAAGGCTGTGATCACCTTGCAGCCTCCATGGGTCAGTATTTTCCAGAAGGAAAATGTCAC
TTTATGGTGTGAGGGGCCTCACCTGCCTGGAGACAGTTCCACACAATGGTTTATCAACGGAACAGCCGTTCAGATCT
CCACGCCTAGTTATAGCATCCCAGAGGCCAGTTTTCAGGACAGTGGCGAATACAGGTGTCAGATAGGTTCCTCAATG
CCAAGTGACCCTGTGCAGTTGCAAATCCACAATGATTGGCTGCTACTCCAGGCCTCCCGCAGAGTCCTCACAGAAGG
AGAACCCCTGGCCTTGAGGTGTCACGGATGGAAGAATAAACTGGTGTACAATGTGGTTTTCTATAGAAATGGAAAAT
CCTTTCAGTTTTCTTCAGATTCGGAGGTCGCCATTCTGAAAACCAACCTGAGTCACAGCGGCATCTACCACTGCTCA
GGCACGGGAAGACACCGCTACACATCTGCAGGAGTGTCCATCACGGTGAAAGAGCTGTTTACCACGCCAGTGCTGAG
AGCATCCGTGTCATCTCCCTTCCCGGAGGGGAGTCTGGTCACCCTGAACTGTGAGACGAATTTGCTCCTGCAGAGAC
CCGGCTTACAGCTTCACTTCTCCTTCTACGTGGGCAGCAAGATCCTGGAGTACAGGAACACATCCTCAGAGTACCAT
ATAGCAAGGGCGGAAAGAGAAGATGCTGGATTCTACTGGTGTGAGGTAGCCACGGAGGACAGCAGTGTCCTTAAGCG
CAGCCCTGAGTTGGAGCTCCAAGTGCTTGGTCCCCAGTCATCAGCTCCT

EVVNATKAVITLQPPWVSIFQKENVTLWCEGPHLPGDSSTQWFINGTAVQISTPSYSIPEASFQDSGEYRCQIGSSM
PSDPVQLQIHNDWLLLQASRRVLTEGEPLALRCHGWKNKLVYNVVFYRNGKSFQFSSDSEVAILKTNLSHSGIYHCS
GTGRHRYTSAGVSITVKELFTTPVLRASVSSPFPEGSLVTLNCETNLLLQRPGLQLHFSFYVGSKILEYRNTSSEYH
IARAEREDAGFYWCEVATEDSSVLKRSPELELQVLGPQSSAP

mFcγRII (CD32) ectodomain

ACTCATGATCTTCCAAAGGCTGTGGTCAAACTCGAGCCCCCGTGGATCCAGGTGCTCAAGGAAGACACGGTGACACT
GACATGCGAAGGGACCCACAACCCTGGGAACTCTTCTACCCAGTGGTTCCACAATGGGAGGTCCATCCGGAGCCAGG
TCCAAGCCAGCTACACGTTTAAGGCCACAGTCAATGACAGTGGAGAATATCGGTGTCAAATGGAGCAGACCCGCCTC
AGCGACCCTGTAGATCTGGGAGTGATTTCTGACTGGCTGCTGCTCCAGACCCCTCAGCTGGTGTTTCTGGAAGGGGA
AACCATCACGCTAAGGTGCCATAGCTGGAGGAACAAACTACTGAACAGGATCTCGTTCTTCCATAATGAAAAATCCG
TGAGGTATCATCACTACAGTAGTAATTTCTCTATCCCAAAAGCCAACCACAGTCACAGTGGGGACTACTACTGCAAA
GGAAGTCTAGGAAGGACACTGCACCAGTCCAAGCCTGTCACCATCACTGTCCAAGGGCCCAAGTCCAGCAGG

THDLPKAVVKLEPPWIQVLKEDTVTLTCEGTHNPGNSSTQWFHNGRSIRSQVQASYTFKATVNDSGEYRCQMEQTRL
SDPVDLGVISDWLLLQTPQLVFLEGETITLRCHSWRNKLLNRISFFHNEKSVRYHHYSSNFSIPKANHSHSGDYYCK
GSLGRTLHQSKPVTITVQGPKSSR

mFcγRIII (CD16) ectodomain

GCTCTTCCGAAGGCTGTGGTGAAACTGGACCCCCCATGGATCCAGGTGCTCAAGGAAGACATGGTGACACTGATGTG
CGAAGGGACCCACAACCCTGGGAACTCTTCTACCCAGTGGTTCCACAACGGGAGGTCCATCCGGAGCCAGGTCCAAG
CCAGTTACACGTTTAAGGCCACAGTCAATGACAGTGGAGAATATCGGTGTCAAATGGAGCAGACCCGCCTCAGCGAC
CCTGTAGATCTGGGAGTGATTTCTGACTGGCTGCTGCTCCAGACCCCTCAGCGGGTGTTTCTGGAAGGGGAAACCAT
CACGCTAAGGTGCCATAGCTGGAGGAACAAACTACTGAACAGGATCTCGTTCTTCCATAATGAAAAATCCGTGAGGT
ATCATCACTACAAAAGTAATTTCTCTATCCCAAAAGCCAACCACAGTCACAGTGGGGACTACTACTGCAAAGGAAGT
CTAGGAAGTACACAGCACCAGTCCAAGCCTGTCACCATCACTGTCCAAGATCCAGCAACTACATCCTCCATCTCTCT
AGTCTGGTACCACACT

ALPKAVVKLDPPWIQVLKEDMVTLMCEGTHNPGNSSTQWFHNGRSIRSQVQASYTFKATVNDSGEYRCQMEQTRLSD
PVDLGVISDWLLLQTPQRVFLEGETITLRCHSWRNKLLNRISFFHNEKSVRYHHYKSNFSIPKANHSHSGDYYCKGS
LGSTQHQSKPVTITVQDPATTSSISLVWYHT

Polymorphism: V81I

mFcγRIV (CD16-2) ectodomain

CAAGCTGGTCTCCAAAAGGCTGTGGTGAACCTAGACCCCAAGTGGGTCAGGGTGCTTGAGGAAGACAGCGTGACCCT
CAGATGCCAAGGCACTTTCTCCCCCGAGGACAATTCTATCAAGTGGTTCCATAACGAAAGCCTCATCCCACACCAGG
ATGCCAACTATGTCATCCAAAGTGCCAGAGTTAAGGACAGTGGAATGTACAGGTGCCAGACAGCCCTCTCCACGATC
AGTGACCCAGTGCAACTAGAGGTCCATATGGGCTGGCTATTGCTTCAGACCACTAAGTGGCTGTTCCAGGAGGGGGA
CCCCATTCATCTGAGATGCCACAGTTGGCAAAACAGACCTGTACGGAAGGTCACCTATTTACAGAACGGCAAAGGCA
AGAAGTATTTCCATGAAAATTCTGAATTACTCATTCCAAAAGCTACACACAATGACAGTGGCTCCTACTTCTGCAGA
GGGCTCATTGGACACAACAACAAATCTTCAGCATCCTTTCGTATAAGCCTAGGCGATCCAGGGTCTCCATCCATGTT
TCCACCGTGGCATCAAATCACATTCTGCCTGCTGATAGGACTCTTGTTTGCAATA

QAGLQKAVVNLDPKWVRVLEEDSVTLRCQGTFSPEDNSIKWFHNESLIPHQDANYVIQSARVKDSGMYRCQTALSTI
SDPVQLEVHMGWLLLQTTKWLFQEGDPIHLRCHSWQNRPVRKVTYLQNGKGKKYFHENSELLIPKATHNDSGSYFCR
GLIGHNNKSSASFRISLGDPGSPSMFPPWHQITFCLLIGLLFAI

mFcγR ectodomain format in gWiz (example: mFcγRIV)

GWIZ –PSTI – SIGNAL SEQ – FCGRECTODOMAIN – $(G_4S)_2$ – BIOTIN ACCEPTOR PEPTIDE – HIS6 TAG – STOP – SALI – GWIZ

CTGCAGATGTGGCAGCTACTACTACCAACAGCTCTGGTACTTACAGCTTTCTCTGGCATTCAAGCTGGTCTCCAAAA
GGCTGTGGTGAACCTAGACCCCAAGTGGGTCAGGGTGCTTGAGGAAGACAGCGTGACCCTCAGATGCCAAGGCACTT
TCTCCCCCGAGGACAATTCTATCAAGTGGTTCCATAACGAAAGCCTCATCCCACACCAGGATGCCAACTATGTCATC
CAAAGTGCCAGAGTTAAGGACAGTGGAATGTACAGGTGCCAGACAGCCCTCTCCACGATCAGTGACCCAGTGCAACT
AGAGGTCCATATGGGCTGGCTATTGCTTCAGACCACTAAGTGGCTGTTCCAGGAGGGGGACCCCATTCATCTGAGAT
GCCACAGTTGGCAAAACAGACCTGTACGGAAGGTCACCTATTTACAGAACGGCAAAGGCAAGAAGTATTTCCATGAA
AATTCTGAATTACTCATTCCAAAAGCTACACACAATGACAGTGGCTCCTACTTCTGCAGAGGGCTCATTGGACACAA
CAACAAATCTTCAGCATCCTTTCGTATAAGCCTAGGCGATCCAGGGTCTCCATCCATGTTTCCACCGTGGCATCAAG
GAGGCGGTGGGTCTGGCGGAGGTGGACACGTGCTTAATGACATTTTCGAGGCCCAAAAAATAGAGTGGCATGAAACC
GGTCATCACCATCACCATCACTGATAAGTCGAC

LQMWQLLLPTALVLTAFSGIQAGLQKAVVNLDPKWVRVLEEDSVTLRCQGTFSPEDNSIKWFHNESLIPHQDANYVI
QSARVKDSGMYRCQTALSTISDPVQLEVHMGWLLLQTTKWLFQEGDPIHLRCHSWQNRPVRKVTYLQNGKGKKYFHE
NSELLIPKATHNDSGSYFCRGLIGHNNKSSASFRISLGDPGSPSMFPPWHQGGGGSGGGGHVLNDIFEAQKIEWHET
GHHHHHH**VD

MSA/IL-2 sequences

MSA/IL-2 without the propeptide in gWiz

GWIZ – PSTI – HUMAN LC LEADER – MOUSE SERUM ALBUMIN – GGGS - MIL2 – HHHHHH – STOP – SALI – GWIZ

Yellow: Forward Sequence Primer
Light Blue: Reverse Sequence Primer

CTGCAGATGAGGGTCCCCGCTCAGCTCCTGGGGCTCCTGCTGCTCTGGCTCCCAGGTGCACGATGTGAAGCACACAA
GAGTGAGATCGCCCATCGGTATAATGATTTGGGAGAACAACATTTCAAAGGCCTAGTCCTGATTGCCTTTTCCCAGT

ATCTCCAGAAATGCTCATACGATGAGCATGCCAAATTAGTGCAGGAAGTAACAGACTTTGCAAAGACGTGTGTTGCC
GATGAGTCTGCCGCCAACTGTGACAAATCCCTTCACACTCTTTTTGGAGATAAGTTGTGTGCCATTCCAAACCTCCG
TGAAAACTATGGTGAACTGGCTGACTGCTGTACAAAACAAGAGCCCGAAAGAAACGAATGTTTCCTGCAACACAAAG
ATGACAACCCCAGCCTGCCACCATTTGAAAGGCCAGAGGCTGAGGCCATGTGCACCTCCTTTAAGGAAAACCCAACC
ACCTTTATGGGACACTATTTGCATGAAGTTGCCAGAAGACATCCTTATTTCTATGCCCCAGAACTTCTTTACTATGC
TGAGCAGTACAATGAGATTCTGACCCAGTGTTGTGCAGAGGCTGACAAGGAAAGCTGCCTGACCCCGAAGCTTGATG
GTGTGAAGGAGAAAGCATTGGTCTCATCTGTCCGTCAGAGAATGAAGTGCTCCAGTATGCAGAAGTTTGGAGAGAGA
GCTTTTAAAGCATGGGCAGTAGCTCGTCTGAGCCAGACATTCCCCAATGCTGACTTTGCAGAAATCACCAAATTGGC
AACAGACCTGACCAAAGTCAACAAGGAGTGCTGCCATGGTGACCTGCTGGAATGCGCAGATGACAGGGCGGAACTTG
CCAAGTACATGTGTGAAAACCAGGCGACTATCTCCAGCAAACTGCAGACTTGCTGCGATAAACCACTGTTGAAGAAA
GCCCACTGTCTTAGTGAGGTGGAGCATGACACCATGCCTGCTGATCTGCCTGCCATTGCTGCTGATTTTGTTGAGGA
CCAGGAAGTGTGCAAGAACTATGCTGAGGCCAAGGATGTCTTCCTGGGCACGTTCTTGTATGAATATTCAAGAAGAC
ACCCTGATTACTCTGTATCCCTGTTGCTGAGACTTGCTAAGAAATATGAAGCCACTCTGGAAAAGTGCTGCGCTGAA
GCCAATCCTCCCGCATGCTACGGCACAGTGCTTGCTGAATTTCAGCCTCTTGTAGAAGAGCCTAAGAACTTGGTCAA
AACCAACTGTGATCTTTACGAGAAGCTTGGAGAATATGGATTCCAAAATGCCATTCTAGTTCGCTACACCCAGAAAG
CACCTCAGGTGTCAACCCCAACTCTCGTGGAGGCTGCAAGAAACCTAGGAAGAGTGGGCACCAAGTGTTGTACACTT
CCTGAAGATCAGAGACTGCCTTGTGTGGAAGACTATCTGTCTGCAATCCTGAACCGTGTGTGTCTGCTGCATGAGAA
GACCCCAGTGAGTGAGCATGTTACCAAGTGCTGTAGTGGATCCCTGGTGGAAAGGCGGCCATGCTTCTCTGCTCTGA
CAGTTGATGAAACATATGTCCCCAAAGAGTTTAAAGCTGAGACCTTCACCTTCCACTCTGATATCTGCACACTTCCA
GAGAAGGAGAAGCAGATTAAGAAACAAACGGCTCTTGCTGAGCTGGTGAAGCACAAGCCCAAGGCTACAGCGGAGCA
ACTGAAGACTGTCATGGATGACTTTGCACAGTTCCTGGATACATGTTGCAAGGCTGCTGACAAGGACACCTGCTTCT
CGACTGAGGGTCCAAACCTTGTCACTAGATGCAAAGACGCCTTAGCCGGAGGGGGCTCCGCACCCACTTCAAGCTCC
ACTTCAAGCTCTACAGCGGAAGCACAGCAGCAGCAGCAGCAGCAGCAGCAGCAGCAGCAGCACCTGGAGCAGCTGTT
GATGGACCTACAGGAGCTCCTGAGCAGGATGGAGAATTACAGGAACCTGAAACTCCCCAGGATGCTCACCTTCAAAT
TTTACTTGCCCAAGCAGGCCACAGAATTGAAAGATCTTCAGTGCCTAGAAGATGAACTTGGACCTCTGCGGCATGTT
CTGGATTTGACTCAAAGCAAAAGCTTTCAATTGGAAGATGCTGAGAATTTCATCAGCAATATCAGAGTAACTGTTGT
AAAACTAAAGGGCTCTGACAACACATTTGAGTGCCAATTCGATGATGAGTCAGCAACTGTGGTGGACTTTCTGAGGA
GATGGATAGCCTTCTGTCAAAGCATCATCTCAACAAGCCCTCAACACCATCACCACCATCACTGATAAGTCGAC

Aglycosylated antibody sequences

TA99 hIgG1 in gWiz

PstI – TA99 leader – TA99 hIgG1 – STOP - SalI

leader: mouse TA99 heavy chain

HC: TA99V_H C_H1, hinge, C_H2, and C_H3 (IgG2a)

CTGCAGATGAAATGGAGCTGGGTCTTTCTCTTCCTGATGGCAATGGTTACAGGGGTCAATTCAGAGGTTCAGCTCCA
ACAGTCTGGGGCTGAGCTTGTGAGGCCAGGGGCCTTGGTCAAGTTGTCCTGCAAAACTTCTGGCTTCAACATTAAAG
ACTACTTTTTACACTGGGTGAGACAGAGGCCTGACCAGGGCCTGGAGTGGATTGGATGGATTAATCCTGATAATGGT
AATACTGTTTATGACCCGAAGTTTCAGGGCACGGCCAGTTTAACAGCAGACACATCCTCCAACACAGTCTACTTGCA
GCTCAGCGGCCTGACATCTGAGGACACTGCCGTCTATTTCTGTACTCGGAGGGACTATACTTATGAAAAGGCTGCTC
TGGACTACTGGGGTCAGGGAGCCTCAGTCATCGTCTCCTCAGCTAGCACCAAGGGCCCATCGGTCTTCCCCCTGGCA
CCCTCCTCCAAGAGCACCTCTGGGGGCACAGCGGCCCTGGGCTGCCTGGTCAAGGACTACTTCCCCGAACCGGTGAC
GGTGTCGTGGAACTCAGGCGCCCTGACCAGCGGCGTGCACACCTTCCCGGCTGTCCTACAGTCCTCAGGACTCTACT
CCCTCAGCAGCGTGGTGACCGTGCCCTCCAGCAGCTTGGGCACCCAGACCTACATCTGCAACGTGAATCACAAGCCC
AGCAACACCAAGGTGGACAAGAAAGTTGAGCCCAAATCTTGTGACAAAACTCACACATGCCCACCGTGCCCAGCACC
TGAACTCCTGGGGGGACCGTCAGTCTTCCTCTTCCCCCCAAAACCCAAGGACACCCTCATGATCTCCCGGACCCCTG
AGGTCACATGCGTGGTGGTGGACGTGAGCCACGAAGACCCTGAGGTCAAGTTCAACTGGTACGTGGACGGCGTGGAG
GTGCATAATGCCAAGACAAAGCCGCGGGAGGAGCAGTACAACAGCACGTACCGTGTGGTCAGCGTCCTCACCGTCCT
GCACCAGGACTGGCTGAATGGCAAGGAGTACAAGTGCAAGGTCTCCAACAAAGCCCTCCCAGCCCCCATCGAGAAAA
CCATCTCCAAAGCCAAAGGGCAGCCCCGAGAACCACAGGTGTACACCCTGCCCCCATCCCGGGATGAGCTGACCAAG
AACCAGGTCAGCCTGACCTGCCTGGTCAAAGGCTTCTATCCCAGCGACATCGCCGTGGAGTGGGAGAGCAATGGGCA
GCCGGAGAACAACTACAAGACCACGCCTCCCGTGCTGGACTCCGACGGCTCCTTCTTCCTCTACAGCAAGCTCACCG
TGGACAAGAGCAGGTGGCAGCAGGGGAACGTCTTCTCATGCTCCGTGATGCATGAGGCTCTGCACAACCACTACACG
CAGAAGAGCCTCTCCCTGTCTCCGGGTAAATGATAAGTCGAC

TA99 hLC (Light Chain)

PstI – LEADER – TA99 HLC – STOP - SalI

leader: mouse TA99 light chain

LC: TA99V_L C_{kappa}

CTGCAGATGAGTGTGCTCACTCAGGTCCTGGCGTTGCTGCTGCTGTGGCTTACAGGTGCCAGATGTGCCATCCAGAT
GTCTCAGTCTCCAGCCTCCCTATCTGCATCTGTGGGAGAAACTGTCACCATCACATGTCGAGCAAGTGGAAATATTT
ACAATTATTTAGCATGGTATCAGCAGAAACAGGGAAAATCTCCTCACCTCCTGGTCTATGATGCAAAAACCTTAGCA
GATGGTGTGCCATCAAGGTTCAGTGGCAGTGGCTCAGGGACACAATATTCTCTCAAGATTAGCAGCCTGCAGACTGA
AGATTCTGGGAATTATTACTGTCAACATTTTTGGAGTCTTCCATTCACGTTCGGCTCGGGGACAAAGTTGGAAATAA
AACGTACGGTGGCTGCACCATCTGTCTTCATCTTCCCGCCATCTGATGAGCAGTTGAAATCTGGAACTGCCTCTGTT
GTGTGCCTGCTGAATAACTTCTATCCCAGAGAGGCCAAAGTACAGTGGAAGGTGGATAACGCCCTCCAATCGGGTAA
CTCCCAGGAGAGTGTCACAGAGCAGGACAGCAAGGACAGCACCTACAGCCTCAGCAGCACCCTGACGCTGAGCAAAG
CAGACTACGAGAAACACAAAGTCTACGCCTGCGAAGTCACCCATCAGGGCCTGAGCTCGCCCGTCACAAAGAGCTTC
AACAGGGGAGAGTGTTAATAGGTCGAC

TA99 hIgG1 N297Q

PstI – TA99 LEADER – TA99 N297Q – STOP - SalI

leader: mouse TA99 heavy chain

HC: TA99V_H C_H1, hinge, C_H2, and C_H3 (IgG2a)

CTGCAGATGAAATGGAGCTGGGTCTTTCTCTTCCTGATGGCAATGGTTACAGGGGTCAATTCAGAGGTTCAGCTCCA
ACAGTCTGGGGCTGAGCTTGTGAGGCCAGGGGCCTTGGTCAAGTTGTCCTGCAAAACTTCTGGCTTCAACATTAAAG
ACTACTTTTTACACTGGGTGAGACAGAGGCCTGACCAGGGCCTGGAGTGGATTGGATGGATTAATCCTGATAATGGT
AATACTGTTTATGACCCGAAGTTTCAGGGCACGGCCAGTTTAACAGCAGACACATCCTCCAACACAGTCTACTTGCA
GCTCAGCGGCCTGACATCTGAGGACACTGCCGTCTATTTCTGTACTCGGAGGGACTATACTTATGAAAAGGCTGCTC
TGGACTACTGGGGTCAGGGAGCCTCAGTCATCGTCTCCTCAGCTAGCACCAAGGGCCCATCGGTCTTCCCCCTGGCA
CCCTCCTCCAAGAGCACCTCTGGGGGCACAGCGGCCCTGGGCTGCCTGGTCAAGGACTACTTCCCCGAACCGGTGAC
GGTGTCGTGGAACTCAGGCGCCCTGACCAGCGGCGTGCACACCTTCCCGGCTGTCCTACAGTCCTCAGGACTCTACT
CCCTCAGCAGCGTGGTGACCGTGCCCTCCAGCAGCTTGGGCACCCAGACCTACATCTGCAACGTGAATCACAAGCCC
AGCAACACCAAGGTGGACAAGAAAGTTGAGCCCAAATCTTGTGACAAAACTCACACATGCCCACCGTGCCCAGCACC
TGAACTCCTGGGGGGACCGTCAGTCTTCCTCTTCCCCCCAAAACCCAAGGACACCCTCATGATCTCCCGGACCCCTG
AGGTCACATGCGTGGTGGTGGACGTGAGCCACGAAGACCCTGAGGTCAAGTTCAACTGGTACGTGGACGGCGTGGAG
GTGCATAATGCCAAGACAAAGCCGCGGGAGGAGCAGTACCAAAGCACGTACCGTGTGGTCAGCGTCCTCACCGTCCT
GCACCAGGACTGGCTGAATGGCAAGGAGTACAAGTGCAAGGTCTCCAACAAAGCCCTCCCAGCCCCCATCGAGAAAA
CCATCTCCAAAGCCAAAGGGCAGCCCCGAGAACCACAGGTGTACACCCTGCCCCCATCCCGGGATGAGCTGACCAAG
AACCAGGTCAGCCTGACCTGCCTGGTCAAAGGCTTCTATCCCAGCGACATCGCCGTGGAGTGGGAGAGCAATGGGCA
GCCGGAGAACAACTACAAGACCACGCCTCCCGTGCTGGACTCCGACGGCTCCTTCTTCCTCTACAGCAAGCTCACCG
TGGACAAGAGCAGGTGGCAGCAGGGGAACGTCTTCTCATGCTCCGTGATGCATGAGGCTCTGCACAACCACTACACG
CAGAAGAGCCTCTCCCTGTCTCCGGGTAAATGATAAGTCGAC

TA99 hIgG1 SGTA

PstI – TA99 LEADER – TA99 SGTA – STOP - SalI

leader: mouse TA99 heavy chain

HC: TA99V_H C_H1, hinge, C_H2, and C_H3 (IgG2a)

CTGCAGATGAAATGGAGCTGGGTCTTTCTCTTCCTGATGGCAATGGTTACAGGGGTCAATTCAGAGGTTCAGCTCCA
ACAGTCTGGGGCTGAGCTTGTGAGGCCAGGGGCCTTGGTCAAGTTGTCCTGCAAAACTTCTGGCTTCAACATTAAAG
ACTACTTTTTACACTGGGTGAGACAGAGGCCTGACCAGGGCCTGGAGTGGATTGGATGGATTAATCCTGATAATGGT
AATACTGTTTATGACCCGAAGTTTCAGGGCACGGCCAGTTTAACAGCAGACACATCCTCCAACACAGTCTACTTGCA
GCTCAGCGGCCTGACATCTGAGGACACTGCCGTCTATTTCTGTACTCGGAGGGACTATACTTATGAAAAGGCTGCTC
TGGACTACTGGGGTCAGGGAGCCTCAGTCATCGTCTCCTCAGCTAGCACCAAGGGCCCATCGGTCTTCCCCCTGGCA
CCCTCCTCCAAGAGCACCTCTGGGGGCACAGCGGCCCTGGGCTGCCTGGTCAAGGACTACTTCCCCGAACCGGTGAC
GGTGTCGTGGAACTCAGGCGCCCTGACCAGCGGCGTGCACACCTTCCCGGCTGTCCTACAGTCCTCAGGACTCTACT
CCCTCAGCAGCGTGGTGACCGTGCCCTCCAGCAGCTTGGGCACCCAGACCTACATCTGCAACGTGAATCACAAGCCC

AGCAACACCAAGGTGGACAAGAAAGTTGAGCCCAAATCTTGTGACAAAACTCACACATGCCCACCGTGCCCAGCACC
TGAACTCCTGGGGGGACCGTCAGTCTTCCTCTTCCCCCCAAAACCCAAGGACACCCTCATGATCTCCCGGACCCCTG
AGGTCACATGCGTGGTGGTGGACGTGAGCCACGAAGACCCTGAGGTCAAGTTCAACTGGTACGTGGACGGCGTGGAG
GTGCATAATGCCAAGACAAAGCCGCGGGAGGAGCAGTACAACGGCGCGTACCGTGTGGTCAGCGTCCTCACCGTCCT
GCACCAGGACTGGCTGAATGGCAAGGAGTACAAGTGCAAGGTCTCCAACAAAGCCCTCCCAGCCCCCATCGAGAAAA
CCATCTCCAAAGCCAAAGGGCAGCCCCGAGAACCACAGGTGTACACCCTGCCCCCATCCCGGGATGAGCTGACCAAG
AACCAGGTCAGCCTGACCTGCCTGGTCAAAGGCTTCTATCCCAGCGACATCGCCGTGGAGTGGGAGAGCAATGGGCA
GCCGGAGAACAACTACAAGACCACGCCTCCCGTGCTGGACTCCGACGGCTCCTTCTTCCTCTACAGCAAGCTCACCG
TGGACAAGAGCAGGTGGCAGCAGGGGAACGTCTTCTCATGCTCCGTGATGCATGAGGCTCTGCACAACCACTACACG
CAGAAGAGCCTCTCCCTGTCTCCGGGTAAATGATAAGTCGAC

TA99 hIgG1 DTT-IYG

PstI – TA99 leader – TA99 DTT-IYG – STOP - SalI

leader: mouse TA99 heavy chain

HC: TA99V_H C_H1, hinge, C_H2, and C_H3 (IgG2a)

CTGCAGATGAAATGGAGCTGGGTCTTTCTCTTCCTGATGGCAATGGTTACAGGGGTCAATTCAGAGGTTCAGCTCCA
ACAGTCTGGGGCTGAGCTTGTGAGGCCAGGGGCCTTGGTCAAGTTGTCCTGCAAAACTTCTGGCTTCAACATTAAAG
ACTACTTTTTACACTGGGTGAGACAGAGGCCTGACCAGGGCCTGGAGTGGATTGGATGGATTAATCCTGATAATGGT
AATACTGTTTATGACCCGAAGTTTCAGGGCACGGCCAGTTTAACAGCAGACACATCCTCCAACACAGTCTACTTGCA
GCTCAGCGGCCTGACATCTGAGGACACTGCCGTCTATTTCTGTACTCGGAGGGACTATACTTATGAAAAGGCTGCTC
TGGACTACTGGGGTCAGGGAGCCTCAGTCATCGTCTCCTCAGCTAGCACCAAGGGCCCATCGGTCTTCCCCCTGGCA
CCCTCCTCCAAGAGCACCTCTGGGGGCACAGCGGCCCTGGGCTGCCTGGTCAAGGACTACTTCCCCGAACCGGTGAC
GGTGTCGTGGAACTCAGGCGCCCTGACCAGCGGCGTGCACACCTTCCCGGCTGTCCTACAGTCCTCAGGACTCTACT
CCCTCAGCAGCGTGGTGACCGTGCCCTCCAGCAGCTTGGGCACCCAGACCTACATCTGCAACGTGAATCACAAGCCC
AGCAACACCAAGGTGGACAAGAAAGTTGAGCCCAAATCTTGTGACAAAACTCACACATGCCCACCGTGCCCAGCACC
TGAACTCCTGGGGGGACCGTCAGTCTTCCTCTTCCCCCCAAAACCCAAGGACACCCTCATGATCTCCCGGACCCCTG
AGGTCACATGCGTGGTGGTGGACGTGAGCCACGAAGACCCTGAGGTCAAGTTCAACTGGTACGTGGACGGCGTGGAG
GTGCATAATGCCAAGACAAAGCCGCGGGAGGAGCAGTACGACACCACGTACCGTGTGGTCAGCGTCCTCACCGTCCT
GCACCAGGACTGGCTGAATGGCAAGGAGTACAAGTGCAAGGTCTCCAACATTTATGGGCCAGCCCCCATCGAGAAAA
CCATCTCCAAAGCCAAAGGGCAGCCCCGAGAACCACAGGTGTACACCCTGCCCCCATCCCGGGATGAGCTGACCAAG
AACCAGGTCAGCCTGACCTGCCTGGTCAAAGGCTTCTATCCCAGCGACATCGCCGTGGAGTGGGAGAGCAATGGGCA
GCCGGAGAACAACTACAAGACCACGCCTCCCGTGCTGGACTCCGACGGCTCCTTCTTCCTCTACAGCAAGCTCACCG
TGGACAAGAGCAGGTGGCAGCAGGGGAACGTCTTCTCATGCTCCGTGATGCATGAGGCTCTGCACAACCACTACACG
CAGAAGAGCCTCTCCCTGTCTCCGGGTAAATGATAAGTCGAC

TA99 hIgG1 DAT-IYG

PstI – TA99 leader – TA99 DAT-IYG – STOP - SalI

leader: mouse TA99 heavy chain

HC: TA99V_H C_H1, hinge, C_H2, and C_H3 (IgG2a)

CTGCAGATGAAATGGAGCTGGGTCTTTCTCTTCCTGATGGCAATGGTTACAGGGGTCAATTCAGAGGTTCAGCTCCA
ACAGTCTGGGGCTGAGCTTGTGAGGCCAGGGGCCTTGGTCAAGTTGTCCTGCAAAACTTCTGGCTTCAACATTAAAG
ACTACTTTTTACACTGGGTGAGACAGAGGCCTGACCAGGGCCTGGAGTGGATTGGATGGATTAATCCTGATAATGGT
AATACTGTTTATGACCCGAAGTTTCAGGGCACGGCCAGTTTAACAGCAGACACATCCTCCAACACAGTCTACTTGCA
GCTCAGCGGCCTGACATCTGAGGACACTGCCGTCTATTTCTGTACTCGGAGGGACTATACTTATGAAAAGGCTGCTC
TGGACTACTGGGGTCAGGGAGCCTCAGTCATCGTCTCCTCAGCTAGCACCAAGGGCCCATCGGTCTTCCCCCTGGCA
CCCTCCTCCAAGAGCACCTCTGGGGGCACAGCGGCCCTGGGCTGCCTGGTCAAGGACTACTTCCCCGAACCGGTGAC
GGTGTCGTGGAACTCAGGCGCCCTGACCAGCGGCGTGCACACCTTCCCGGCTGTCCTACAGTCCTCAGGACTCTACT
CCCTCAGCAGCGTGGTGACCGTGCCCTCCAGCAGCTTGGGCACCCAGACCTACATCTGCAACGTGAATCACAAGCCC
AGCAACACCAAGGTGGACAAGAAAGTTGAGCCCAAATCTTGTGACAAAACTCACACATGCCCACCGTGCCCAGCACC
TGAACTCCTGGGGGGACCGTCAGTCTTCCTCTTCCCCCCAAAACCCAAGGACACCCTCATGATCTCCCGGACCCCTG
AGGTCACATGCGTGGTGGTGGACGTGAGCCACGAAGACCCTGAGGTCAAGTTCAACTGGTACGTGGACGGCGTGGAG
GTGCATAATGCCAAGACAAAGCCGCGGGAGGAGCAGTACGACGCCACGTACCGTGTGGTCAGCGTCCTCACCGTCCT
GCACCAGGACTGGCTGAATGGCAAGGAGTACAAGTGCAAGGTCTCCAACATTTATGGGCCAGCCCCCATCGAGAAAA

CCATCTCCAAAGCCAAAGGGCAGCCCCGAGAACCACAGGTGTACACCCTGCCCCCATCCCGGGATGAGCTGACCAAG
AACCAGGTCAGCCTGACCTGCCTGGTCAAAGGCTTCTATCCCAGCGACATCGCCGTGGAGTGGGAGAGCAATGGGCA
GCCGGAGAACAACTACAAGACCACGCCTCCCGTGCTGGACTCCGACGGCTCCTTCTTCCTCTACAGCAAGCTCACCG
TGGACAAGAGCAGGTGGCAGCAGGGGAACGTCTTCTCATGCTCCGTGATGCATGAGGCTCTGCACAACCACTACACG
CAGAAGAGCCTCTCCCTGTCTCCGGGTAAATGATAAGTCGAC

TA99 hIgG1 HAT-IYG

PstI – TA99 leader – TA99 HAT-IYG – STOP - SalI

leader: mouse TA99 heavy chain

HC: TA99V_H C_H1, hinge, C_H2, and C_H3 (IgG2a)

CTGCAGATGAAATGGAGCTGGGTCTTTCTCTTCCTGATGGCAATGGTTACAGGGGTCAATTCAGAGGTTCAGCTCCA
ACAGTCTGGGGCTGAGCTTGTGAGGCCAGGGGCCTTGGTCAAGTTGTCCTGCAAAACTTCTGGCTTCAACATTAAAG
ACTACTTTTTACACTGGGTGAGACAGAGGCCTGACCAGGGCCTGGAGTGGATTGGATGGATTAATCCTGATAATGGT
AATACTGTTTATGACCCGAAGTTTCAGGGCACGGCCAGTTTAACAGCAGACACATCCTCCAACACAGTCTACTTGCA
GCTCAGCGGCCTGACATCTGAGGACACTGCCGTCTATTTCTGTACTCGGAGGGACTATACTTATGAAAAGGCTGCTC
TGGACTACTGGGGTCAGGGAGCCTCAGTCATCGTCTCCTCAGCTAGCACCAAGGGCCCATCGGTCTTCCCCCTGGCA
CCCTCCTCCAAGAGCACCTCTGGGGGCACAGCGGCCCTGGGCTGCCTGGTCAAGGACTACTTCCCCGAACCGGTGAC
GGTGTCGTGGAACTCAGGCGCCCTGACCAGCGGCGTGCACACCTTCCCGGCTGTCCTACAGTCCTCAGGACTCTACT
CCCTCAGCAGCGTGGTGACCGTGCCCTCCAGCAGCTTGGGCACCCAGACCTACATCTGCAACGTGAATCACAAGCCC
AGCAACACCAAGGTGGACAAGAAAGTTGAGCCCAAATCTTGTGACAAAACTCACACATGCCCACCGTGCCCAGCACC
TGAACTCCTGGGGGGACCGTCAGTCTTCCTCTTCCCCCCAAAACCCAAGGACACCCTCATGATCTCCCGGACCCCTG
AGGTCACATGCGTGGTGGTGGACGTGAGCCACGAAGACCCTGAGGTCAAGTTCAACTGGTACGTGGACGGCGTGGAG
GTGCATAATGCCAAGACAAAGCCGCGGGAGGAGCAGTACCACGCCACGTACCGTGTGGTCAGCGTCCTCACCGTCCT
GCACCAGGACTGGCTGAATGGCAAGGAGTACAAGTGCAAGGTCTCCAACATTTATGGGCCAGCCCCCATCGAGAAAA
CCATCTCCAAAGCCAAAGGGCAGCCCCGAGAACCACAGGTGTACACCCTGCCCCCATCCCGGGATGAGCTGACCAAG
AACCAGGTCAGCCTGACCTGCCTGGTCAAAGGCTTCTATCCCAGCGACATCGCCGTGGAGTGGGAGAGCAATGGGCA
GCCGGAGAACAACTACAAGACCACGCCTCCCGTGCTGGACTCCGACGGCTCCTTCTTCCTCTACAGCAAGCTCACCG
TGGACAAGAGCAGGTGGCAGCAGGGGAACGTCTTCTCATGCTCCGTGATGCATGAGGCTCTGCACAACCACTACACG
CAGAAGAGCCTCTCCCTGTCTCCGGGTAAATGATAAGTCGAC

TA99 hIgG1 299A-IYG

PstI – TA99 leader – TA99 299A-IYG – STOP - SalI

leader: mouse TA99 heavy chain

HC: TA99V_H C_H1, hinge, C_H2, and C_H3 (IgG2a)

CTGCAGATGAAATGGAGCTGGGTCTTTCTCTTCCTGATGGCAATGGTTACAGGGGTCAATTCAGAGGTTCAGCTCCA
ACAGTCTGGGGCTGAGCTTGTGAGGCCAGGGGCCTTGGTCAAGTTGTCCTGCAAAACTTCTGGCTTCAACATTAAAG
ACTACTTTTTACACTGGGTGAGACAGAGGCCTGACCAGGGCCTGGAGTGGATTGGATGGATTAATCCTGATAATGGT
AATACTGTTTATGACCCGAAGTTTCAGGGCACGGCCAGTTTAACAGCAGACACATCCTCCAACACAGTCTACTTGCA
GCTCAGCGGCCTGACATCTGAGGACACTGCCGTCTATTTCTGTACTCGGAGGGACTATACTTATGAAAAGGCTGCTC
TGGACTACTGGGGTCAGGGAGCCTCAGTCATCGTCTCCTCAGCTAGCACCAAGGGCCCATCGGTCTTCCCCCTGGCA
CCCTCCTCCAAGAGCACCTCTGGGGGCACAGCGGCCCTGGGCTGCCTGGTCAAGGACTACTTCCCCGAACCGGTGAC
GGTGTCGTGGAACTCAGGCGCCCTGACCAGCGGCGTGCACACCTTCCCGGCTGTCCTACAGTCCTCAGGACTCTACT
CCCTCAGCAGCGTGGTGACCGTGCCCTCCAGCAGCTTGGGCACCCAGACCTACATCTGCAACGTGAATCACAAGCCC
AGCAACACCAAGGTGGACAAGAAAGTTGAGCCCAAATCTTGTGACAAAACTCACACATGCCCACCGTGCCCAGCACC
TGAACTCCTGGGGGGACCGTCAGTCTTCCTCTTCCCCCCAAAACCCAAGGACACCCTCATGATCTCCCGGACCCCTG
AGGTCACATGCGTGGTGGTGGACGTGAGCCACGAAGACCCTGAGGTCAAGTTCAACTGGTACGTGGACGGCGTGGAG
GTGCATAATGCCAAGACAAAGCCGCGGGAGGAGCAGTACAACAGCGCGTACCGTGTGGTCAGCGTCCTCACCGTCCT
GCACCAGGACTGGCTGAATGGCAAGGAGTACAAGTGCAAGGTCTCCAACATTTATGGGCCAGCCCCCATCGAGAAAA
CCATCTCCAAAGCCAAAGGGCAGCCCCGAGAACCACAGGTGTACACCCTGCCCCCATCCCGGGATGAGCTGACCAAG
AACCAGGTCAGCCTGACCTGCCTGGTCAAAGGCTTCTATCCCAGCGACATCGCCGTGGAGTGGGAGAGCAATGGGCA
GCCGGAGAACAACTACAAGACCACGCCTCCCGTGCTGGACTCCGACGGCTCCTTCTTCCTCTACAGCAAGCTCACCG
TGGACAAGAGCAGGTGGCAGCAGGGGAACGTCTTCTCATGCTCCGTGATGCATGAGGCTCTGCACAACCACTACACG
CAGAAGAGCCTCTCCCTGTCTCCGGGTAAATGATAAGTCGAC

APPENDIX B: MATLAB MODEL

Example code for modeling dimer concentration from wild-type TA99 hIgG1 binding to the human FcγRs. Same code was expanded to all of the aglycosylated variants.

```
function phago

clear all
close all

options = optimset('MaxFunEval',1e8, 'MaxIter', 1e6);

x = ones(29,1); %will have to change # depending upon total # of
unknowns/equations to be solved
[x] = fsolve(@myfun, x, options)

save('variables.mat','x')

end

%for WT
function F=myfun(x)

%Original Parameters
Ab = 0.1; %antibody concentration uM
B16_TRP1 = 33904; %antigen # per cell
Mac_FcR = 3e5; %total Fc gamma Receptor per cell (wofsy et al.) -- will be
assumed to be the same for all different types of FcgR
Nav = 6.022e23; %avogadro's number
B16_dia = 10; %diameter of B16F10 in um
Mac_dia = 21; %diameter of macrophage in um
contactArea = 104.7; %um^2 = 1/3 of the surface area of the B16 cells

%Calculated areas and volumes
Mac_vol = 4/3*pi*(Mac_dia/2)^3*1e-15; %volume of macrophage cell converted to
liters
Mac_sa = 4*pi*(Mac_dia/2)^2; % surface area of macrophage cell in um^2
B16_vol = 4/3*pi*(B16_dia/2)^3*1e-15; %volume of B16F10 cell converted to
liters

%Affinity parameters
%all Kd except Kdiff are uM
Kdab = 6.1e-4; % Antibody binding affinity to antigen
Kdiff = (Mac_sa-contactArea)/contactArea; % equation from paper -- rate of
diffusion of Free FcgR into the Contact Volume
%Determining Kcross
kx1Ro = 0.1; %s^-1              (slow), cross-linking(wofsy et al.)
Ro = (Mac_FcR/Mac_vol)/(Nav); %M                  initial cell surface Fc
gamma receptor expression(wofsy et al.)
k_onx = kx1Ro/Ro; %M^-1s^-1     dimer cross-linking rate constant
k_offx = 1e-5; %s^-1               dimer dissociation rate constant (wofsy et
al) (from Haugh = 0.016min^1) -->change using same order of magnitude
Kcross = k_offx/k_onx * 1e6; %uM          rate constant of dimers
crosslinking (i.e. signaling)
```

```
%Expand here: affinity parameters of all antibody Fc variants to other FcgR
KdIa = 0.003; % Antibody Fc (WT) binding affinity to FcgRIa
KdIIaH = 1.148; % Antibody Fc (WT) binding affinity to FcgRIIaH
KdIIaR = 8.015; % Antibody Fc (WT) binding affinity to FcgRIIaR
KdIIb = 3.516; % Antibody Fc (WT) binding affinity to FcgRIIb
KdIIIaV = 1.703; % Antibody Fc (WT) binding affinity to FcgRIIIaV
KdIIIaF = 4.538; % Antibody Fc (WT) binding affinity to FcgRIIIaF

% Calculated known concentrations
Rt = (Mac_FcR/Nav)/Mac_vol * 1e6; %total Fc gamma receptor concentration uM
Ag = (B16_TRP1/Nav)/B16_vol * 1e6; %total antigen concentration uM

%outputs concentrations of Receptors in the contact volume, bound antibody,
complexes, and dimers in uM
F = [Rt-x(1)-Kdiff*x(1); %x(1) solves for FcgR concentration in the contact
volume
Ag*Ab - Kdab*x(2); %x(2) solves for concentration antibody bound to it's
antigen

%x(3-8) solves for concentration of complexes formed of bound antibody and
FcgR in the contact volume
    x(1)*x(2) - KdIa*x(3);
    x(1)*x(2) - KdIIaH*x(4);
    x(1)*x(2) - KdIIaR*x(5);
    x(1)*x(2) - KdIIb*x(6);
    x(1)*x(2) - KdIIIaV*x(7);
    x(1)*x(2) - KdIIIaF*x(8);

    x(3)*x(3) - Kcross*x(9);
    x(3)*x(4) - Kcross*x(10);
    x(3)*x(5) - Kcross*x(11);
    x(3)*x(6) - Kcross*x(12);
    x(3)*x(7) - Kcross*x(13);
    x(3)*x(8) - Kcross*x(14);

    x(4)*x(4) - Kcross*x(15);
    x(4)*x(5) - Kcross*x(16);
    x(4)*x(6) - Kcross*x(17);
    x(4)*x(7) - Kcross*x(18);
    x(4)*x(8) - Kcross*x(19);

    x(5)*x(5) - Kcross*x(20);
    x(5)*x(6) - Kcross*x(21);
    x(5)*x(7) - Kcross*x(22);
    x(5)*x(8) - Kcross*x(23);

    x(6)*x(6) - Kcross*x(24);
    x(6)*x(7) - Kcross*x(25);
    x(6)*x(8) - Kcross*x(26);

    x(7)*x(7) - Kcross*x(27);
    x(7)*x(8) - Kcross*x(28);

    x(8)*x(8) - Kcross*x(29)];

end
```